

1-1-1998

A study of the influence of physical parameters on the drying of porous media

Jason C Viggato

University of Nevada, Las Vegas

Follow this and additional works at: <https://digitalscholarship.unlv.edu/rtds>

Repository Citation

Viggato, Jason C, "A study of the influence of physical parameters on the drying of porous media" (1998). *UNLV Retrospective Theses & Dissertations*. 859.

<http://dx.doi.org/10.25669/s4bi-4xej>

This Thesis is protected by copyright and/or related rights. It has been brought to you by Digital Scholarship@UNLV with permission from the rights-holder(s). You are free to use this Thesis in any way that is permitted by the copyright and related rights legislation that applies to your use. For other uses you need to obtain permission from the rights-holder(s) directly, unless additional rights are indicated by a Creative Commons license in the record and/or on the work itself.

This Thesis has been accepted for inclusion in UNLV Retrospective Theses & Dissertations by an authorized administrator of Digital Scholarship@UNLV. For more information, please contact digitalscholarship@unlv.edu.

INFORMATION TO USERS

This manuscript has been reproduced from the microfilm master. UMI films the text directly from the original or copy submitted. Thus, some thesis and dissertation copies are in typewriter face, while others may be from any type of computer printer.

The quality of this reproduction is dependent upon the quality of the copy submitted. Broken or indistinct print, colored or poor quality illustrations and photographs, print bleedthrough, substandard margins, and improper alignment can adversely affect reproduction.

In the unlikely event that the author did not send UMI a complete manuscript and there are missing pages, these will be noted. Also, if unauthorized copyright material had to be removed, a note will indicate the deletion.

Oversize materials (e.g., maps, drawings, charts) are reproduced by sectioning the original, beginning at the upper left-hand corner and continuing from left to right in equal sections with small overlaps. Each original is also photographed in one exposure and is included in reduced form at the back of the book.

Photographs included in the original manuscript have been reproduced xerographically in this copy. Higher quality 6" x 9" black and white photographic prints are available for any photographs or illustrations appearing in this copy for an additional charge. Contact UMI directly to order.

UMI

A Bell & Howell Information Company
300 North Zeeb Road, Ann Arbor MI 48106-1346 USA
313/761-4700 800/521-0600

A STUDY OF THE INFLUENCE OF PHYSICAL PARAMETERS ON THE DRYING
OF POROUS MEDIA

by

Jason C. Viggato

Bachelor of Technology
State University of New York College at Buffalo
1996

A thesis submitted in partial fulfillment
of the requirements for the degree of

Master of Science

in

Mechanical Engineering

**Department of Mechanical Engineering
University of Nevada, Las Vegas
May 1998**

UMI Number: 1390662

**UMI Microform 1390662
Copyright 1998, by UMI Company. All rights reserved.**

**This microform edition is protected against unauthorized
copying under Title 17, United States Code.**

UMI
300 North Zeeb Road
Ann Arbor, MI 48103



Thesis Approval

The Graduate College
University of Nevada, Las Vegas

APRIL 22, 1998

The Thesis prepared by

JASON C. VIGGATO

Entitled

A STUDY OF THE INFLUENCE OF PHYSICAL PARAMETERS ON THE DRYING OF
POROUS MEDIA

is approved in partial fulfillment of the requirements for the degree of

MASTER OF SCIENCE IN MECHANICAL ENGINEERING

Examination Committee Chair

Dean of the Graduate College

Examination Committee Member

Examination Committee Member

Graduate College Faculty Representative

ABSTRACT

A Study of the Influence of Physical Parameters on the Drying of Porous Media

by

Jason C. Viggato

Dr. Robert Boehm, Examination Committee Chair
Professor of Mechanical Engineering
University of Nevada, Las Vegas

An experimental setup is developed to observe the mass transfer that occurs in the drying of saturated porous media due to bulk flow of gas. The analysis and equations are developed in a one-dimensional perspective, and focus on the convection and evaporation that results. Humidity readings are monitored at various locations and used in the analysis of the results. These procedures are used in test cases for Steel spheres and Ceramic beads both 4.5 mm in diameter at .25 L/min, .5 L/min, .75 L/min and 1 L/min flow rates.

Drying times and humidity plots versus time for both steel and ceramic are witnessed to be similar in nature. A correlation for the drying time is developed through use of Sherwood number, Reynolds number, and Schmidt number. This is achieved by using the non-dimensional quantities and acquiring a linear regression and equation. The coefficients and exponent values of the general equation for the Sherwood number are then solved.

SYMBOLS

A	total surface area per unit volume
c	specific heat
c_p	specific heat at constant pressure
d_p	diameter of particle
D_{12}	coefficient of diffusion
g	gravitational constant
h	enthalpy
h_m	mass transfer coefficient
h_{vap}	latent heat of evaporation
K	permeability
k_{ri}	wetting phase relative permeability
k_{rg}	non-wetting phase permeability
k	thermal conductivity
L	length
m_e	mass flow rate due to evaporation
n_a	evaporation rate
P	pressure
P_c	capillary pressure
P_{sg}	saturated vapor pressure

P_{sg}	saturated vapor pressure
R	universal gas constant
Re	Reynolds number = $\rho u D / \mu$
RH	relative humidity
S_l	liquid phase saturation
S_g	gas phase saturation
S	reduced saturation $(S - S_l) / (1 - S_l - S_g)$
S_{bed}	surface area of bed per unit volume
Sc	Schmidt number = ν / D_{12}
Sh	Sherwood number = $h_m d_p / D_{12}$
T	temperature
t	time
u	critical bed velocity
V	volume
v	specific volume

Greek Symbols

β	volumetric thermal expansion coefficient
ϵ	phase volume fraction
μ	dynamic viscosity
ρ	density
ϕ	porosity

Subscripts

g	gas phase
-----	-----------

l	liquid phase
s	solid phase
0	reference

TABLE OF CONTENTS

ABSTRACT	iii
LIST OF FIGURES	viii
ACKNOWLEDGEMENTS	x
CHAPTER 1 INTRODUCTION	1
CHAPTER 2 EXPERIMENTAL STUDY	5
2.1 Experimental Setup	5
2.2 Experimental Procedure	8
CHAPTER 3 DATA REDUCTION	11
CHAPTER 4 DISCUSSION AND RESULTS	14
4.1 Steel Sphere Tests	15
4.2 Ceramic Bead Tests	18
4.3 Comparison of Steel and Ceramic Tests	30
4.4 Non-Dimensional Curvefit	32
CHAPTER 5 SUMMARY AND CONCLUSION	35
APPENDICES	
APPENDIX I: Development of Theory	36
APPENDIX II: Humidity Sensor Calibrations-Steel	44
APPENDIX III: Humidity Sensor Calibrations-Ceramic	53
APPENDIX IV: Mass of Water Lost Calibrations-Steel	62
APPENDIX V: Mass of Water Lost Calibrations-Ceramic	67
APPENDIX VI: Reynolds Number Calculations	72
APPENDIX VII: Calculations-Steel	75
APPENDIX VIII: Calculations-Ceramic	84
BIBLIOGRAPHY	93
VITA	96

LIST OF FIGURES

Figure 1	Experimental Setup Schematic Diagram	6
Figure 2	Experimental Test Section Cross-Sectional View Diagram	7
Figure 3	Inlet and Outlet Humidity vs. Time-Steel .25 L/min	16
Figure 4	Inlet and Outlet Humidity vs. Time-Steel .5 L/min	17
Figure 5	Inlet and Outlet Humidity vs. Time-Steel .75 L/min	19
Figure 6	Inlet and Outlet Humidity vs. Time-Steel 1 L/min	20
Figure 7	Inlet and Outlet Humidity vs. Time-Ceramic .25 L/min	22
Figure 8	Inlet and Outlet Humidity vs. Time-Ceramic .5 L/min	23
Figure 9	Inlet and Outlet Humidity vs. Time-Ceramic .75 L/min	24
Figure 10	Inlet and Outlet Humidity vs. Time-Ceramic 1 L/min	25
Figure 11	Mass of Water Lost vs. Time-Steel Test Flow Rates	26
Figure 12	Mass of Water Lost vs. Time-Ceramic Test Flow Rates	27
Figure 13	Evaporation Rate Regression-Steel Flow Rates	28
Figure 14	Evaporation Rate Regression-Ceramic Flow Rates	29
Figure 15	Dimensionless Representation of Mass Transfer Measurements-Steel	33
Figure 16	Dimensionless Representation of Mass Transfer Measurements-Ceramic	34
Figure 17	Inlet Humidity of Nitrogen Gas vs. Voltage Calibration-Steel Test # 1	45
Figure 18	Outlet Humidity vs. Voltage Calibration-Steel Test # 1	46
Figure 19	Inlet Humidity of Nitrogen Gas vs. Voltage Calibration-Steel Test # 2	47
Figure 20	Outlet Humidity vs. Voltage Calibration-Steel Test # 2	48
Figure 21	Inlet Humidity of Nitrogen Gas vs. Voltage Calibration-Steel Test # 3	49
Figure 22	Outlet Humidity vs. Voltage Calibration-Steel Test # 3	50
Figure 23	Inlet Humidity of Nitrogen Gas vs. Voltage Calibration-Steel Test # 4	51
Figure 24	Outlet Humidity vs. Voltage Calibration-Steel Test # 4	52
Figure 25	Inlet Humidity of Nitrogen Gas vs. Voltage Calibration-Ceramic Test # 1	54
Figure 26	Outlet Humidity vs. Voltage Calibration-Ceramic Test # 1	55
Figure 27	Inlet Humidity of Nitrogen Gas vs. Voltage Calibration-Ceramic Test # 2	56
Figure 28	Outlet Humidity vs. Voltage Calibration-Ceramic Test # 2	57
Figure 29	Inlet Humidity of Nitrogen Gas vs. Voltage	

	Calibration-Ceramic Test # 3	58
Figure 30	Outlet Humidity vs. Voltage Calibration-Ceramic Test # 3	59
Figure 31	Inlet Humidity of Nitrogen Gas vs. Voltage Calibration-Ceramic Test # 4	60
Figure 32	Outlet Humidity vs. Voltage Calibration- Ceramic Test # 4	61
Figure 33	Mass of Water Lost vs. Time Calibration- Steel .25 L/min	63
Figure 34	Mass of Water Lost vs. Time Calibration- Steel .5 L/min	64
Figure 35	Mass of Water Lost vs. Time Calibration- Steel .75 L/min	65
Figure 36	Mass of Water Lost vs. Time Calibration- Steel 1 L/min	66
Figure 37	Mass of Water Lost vs. Time Calibration- Ceramic .25 L/min	68
Figure 38	Mass of Water Lost vs. Time Calibration- Ceramic .5 L/min	69
Figure 39	Mass of Water Lost vs. Time Calibration- Ceramic .75 L/min	70
Figure 40	Mass of Water Lost vs. Time Calibration- Ceramic 1 L/min	71

ACKNOWLEDGEMENTS

I would like to take the time to thank my entire family, especially my mother-Gail Viggato, father-Charles Viggato and brother- Jeff Viggato for both the financial and moral support needed to accomplish the requirements for the Master of Science degree. At this time, I would also like to take a moment to remember a family friend, the late Paul “Doc” Culkowski, Ph.D. and thank him for the valuable guidance and support that he gave to me during both personal and educational difficulties. It is in great part due to him that I am still pursuing Mechanical Engineering. I would also like to thank my advisor Robert Boehm, Ph.D. and Yi-Tung Chen, Ph.D. for their time, guidance and suggestions throughout the entire course of study and research.

CHAPTER 1

INTRODUCTION

The study of drying in porous media is becoming increasingly more important as society faces more intricate needs and problems related to energy consumption. Many areas of engineering such as catalytic converters, pharmaceutical products, waste disposal, water migration, geothermal energy management, insulation and oil and gas flows to list a few, all utilize the principles of combined heat and mass transfer, fluid flow or both through porous media. Keey (1992) states that the majority of industrialized countries consume between seven and fifteen percent of their total energy in drying processes.

Numerous studies involving heat and mass transfer with phase change have been conducted in various applications. Francis et al. (1996) have investigated jet impingement drying processes for semi-porous textile composites. Plumb et al. (1992) performed studies in heat and mass transfer in drying of packed beds. Keey et al. (1994) model the temperature profiles within boards during high temperature drying processes. It is postulated for heartwood that an evaporative plane moves through the board.

Recent development of the Yucca Mountain Nuclear Waste Repository has been the source for great debate and some concern over the accuracy and safety of performed studies and calculations. Boehm et al. (1995a, 1995b) studies indicate that the humidity values in vacant spaces near porous formations may be underestimated in sub-residual

conditions when arbitrarily fixed capillary pressures are used in numerical codes. The outlet humidities are considerably higher than those predicted using most repository codes.

Gong and Mujumdar (1994) study the influence of an impermeable surface on pore steam pressure during drying of refractory concrete slabs. In this study, a finite element model for the drying process is described. Tests indicate that an impermeable surface can produce very high pore pressure in the drying process, and the potential for explosive spalling is greatly increased.

Sun and Woods (1997) simulate the heat and moisture transfer processes during deep grain bed drying. Here a deep barley bed is used as an example of grain drying. It is witnessed that when the bed temperature approaches the drying temperature, the moisture removed by the drying air may cause a temperature drop in the bed due to evaporative cooling. Walker et al. (1997) studies the effect of humidity on NPK fertilizer drying. It is shown that the correlation between product temperature and moisture content can't be explained by the diffusion drying theory, but indicates evidence for the humidity drying theory.

Chou and Chua (1997) investigate the receding evaporation front in convective food drying. Observations are made that show the front moves faster at the early stage of drying. A longer time is required for the drying front to move the same distance as drying progresses. There comes a time when the front is stationary and the specimen may be regarded as having reached a quasi-thermal equilibrium with the air. As airflow increases, so does the moisture removal rate.

When the surface area of drying increases and other physical dimensions remain constant, the volume up to each depth sustains a higher amount of moisture. Moisture up to each depth has to be completely dried before the front may start to recede from the surface. The receding speed is found to be highly dependent on the exposed drying surface of the product and the drying conditions of the air. It is shown that the square root of the drying time varies linearly with the transient position of the front. The receding front is shown to be related to the drying rate of the product as the front decelerates inward to the center of the material.

La Comber et al. (1997) study the effects of particle size on the drying of milled peat. Studies from various sources indicate that the drying rate of peat in powder form on the surface of a bog is highly dependent on its particle size distribution. A drying chamber was constructed and small (2-5.6 mm), medium (5.6-9.5 mm) and large (9.5 –16 mm) diameter particles are tested. Results show that large diameter particles dry 10-25 % percent faster than the smaller particles depending on the peat type.

Bastian (1997) creates a synthesis of scientific activity in the area of heat and moisture transfers in capillary-porous medium. The transfers are characterized by two independent variables- temperature and water content. Parameters are set for various scenarios of porous drying through heat transfer and mass transfer. Bertmieu et al. (1997) develop a simulation through use of a mathematical model to design an industrial drier for natural rubber in granule form.

As good as the numerical codes such as FEHM are, there is still need for further experimental study of the heat and mass transfer phenomena that occur in porous media. This experimental study is performed to witness the effects of drying of residually

saturated granular porous media by bulk flow of nitrogen gas on humidity and temperature through use of different porous material types. Of the data collected, the most emphasis is put on the humidity readings of the gas flow exiting the porous continuum.

Humidity readings of the exit flow from the media are plotted versus time. These tests are performed from the time of residual saturation and ended at the time that the porous media is completely dried (when the humidity value reaches the humidity value of the incoming nitrogen gas). Tests are run for the materials using four different flow rates of nitrogen gas- 0.25 L/min, 0.5 L/min, 0.75 L/min and 1 L/min.

The results are then compared and a correlation for bed mass transfer rates is made from experimental values for both steel spheres and ceramic beads of 4.5 mm diameters. Empirical correlations are made for both the steel and the ceramic beads through use of Sherwood numbers, Reynolds numbers, and Schmidt numbers which are acquired through non-dimensionalization of the experimental data collected.

CHAPTER 2

EXPERIMENTAL STUDY

2.1 Experimental Setup

The experimental setup is shown in the schematic depicted in Figure 1. It consists of a nitrogen bottle that is the source of the flow for the gas that is used in the drying process. The flow runs through a servo valve into a Controller/Meter (error of $\pm 1\%$) connected to a computer data acquisition device that monitors the flow rate. Flow then proceeds into a cylindrical container that contains a capacitance humidity sensor with a maximum error of 1% and a thermocouple connected to the data acquisition to monitor inlet relative humidity readings and temperature at various time intervals.

After passing through the initial humidity sensor, the gas flows into the test section containing the porous media. The test section consists of a 0.406 m (16") long aluminum cylinder, with an inside diameter of 0.0381 m (1.5") and two windows for visual observations. The inside of the container walls contain thirteen 30 gauge K-type thermocouples that have a maximum error of 0.75%. The thermocouples are at various locations along the length of the cylinder. Gas and water vapor then flow out a tube, where another humidity sensor records the outlet readings. Figure 2 shows a cross sectional view of the test bed.

A thermocouple outside of the system is present and measures the ambient temperature. The data acquisition software LabView collects all the temperature and

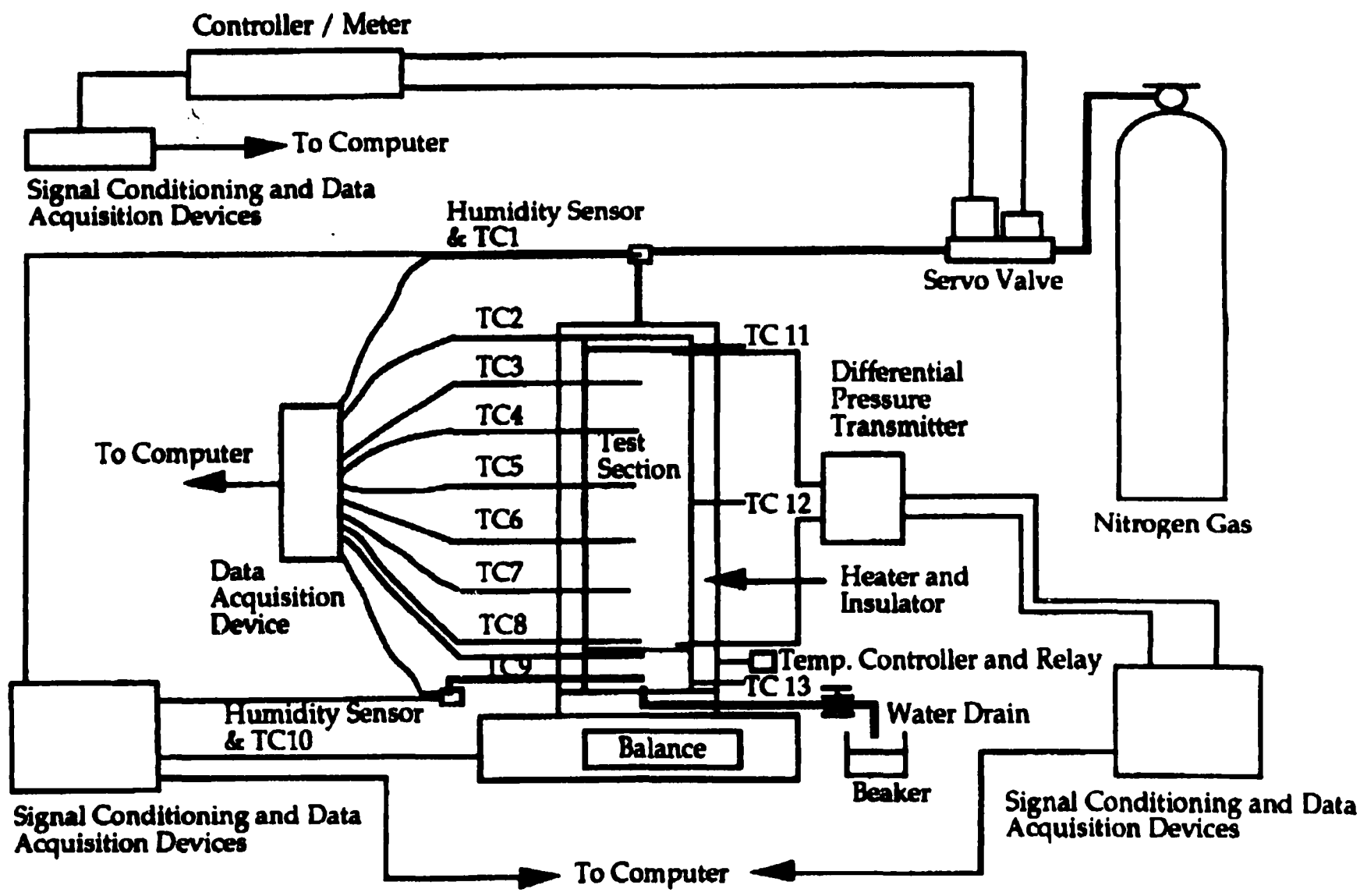


Figure 1. Experimental Setup Schematic Diagram

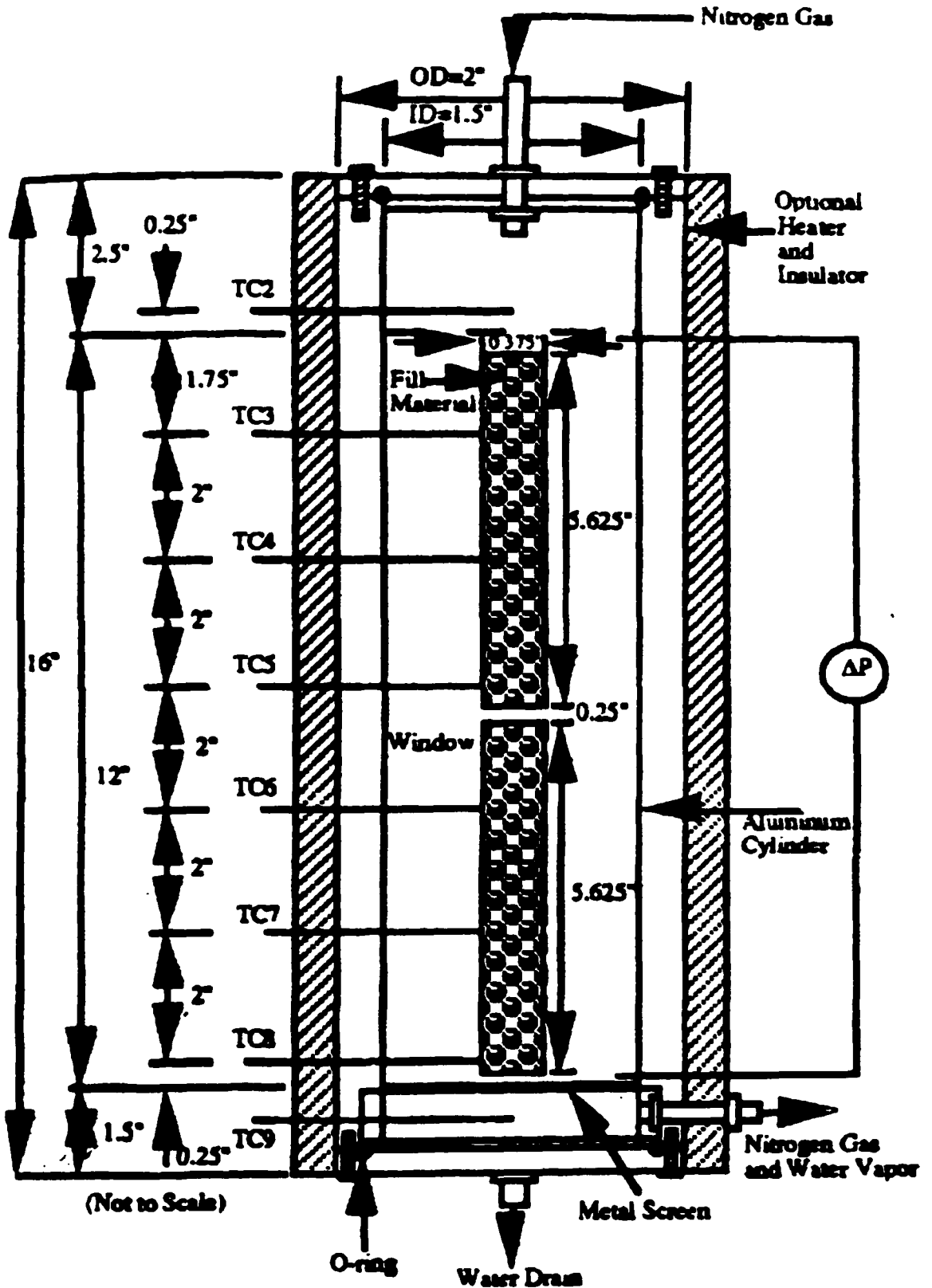


Figure 2. Experimental Test Section Cross-Sectional View Diagram

voltage readings (relative humidity) from the digital signal conditioning and data acquisition devices, and a digital scale is used to weigh the container dry and wet.

2.2 Experimental Procedure

The humidity sensors at the inlet and outlet of the test section are first calibrated using the ASTM E104-85 method. Since the sensors are so sensitive, the calibrations are performed before each run of the experiment. This is especially pertinent to the outlet sensor, because this sensor is exposed to the most change in ambient conditions; such as temperature and humidity changes. This calibration consists of using lithium chloride, sodium chloride, and potassium sulfate in saturated solutions at various temperatures.

Humidity sensors are placed just above the saturated solution, and readings are taken in the test tube for each material. The values for the corresponding relative humidity percentages for differing temperatures and substances may be viewed in Table 1 (ASTM Standard 1991).

The highest temperature available for calibration on the ASTM standard is 50°C, so a calibration at the boiling point is unavailable. This limitation doesn't pose a problem in this experiment because the flows and medium are at room temperature, about 77°F.

After the calibration, the test section is weighed at both dry and wetted conditions. This will give an idea of how much water vapor has been displaced at the end of the experiment (porous bed is completely dry). To achieve wetted conditions, the test section is saturated by filling the porous medium with distilled water and then drained. All tubes are now connected and the power to the voltage regulator, data acquisition, and computers is turned on. The LabView data acquisition software is started for both the temperature readings and the voltage data, and then the nitrogen gas is allowed to enter

Table 1- ASTM Standard: Relative Humidity Values for Saturated Aqueous Salt Solutions

EQUILIBRIUM RELATIVE HUMIDITY VALUES FOR SELECTED SATURATED AQUEOUS SALT SOLUTIONS

Temperature (°C)	Lithium Chloride ^a LiCl H ₂ O, %	Potassium Acetate ^a KC ₂ H ₃ O ₂	Magnesium Chloride ^a MgCl ₂ 6H ₂ O, %	Potassium Carbonate ^a K ₂ CO ₃ 2H ₂ O, %	Magnesium Nitrate ^a Mg(NO ₃) ₂ 6H ₂ O, %	Sodium Chloride ^a NaCl, %	Potassium Chloride ^a KCl, %	Barium Chloride ^a BaCl ₂ 2H ₂ O, %	Potassium Nitrate ^a KNO ₃ , %	Potassium Sulfate ^a K ₂ SO ₄ , %
0	11.2 ± 0.5	...	33.7 ± 0.3	43.1 ± 0.7	60.4 ± 0.6	75.5 ± 0.3	88.6 ± 0.5	...	96.3 ± 2.9	98.8 ± 2.1
5	11.3 ± 0.5	...	33.6 ± 0.3	43.1 ± 0.5	59.9 ± 0.4	75.7 ± 0.3	87.7 ± 0.5	93 ± 2	96.3 ± 2.1	98.5 ± 0.9
10	11.3 ± 0.4	23.4 ± 0.5	33.5 ± 0.2	43.1 ± 0.4	57.4 ± 0.3	76.7 ± 0.2	86.8 ± 0.4	93 ± 2	96.0 ± 1.4	98.2 ± 0.8
15	11.3 ± 0.4	23.4 ± 0.3	33.3 ± 0.2	43.2 ± 0.3	56.9 ± 0.3	75.8 ± 0.2	85.9 ± 0.3	92 ± 2	95.4 ± 1.0	97.9 ± 0.6
20	11.3 ± 0.3	23.1 ± 0.2	33.1 ± 0.2	43.2 ± 0.3	54.4 ± 0.2	75.5 ± 0.1	85.1 ± 0.3	91 ± 2	94.6 ± 0.7	97.6 ± 0.5
25	11.3 ± 0.3	22.5 ± 0.3	32.8 ± 0.2	43.2 ± 0.4	52.9 ± 0.2	76.3 ± 0.1	84.3 ± 0.3	90 ± 2	93.6 ± 0.6	97.3 ± 0.5
30	11.3 ± 0.2	21.6 ± 0.5	32.4 ± 0.1	43.2 ± 0.5	51.4 ± 0.2	75.1 ± 0.1	83.6 ± 0.3	89 ± 2	92.3 ± 0.6	97.0 ± 0.4
35	11.3 ± 0.2	...	32.1 ± 0.1	...	49.9 ± 0.3	74.9 ± 0.1	83.0 ± 0.3	88 ± 2	90.8 ± 0.6	96.7 ± 0.4
40	11.2 ± 0.2	...	31.6 ± 0.1	...	48.4 ± 0.4	74.7 ± 0.1	82.3 ± 0.3	87 ± 2	89.0 ± 1.2	96.4 ± 0.4
45	11.2 ± 0.2	...	31.1 ± 0.1	...	46.9 ± 0.5	74.5 ± 0.2	81.7 ± 0.3	...	87.0 ± 1.6	96.1 ± 0.4
50	11.1 ± 0.2	...	30.5 ± 0.1	...	45.4 ± 0.6	74.4 ± 0.2	81.2 ± 0.3	...	84.8 ± 2.5	95.8 ± 0.5

^a See "Humidity Fixed Points of Binary Saturated Aqueous Solutions," by L. Greenspan. Published in the Journal of Research by the National Institute of Standards and Technology, Vol 81A, 1977, pp. 89-94.

^b See the German standard, DIN 50006, Constant Climates Over Aqueous Solutions, (referenced in 2.2).

the system by opening the valve and regulator on the bottle. Flow of gas is continued until the porous medium is completely dried, or in other words, the relative humidity in the exiting flow is equal to the humidity of the inlet gas; approximately 5 to 9.5 percent.

Readings are taken every 20 minutes or every hour for the weight of the system depending on the flow rate. Smaller time intervals are used for high flow rates and larger intervals for the slower rates. This will indicate the amount of water evaporated over each time interval. The time for this condition to occur will vary according to the flow rate of the incoming gas. High flow rates such as 1 L/min may take around 2 hours and lower flow rates even longer.

Procedures listed above are done for two different materials. The first consists of steel spheres, the same used in BB guns, with a diameter of 4.5 mm. The BB's have a thermal conductivity (k) of approximately 58.7 W/m·K at about 20°C. The ceramic beads are also spherical and hollow of 4.5 mm diameter, and have a thermal conductivity of approximately 0.1 W/m·K.

CHAPTER 3

DATA REDUCTION

Since there are numerous data points gathered over the course of one experiment, it is necessary to reduce them in a way that is easy to analyze the trends that occur. The best way to compare the results from the different materials used is to plot the data on similar scale graphs. This is done for the relative humidity readings from humidity sensors.

Before the humidity results can be plotted, a correlation between the voltage data and that of relative humidity must be established. This correlation goes back to the calibration of the humidity sensors prior to running the experiment. The voltages that were obtained during the calibration process correspond to relative humidities of the different substances at varying temperatures. A graph is then produced by plotting voltage versus the humidity listed in the ASTM standard for various temperatures that were calibrated. A linear regression is then used to smooth out any irregularity that may occur with the data points. This plot will then serve as a chart to convert voltage readings to relative humidity. Calibrations for both inlet and outlet sensors are shown in the appendices.

Values for humidities of the various test cases may now be plotted versus time using the equation acquired for the line of the voltage versus humidity calibration. All tests are then compared to one another and conclusions are made through analysis of the

plots for the varying flow rates. These plots are discussed in the following discussion and results section.

An empirical correlation is then made from the humidity plots to determine a general equation. This is accomplished by solving for values of Reynolds number and Sherwood number through known data. An evaporation rate is acquired from data and then a mass transfer coefficient may be obtained. This is done by creating a calibration plot of the mass of water lost versus time. The area of particular interest is the section of constant mass loss rate; in other words, the “flat” areas in the beginning and end of tests are neglected.

The calibration plot for the evaporation rate is established using the area of the curve described above, and a linear regression is performed to acquire an equation that is representative of the mass transfer per unit time (evaporation rate). The slope of the line will represent the mass divided by time, thus giving the evaporation rate. From these values, the mass transfer coefficient is determined and then a Sherwood number (Sh) value is known, and is plotted versus the Reynolds number on a log-log scale.

This procedure will non-dimensionalize the experimental parameters, and then produce a non-dimensional correlation, from which coefficients may be determined. After acquiring a plot and the corresponding equation to the curve, and coefficients, a correlation for the Sherwood number is then made from the data for both steel and ceramic packed beds. The equation for the Sherwood (Sh) number will give design parameters for mass transfer through use of the Reynolds number (Re) and the Schmidt number (Sc). A typical form of the Sherwood equation would look like:

$$Sh = c Re^a Sc^b$$

where a , b and c are all values acquired through the equation given in the correlation of the data. Since all tests are performed at room temperature, the Schmidt number remains constant. The Sherwood number equation is then formulated in the following manner:

$$Sh = (cSc^b) Re^a$$

where cSc^b is a constant. This is done by comparing the equation of the curve of the log-log plot to that of a line with the equation:

$$\log y = m \log x + \log k$$

where $\log y$ would correspond to the Sherwood number, m the exponent a , of the Reynolds number (x) and k the Schmidt number to an exponent value multiplied by the constant c .

CHAPTER 4

DISCUSSION AND RESULTS

Many different phenomena are witnessed over the course of the experimental and correlation study. The nitrogen gas flowing from the inlet shows approximate values of 5 to 9.5 percent humidity at room temperature or about 24 °C. The Reynolds number for 1 L/min flow rate is 0.421, 0.75 L/min is 0.316, 0.5 L/min is 0.211 and 0.25 L/min is 0.105. The Reynolds number is calculated based on the diameter of the particle. The inlet and outlet humidity calibrations may be seen in Appendix II and III. As an example, a voltage of 2.142 V could be approximately 5 percent and 2.1395 V about 9.5 percent humidity depending on the individual calibrations. These values vary slightly from test to test, but in general it is known from various calibrations performed and Boehm et al. (1995a, 1995b) experiments, that humidity values of commercial grade bottled nitrogen gas at room temperature are in this range. All tests are run until values of about 5 to 9.5 percent are reached. When this value is reached, it is the humidity of the nitrogen gas that is being read by the humidity sensor, the lowest possible exit humidity attainable while gas flow exists. Evaporation rate plots are shown for both steel and ceramic in Figures 13 and 14.

4.1 Steel Sphere Tests

For the first test, steel at 0.25 L/min, .0197 kg of water was weighed initially. The test ended after 32,425 seconds (9.01 hours). The second test, steel at 0.5 L/min, the weight of the test section dry is 3.509 kg and wet is 3.529 kg. Therefore approximately .02 kg of water is evaporated during the drying process of the test section. The drying time for this test was 11,530 seconds (3.2 hours). Test run number three, 0.75 L/min, has a dry weight of 3.509 kg and wet is 3.5297 kg, thus having .0207 kg of water. The drying time for this test is 9,555 seconds (2.65 hours). For the fourth test, steel at 1 L/min, the dry weight is 3.509 kg and the wet is 3.5305, and about .0215 kg of water is evaporated. Drying occurred in 8,950 seconds (2.49 hours).

Figure 3 shows the outlet humidity versus time for the 0.25 L/min test. There are approximately one thousand seconds of constant humidity and then a fairly exponential decline occurs to ten thousand seconds. From this point to fifteen thousand seconds, there is a gradual increase in humidity and then constant decline to the end of the test. The inlet humidity is steady at approximately 6.5 percent throughout (Figure 3). The mass rate of the water lost through evaporation has a flat section in the first two hours and in the last two, with steady loss rate in the middle of the test (Figure 11).

In the second test, the steel at 0.5 L/min outlet humidity versus time may be viewed in Figure 4. The outlet humidity is 100% for about fifteen hundred seconds. After this the decline is fairly exponential over the entire test. Figure 4, the inlet humidity of nitrogen starts at 8 percent and indicates a decrease in humidity and then shows values of 6 percent throughout. The mass of water lost shows low rates of transfer up to the first forty minutes, and the last forty minutes of the experiment.

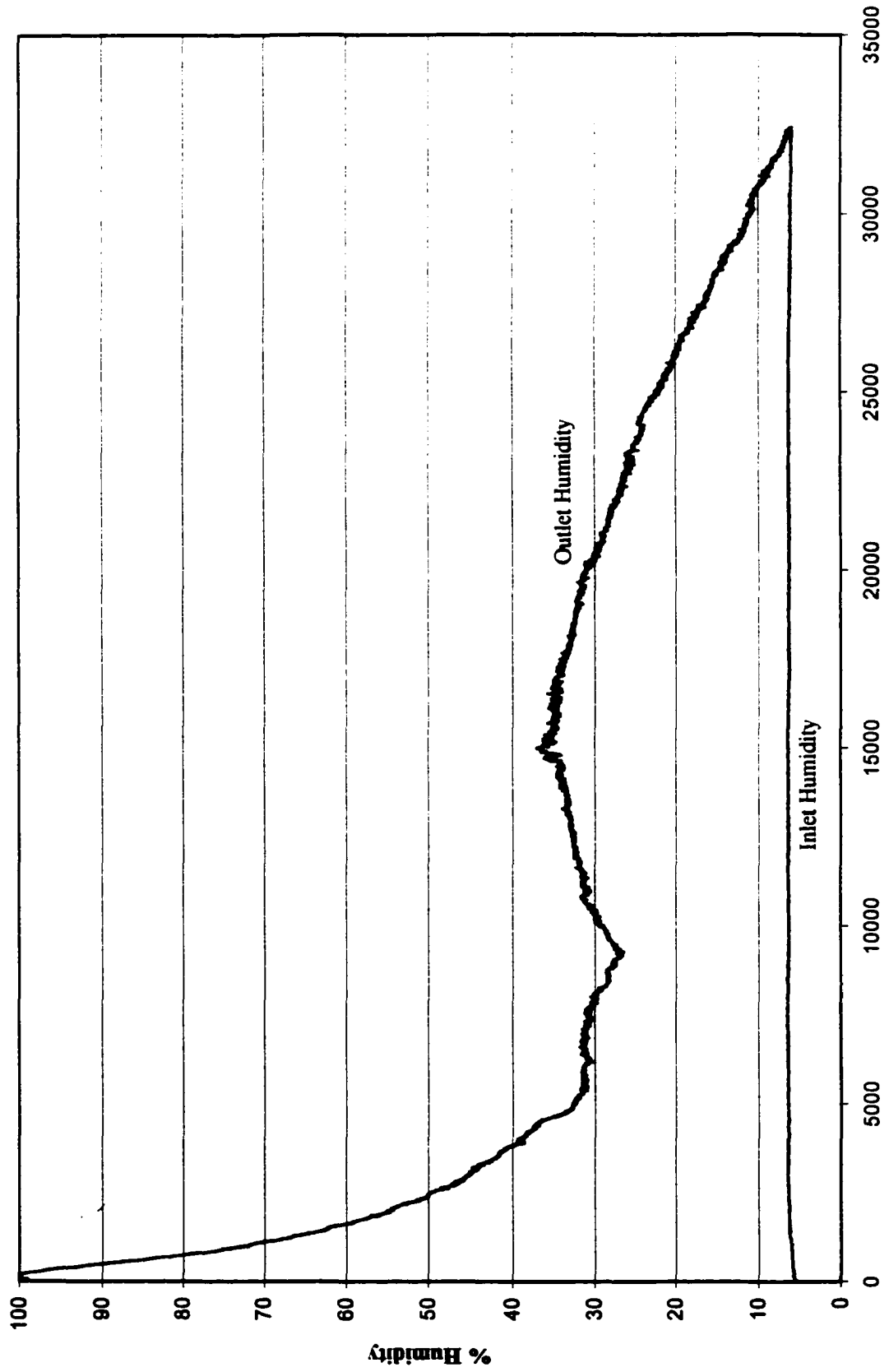


Figure 3. Inlet and Outlet Humidity vs. Time- Steel .25 L/min

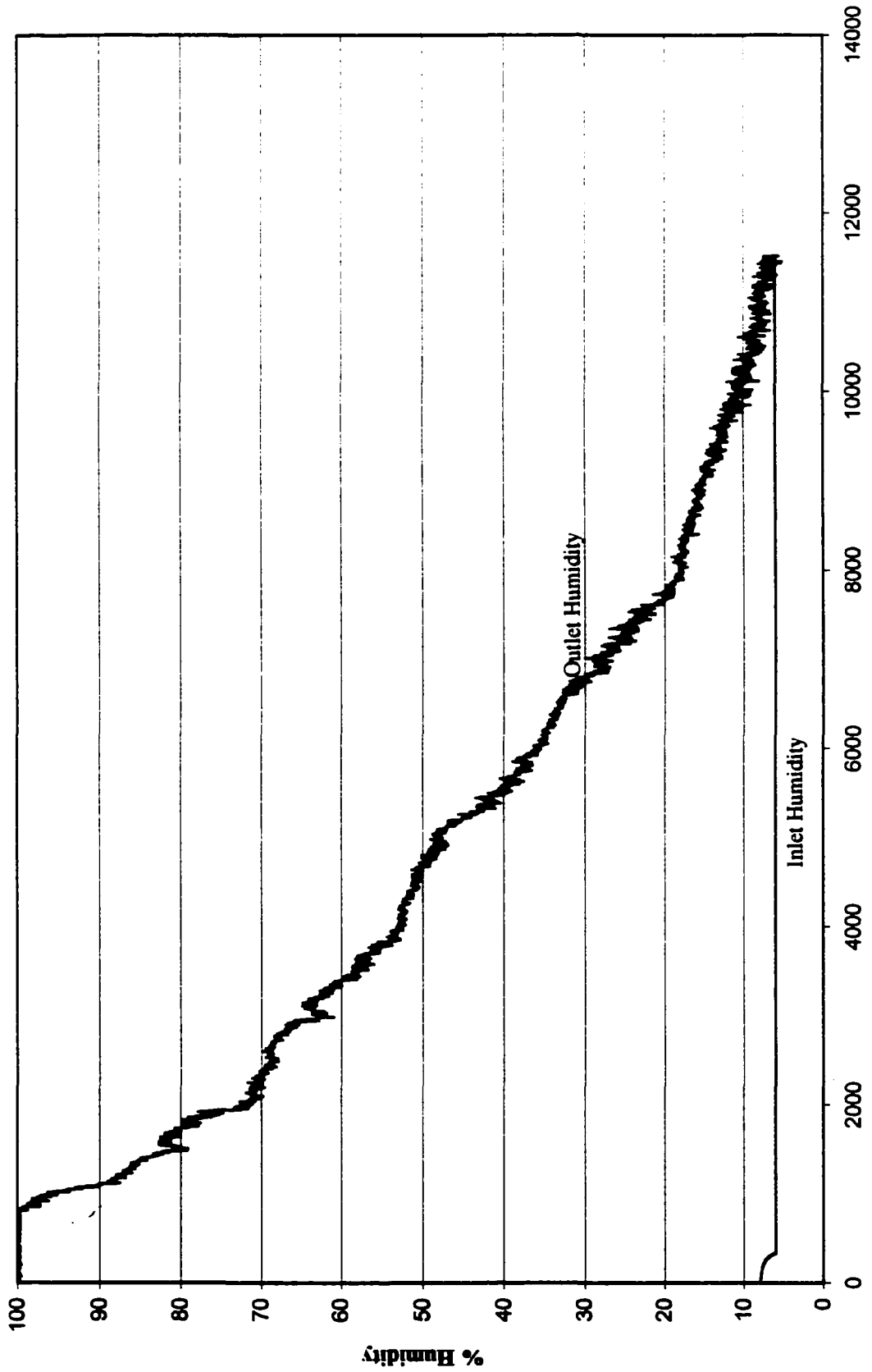


Figure 4. Inlet and Outlet Humidity vs. Time- Steel .5 L/min

Experiment three, 0.75 L/min, shows once again a decay resembling an exponential curve (Figure 5). The first fifteen hundred seconds show values of high humidity and then a constant decline through about eight thousand seconds. The last sections of the test show very slow decline. The inlet humidity was 6 percent through most of the test. Figure 11 shows the mass of water lost and has flat sections in the first twenty minutes and last thirty.

Test four, steel 1L/min, shows more of an exponential decay of humidity values over time (Figure 6). The inlet humidity of nitrogen is mostly constant, with the exception of about five spikes throughout the approximately 9000 seconds. The cause of these fluctuations is not known. One explanation could be the conditions the tank was filled at. A second is that as the test progresses, lower pressure of the contents results due to consumption. This may also have an effect on inlet humidity values. The mass transfer rate is low for the first twenty minutes and is flat in the region from one hundred to one hundred forty minutes.

4.2 Ceramic Bead Tests

Test number one has a dry weight of 2.631 kg and wet 2.669, having a weight of water .0386 kg. The drying time for this test is 33,725 seconds (9.37 hours). For the ceramic beads in test number two, the dry weight is 2.6308 and wet is 2.6694 kg. This test finished drying in 11,140 seconds (3.09 hours). The third test, 0.75 L/min, the weight of the water present is .039 kg. It is finished in 9980 seconds (2.77 hours). Test number four produces .0393 kg of water evaporated over the entire process. The drying time of test four is 9,325 seconds (2.59 hours) for the 1 L/min flowrate.

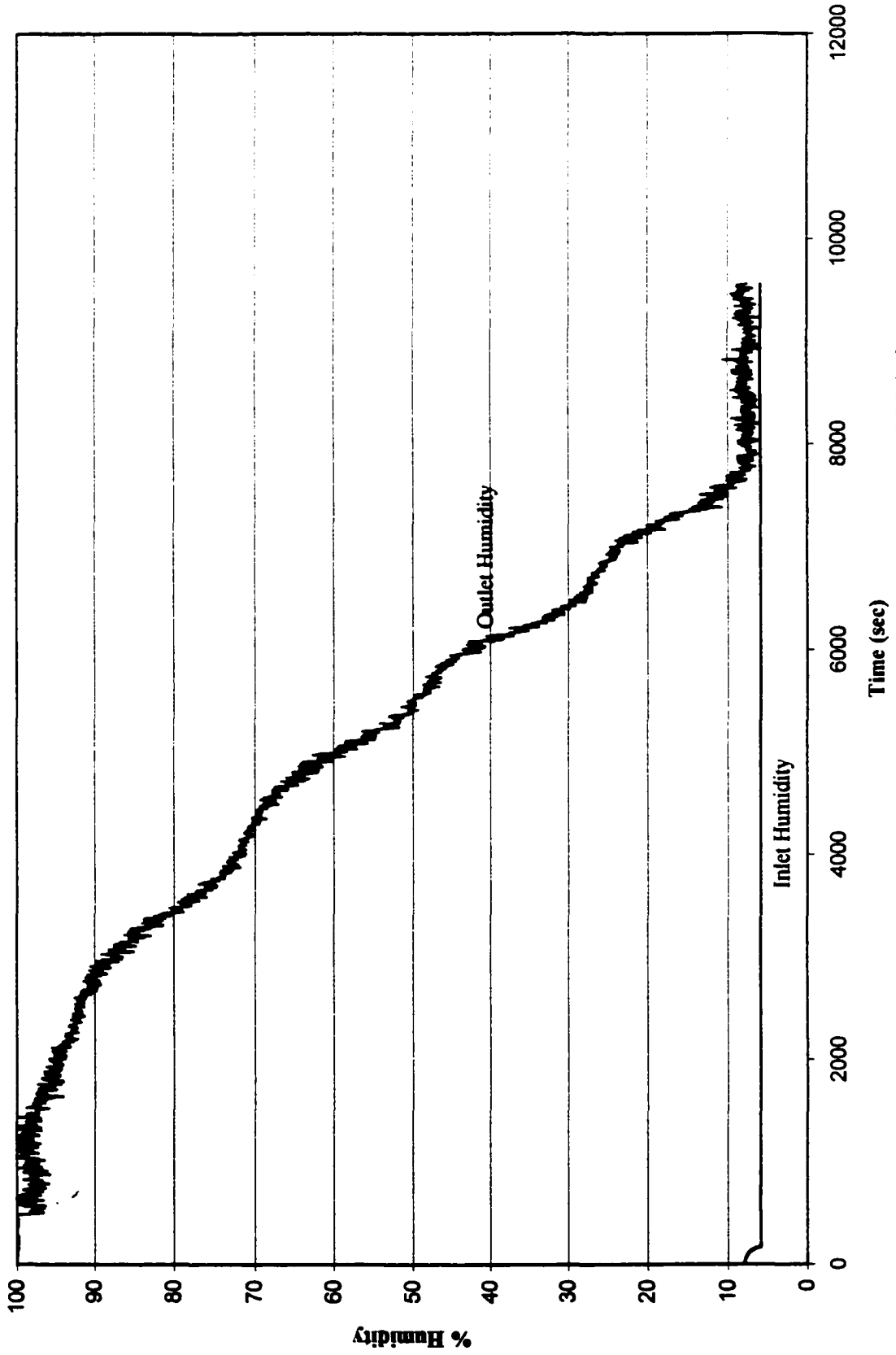


Figure 5. Inlet and Outlet Humidity vs. Time- Steel .75 L/min

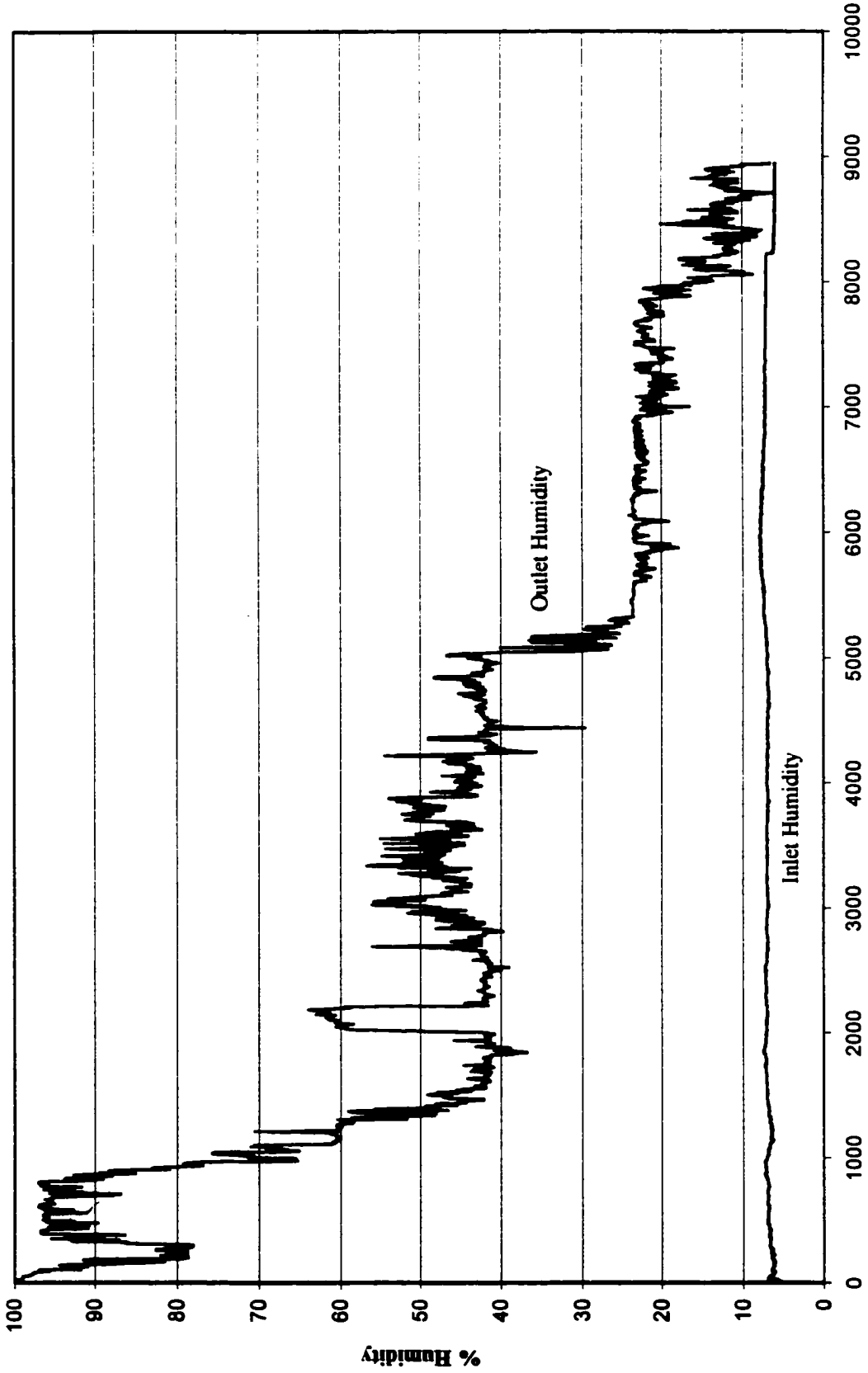


Figure 6. Inlet and Outlet Humidity vs. Time- Steel 1 L/min

Test one, 0.25 L/min, shows similar characteristics of previous curves. Flat sections are evident in the beginning and consistent decay follows (Figure 7). Inlet humidity readings are six percent through the majority of the test. The mass lost is slow for the first and last two hours (Figure 12).

Figure 8 shows the outlet humidity of the ceramic bead test at 0.5 L/min. A very smooth decay is witnessed over most of the test. A look at Figure 8, the inlet humidity of nitrogen, shows a higher humidity for about 500 seconds (8 to 9 percent) and then is constant through out (6 percent). In Figure 12, similar mass lost trends are present.

In test number three, the first one thousand seconds are at 100 percent humidity and then a decline starts (Figure 9). There is a spike around three thousand seconds, and then the rest of the test is similar to previous runs. The inlet humidity is very consistent at about six percent. The mass loss chart (Figure 12) shows flat sections in the first twenty minutes and in the last twenty minutes.

The fourth and final test is that of ceramic beads at a flow rate of 1 L/min (Figure 10). The outlet humidity curve also shows a somewhat exponential decay, with one major spike around 7000 seconds. The inlet humidity is a bit unstable according to Figure 10. However, the plot looks worse than it is in actuality, because humidity readings only vary by 2 or 3 percent. As stated before, it is not known why this inlet humidity varies as much as it does. The transfer of water also is similar to previous tests conducted (Figure 12).

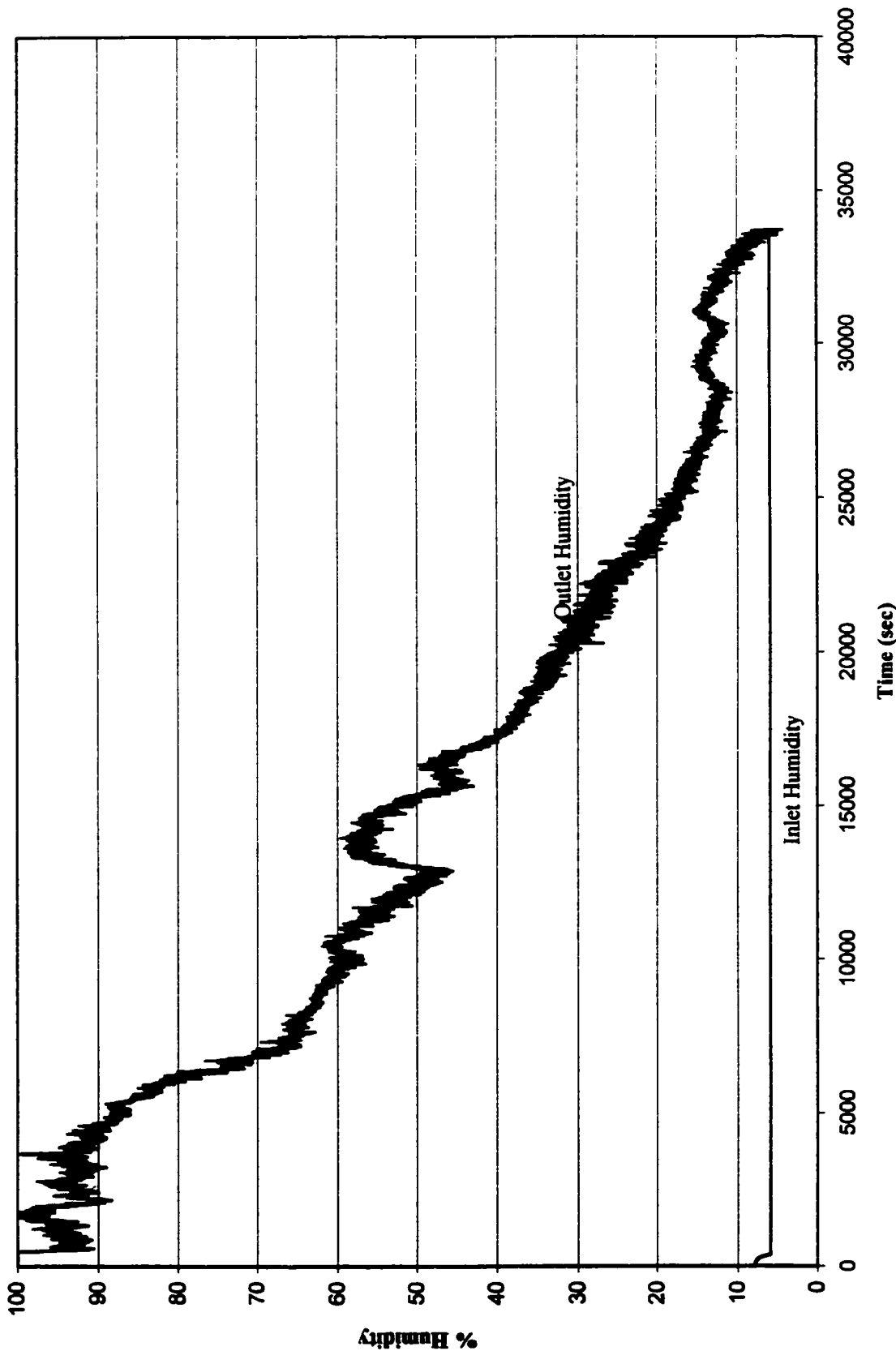


Figure 7. Inlet and Outlet Humidity vs. Time- Ceramic .25 L/min

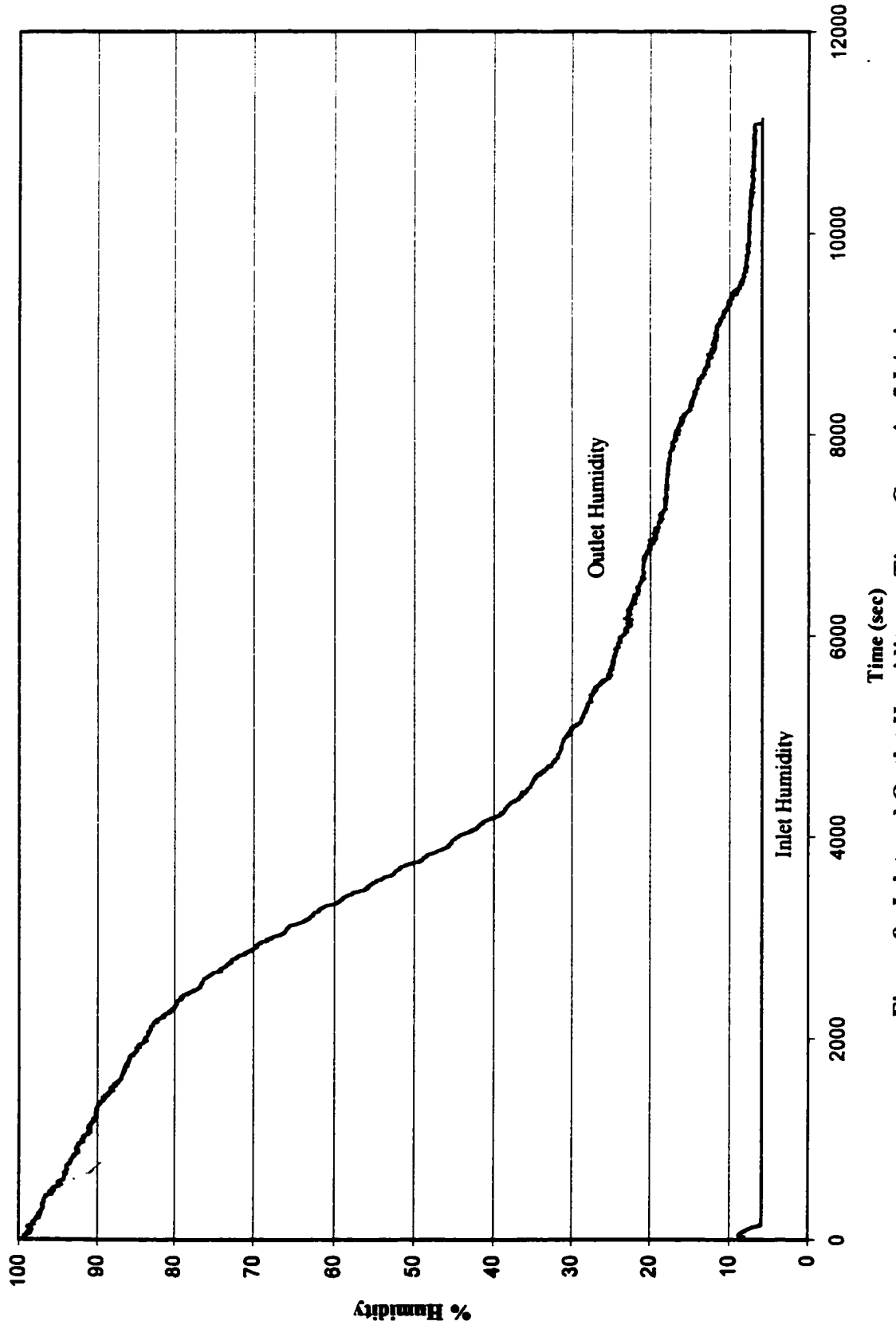


Figure 8. Inlet and Outlet Humidity vs. Time- Ceramic .5 L/min

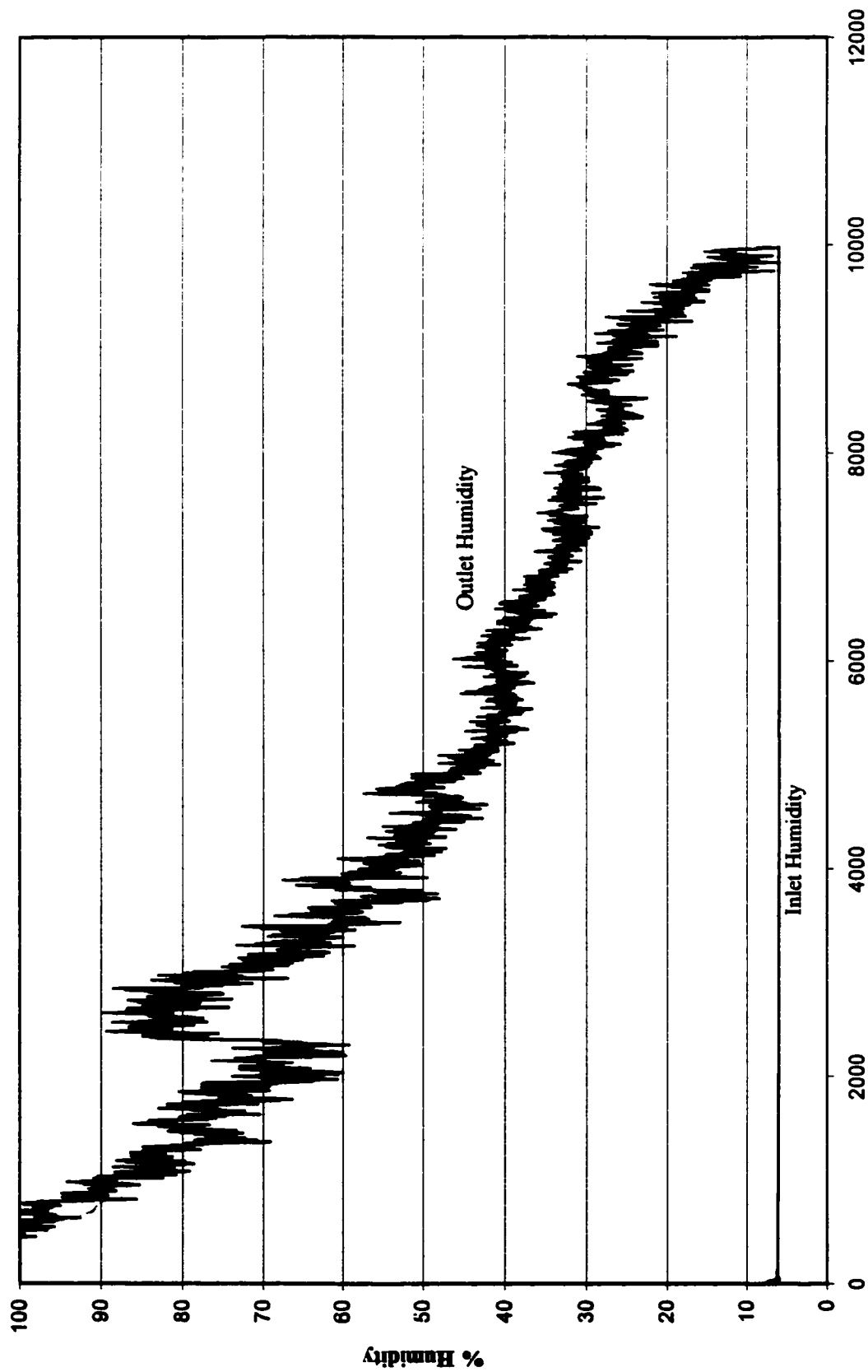


Figure 9. Inlet and Outlet Humidity vs. Time- Ceramic .75 L/min

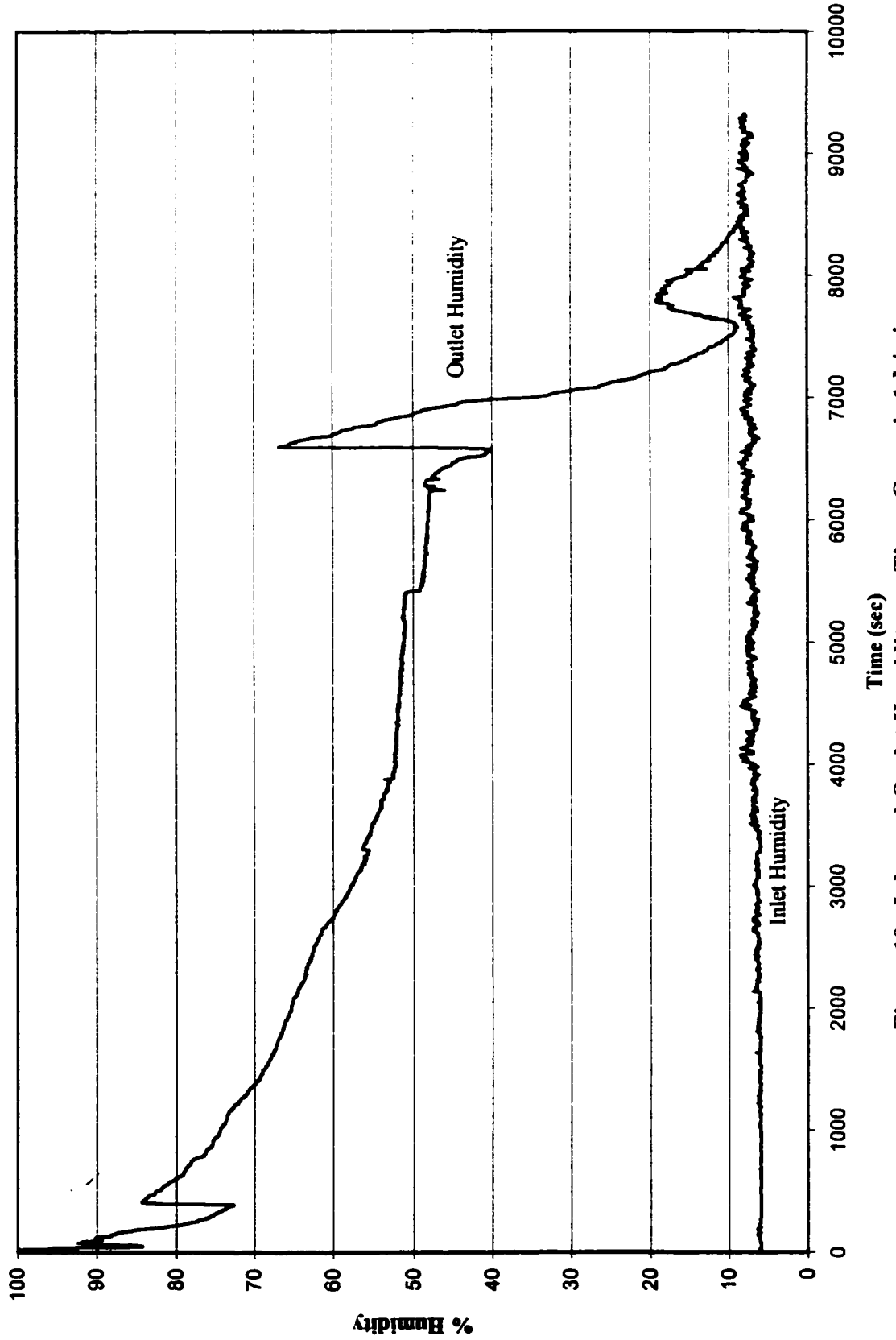


Figure 10. Inlet and Outlet Humidity vs. Time- Ceramic 1 L/min

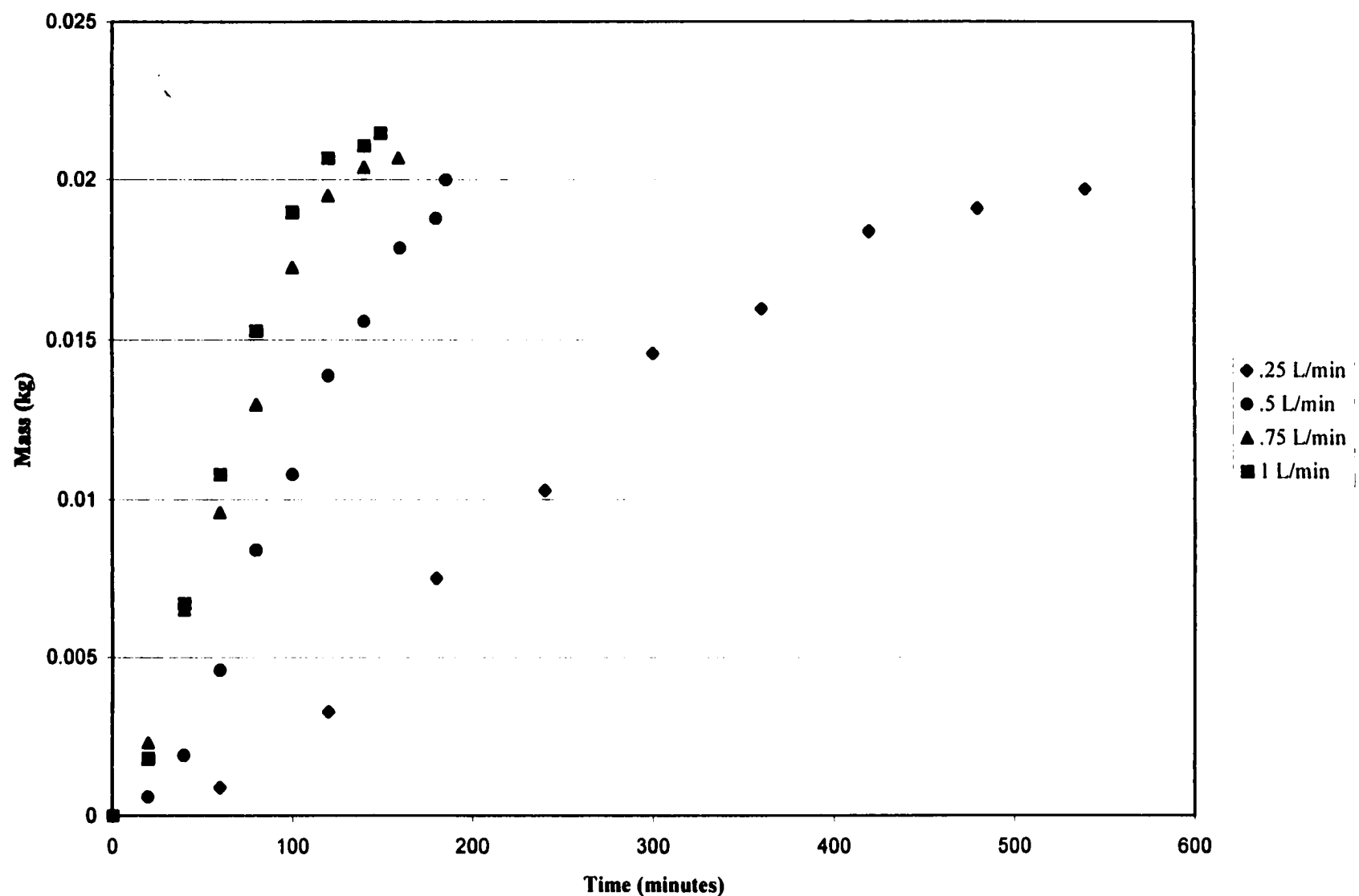


Figure 11. Mass of Water Lost vs. Time- Steel Test Flow Rates

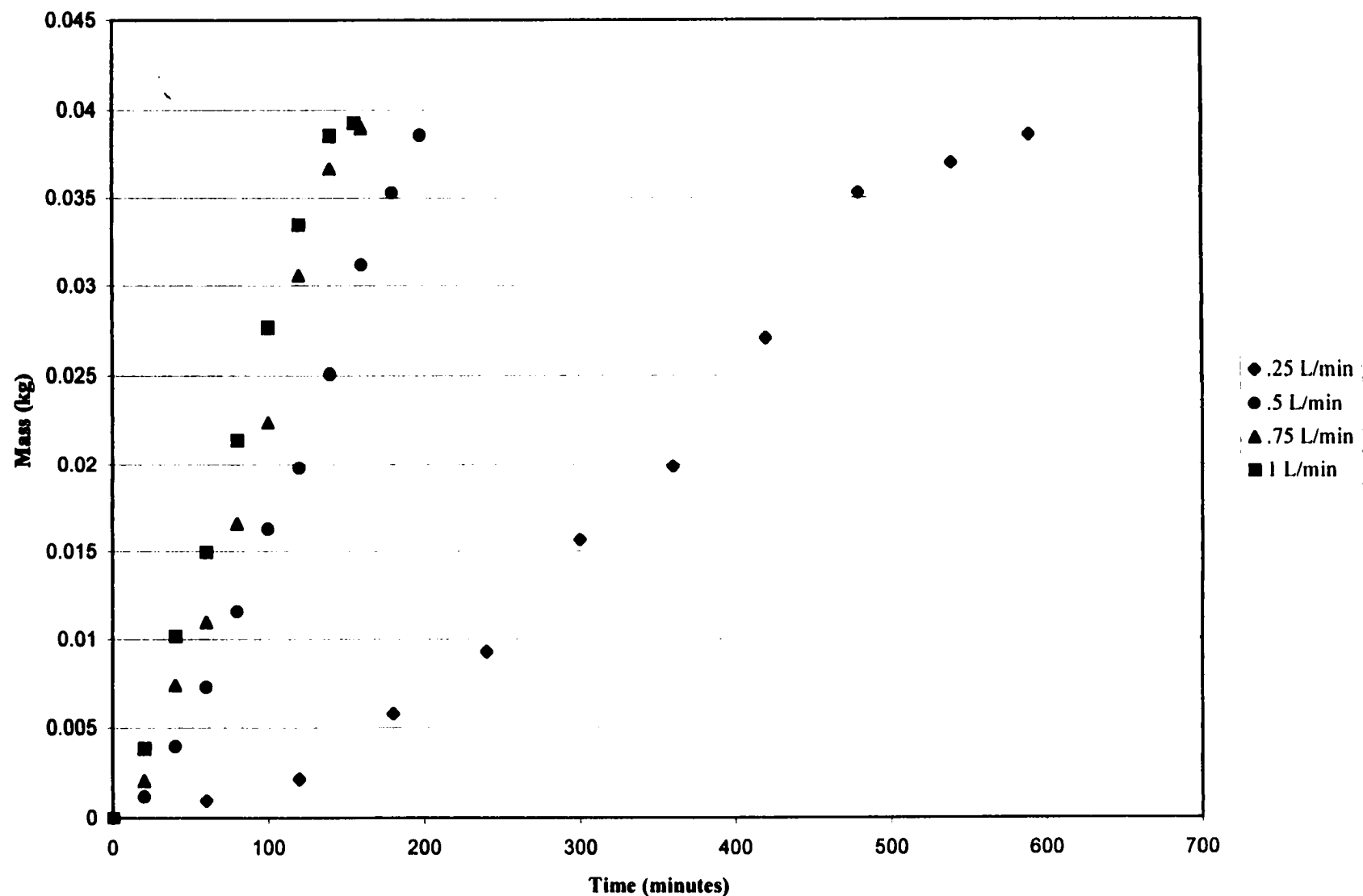


Figure 12. Mass of Water Lost vs. Time- Ceramic Test Flow Rates

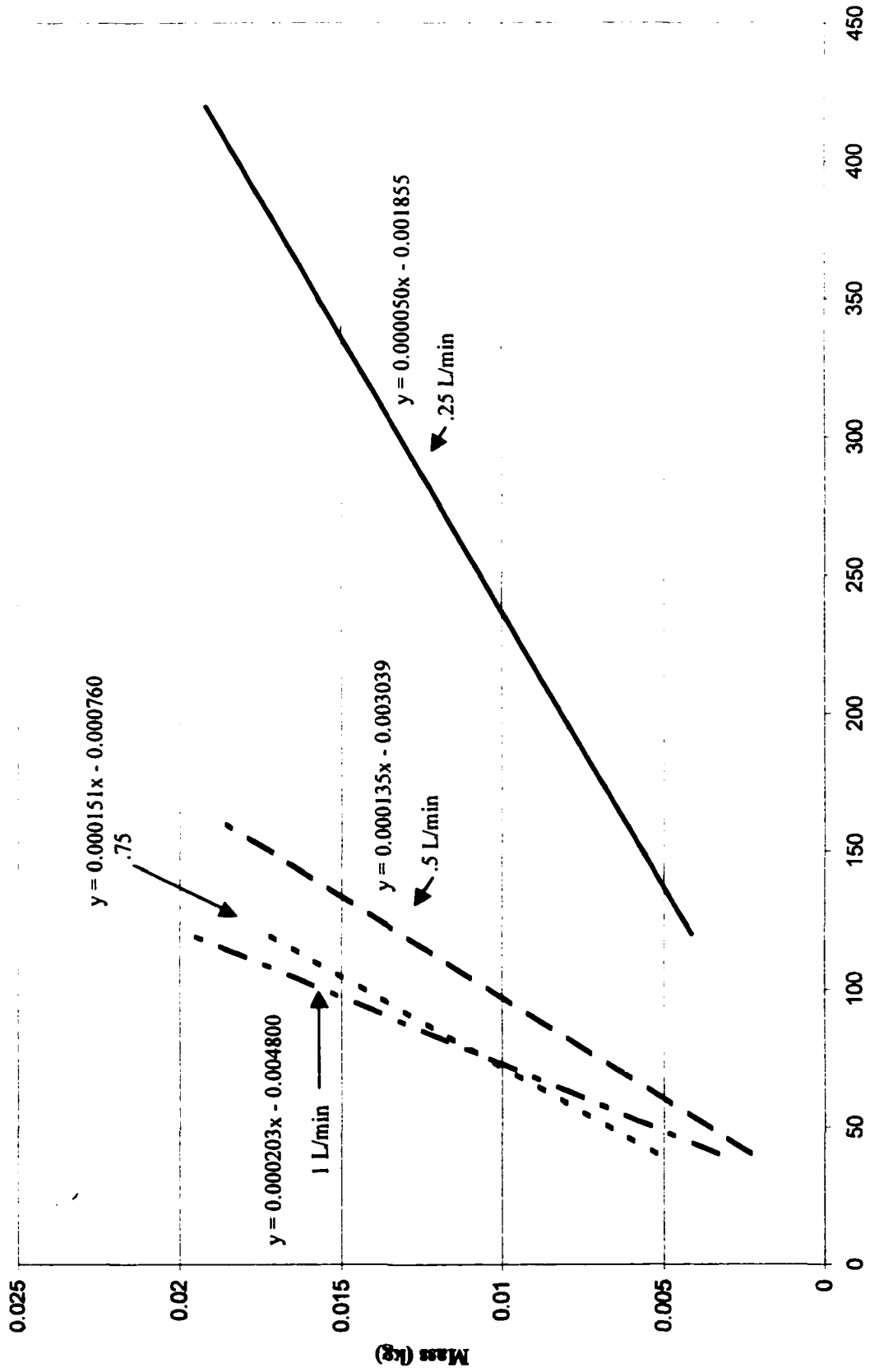


Figure 13. Evaporation Rate Regressions- Steel Flow Rates

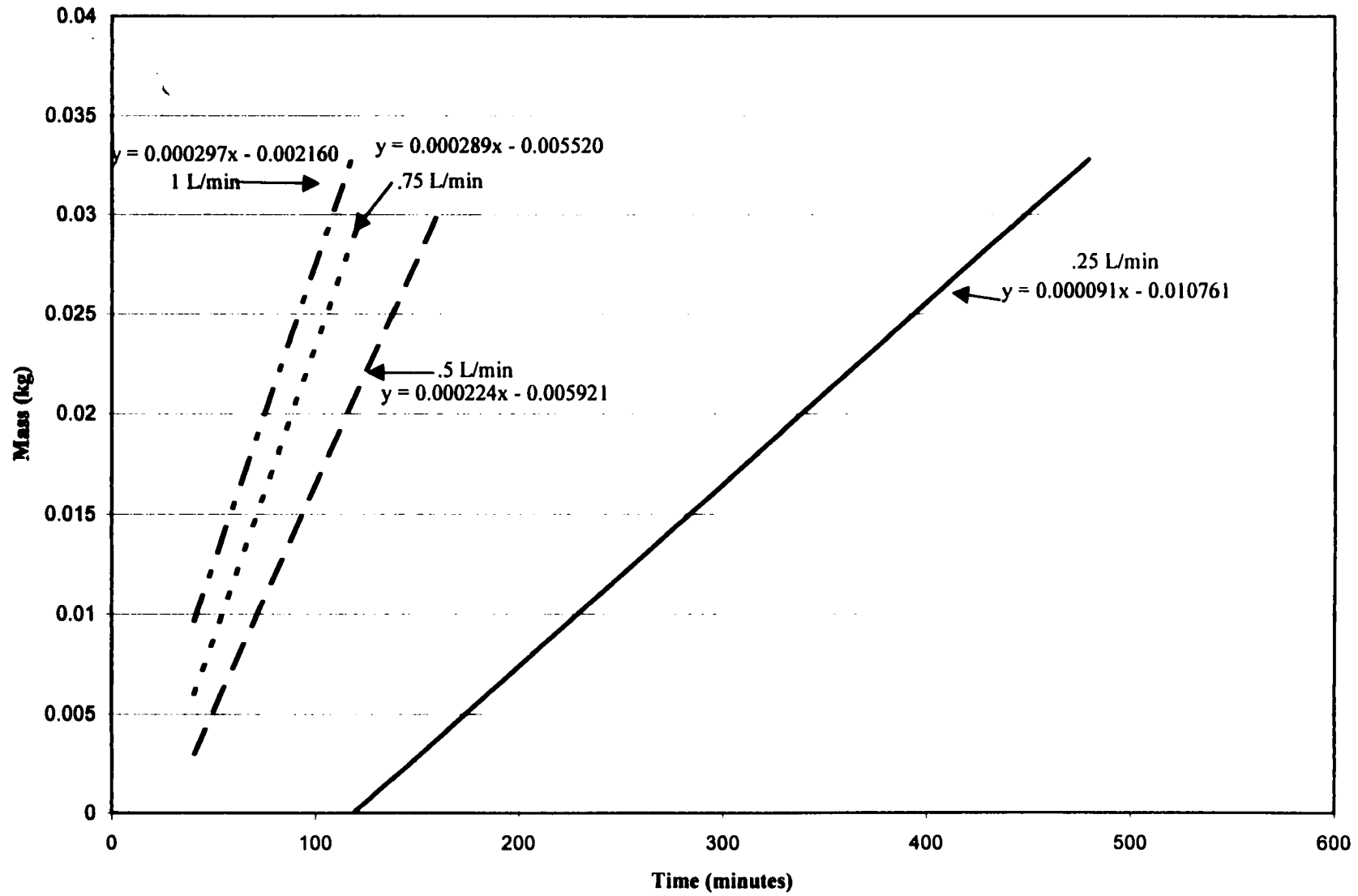


Figure 14. Evaporation Rate Regressions- Ceramic Flow Rates

4.3 Comparison of Steel and Ceramic Experiments

An analysis of all the humidity plots simultaneously for the most part shows similar plots throughout for both materials and all flow rates with few exceptions. Table 2 and Table 3 show the Reynolds number and Sherwood number values for each test.

All tests at the same flow rate, regardless of material, show extremely close drying times. In example, the 1 L/min steel and 1 L/min ceramic beads dried at nearly the same time and the same is true for the 0.5 L/min drying flow rates. Drying times for different flow rates for steel are listed Table 4 and values for ceramic in Table 5.

Some sources of problems encountered that are worth noting follow. The ceramic beads aren't perfectly round like the spheres. This could form a slightly less than perfect bed and also cause some deviation in results. There is also some variation in the inlet humidity, mostly in approximately the first 500 seconds. It is not clear as to why only a few of the tests show jumps in the inlet humidity. This is most evident in the ceramic 1 L/min test, but as noted before, the variations aren't as bad as they look. Even with the fluctuations, there shouldn't be a great impact on drying times because the jumps are only a few percent change in humidity.

Compared to Boehm et al. (1995a, 1995b) experiments with glass beads of 1 mm diameter, outlet humidity curves vary. Previous experiments for the glass beads at room temperature with a Reynolds number of 0.868 show a constant outlet humidity of nearly 100 % for a little more than half of the drying time, and then a sharp decrease followed by constant decrease until completion. All tests observed regardless of material (steel or ceramic) showed short periods of 100% values and then constant decay. This is most

Table 2-Steel- Reynolds Numbers and Sherwood Numbers

Flow Rate	Reynolds Number	Sherwood Number
0.25 L/min	0.267	114.076
0.5 L/min	0.533	305.39
0.75 L/min	0.8	341.629
1 L/min	1.066	465.61

Table 3- Ceramic: Reynolds Numbers and Sherwood Number

Flow Rate	Reynolds Number	Sherwood Number
0.25 L/min	0.267	205.358
0.5 L/min	0.533	506.676
0.75 L/min	0.8	653.806
1 L/min	1.066	684.974

Table 4- Steel: Total Mass of Water and Drying Times

Flow Rate	Total Mass of Water	Time
0.25 L/min	0.0197 kg	9.01 hours
0.5 L/min	0.02 kg	3.2 hours
0.75 L/min	0.0207 kg	2.65 hours
1 L/min	0.0215 kg	2.49 hours

Table 5- Ceramic: Total Mass of Water and Drying Times

Flow Rate	Total Mass of Water	Time
0.25 L/min	0.0386 kg	9.37 hours
0.5 L/min	0.0386 kg	3.09 hours
0.75 L/min	0.039 kg	2.77 hours
1 L/min	0.0393 kg	2.59 hours

likely due to the use of 4.5 times larger spheres. Material may also play a role, because different materials have different values of surface tension.

4.4 Non-Dimensional Curvefit

The Reynolds numbers and Sherwood numbers acquired through the calculations from the data are used to obtain a correlation for both steel and ceramic materials. The Sherwood number is plotted versus the Reynolds number on a log-log scale for the 0.25 L/min, 0.5 L/min, 0.75 L/min and 1 L/min for steel and ceramic. A linear regression of the points is then taken and an equation in the form $y = mx + k$ is achieved along with an R^2 value. These values may be seen in Figure 15 for steel and Figure 16 for ceramic tests. The steel test produced a R^2 value of .9445. The ceramic test had a slightly lower value of .9281. Both test values give fairly good fit values. Some possible reasons for less than perfect correlations may be the packing of the bed, irregularity of ceramic beads and variations in inlet humidity levels in a few tests. The ceramic also may have been able to hold more water, thus giving a state slightly beyond residually saturated.

After solving for the values of the coefficients, empirical equations are obtained for steel and ceramic spheres. For steel the following equation for the Sherwood number is obtained:

$$Sh = 2.6613 Re^{.9842}$$

The ceramic data yields a Sherwood number that looks like the following:

$$Sh = 2.8729 Re^{.8988}$$

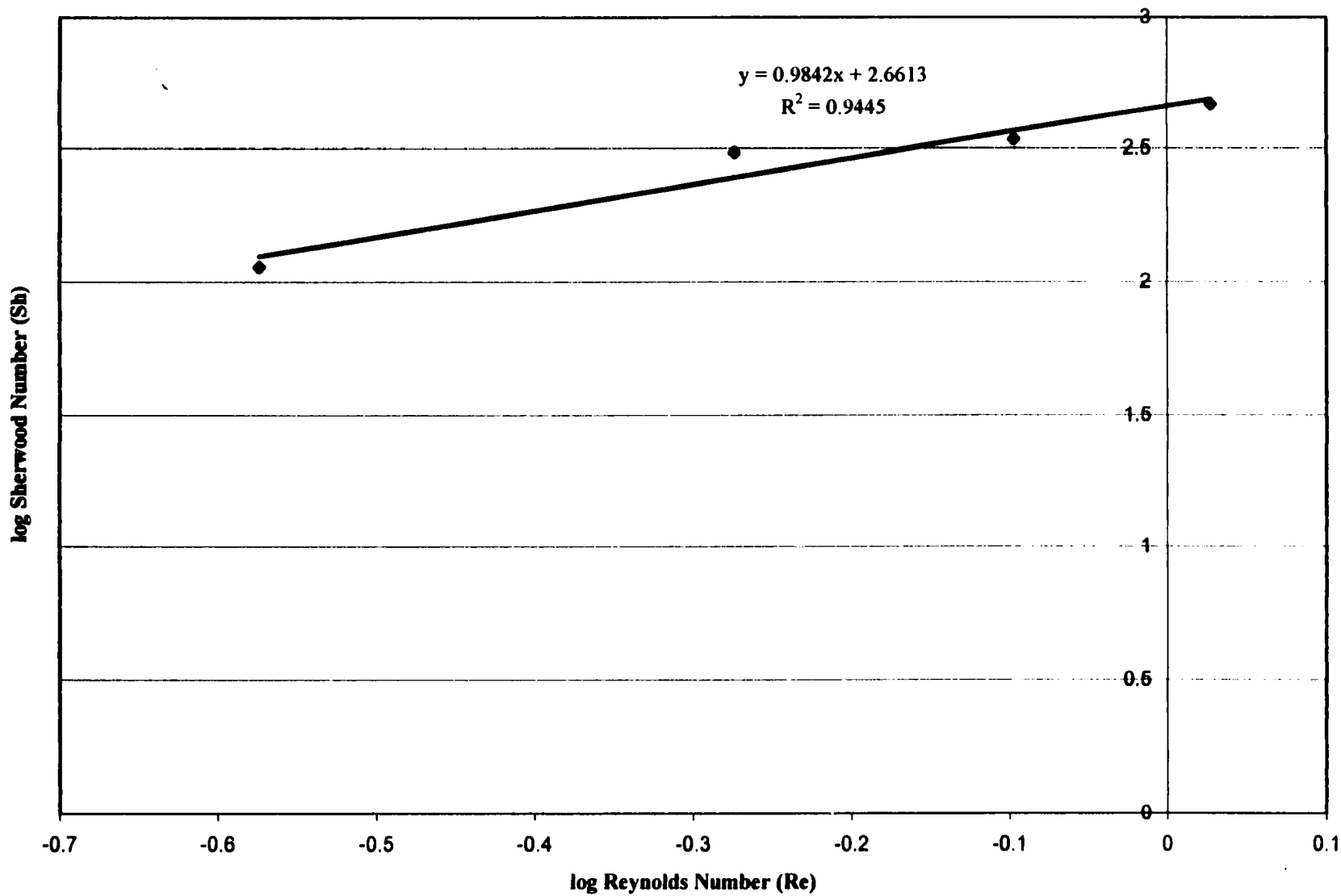


Figure 15. Dimensionless Representation of Mass Transfer Measurements for Steel

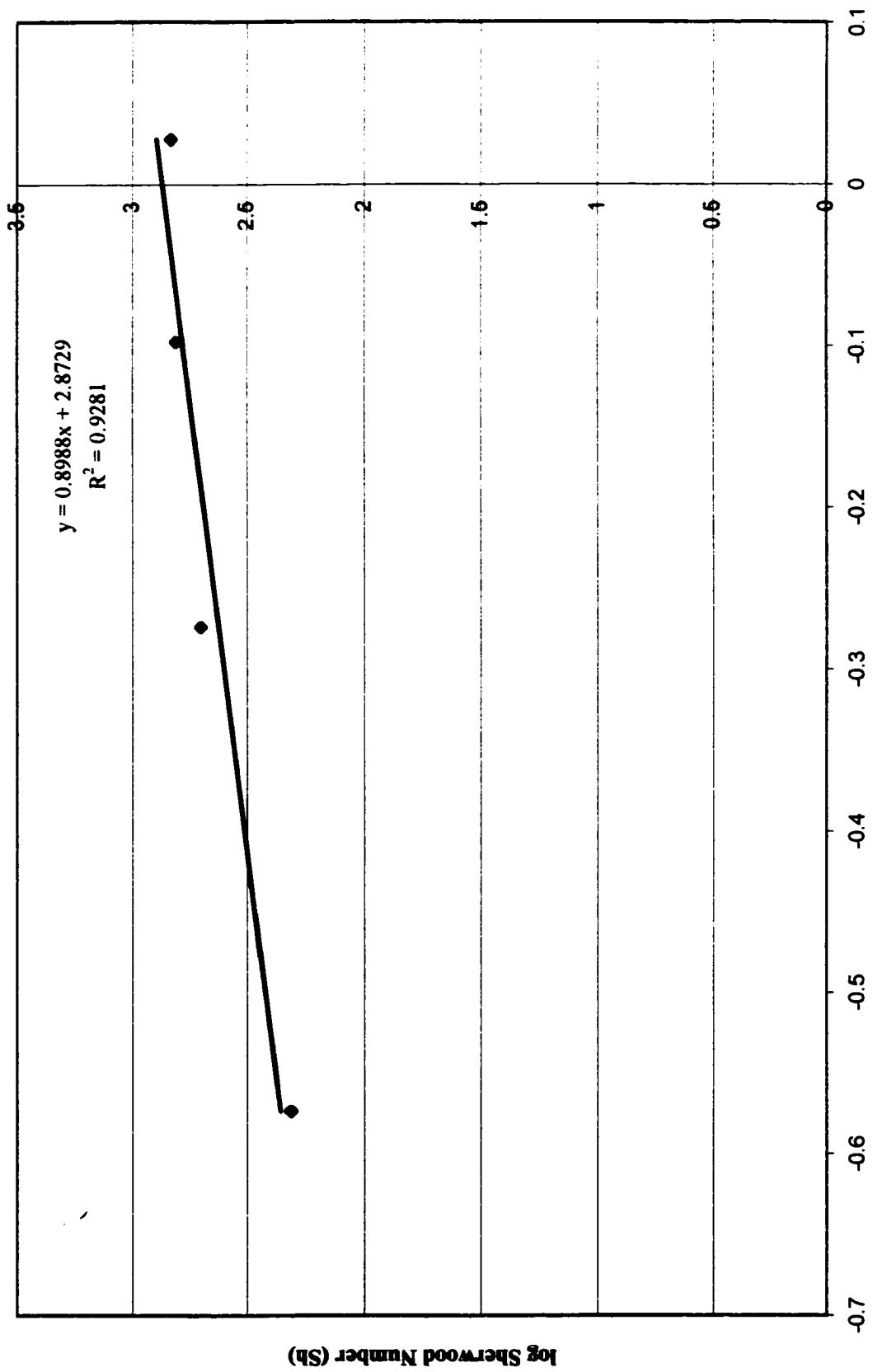


Figure 16. Dimensionless Representation of Mass Transfer Measurements for Ceramic

Both equations are valid in the ranges of $0.267 \leq Re \leq 1.066$. The above equations are derived through use of flow rates at room temperature conditions. Further study could improve on the accuracy and verify results found in this study.

CHAPTER 5

SUMMARY AND CONCLUSIONS

Evaporative drying experiments are conducted for both steel and ceramic porous media fills. The inlet and outlet humidities have been monitored and plotted versus time. Most of the curves are similar in nature for drying rates of each material and flow rate. The drying times were extremely close at similar flow rates regardless of the material. A comparison of the mass of water and the drying times for each material and flow rate may be seen in Table 5. Thermocouple readings showed temperature changes in the media due to evaporative cooling only varying by a couple of degrees in the experiments performed. Empirical correlations for Sherwood number have been acquired for steel and ceramic spheres in the range of $0.267 \leq Re \leq 1.066$. The correlation for steel with a constant Schmidt number at room temperature is:

$$Sh = 2.6613 Re^{.9842}$$

The equation for ceramic was found to be:

$$Sh = .2872 Re^{.8988}$$

APPENDIX I

DEVELOPMENT OF THEORY

Although the test is experimental in nature, most of the theory presented is for background knowledge. However, several of the equations listed are used in the analysis, and may be seen in the calculations in Appendix VI, VII, and VIII. The model has been developed in a one-dimensional, two phase, transient flow with evaporative processes through a residually saturated porous medium.

Fluid flow through a porous media presents difficulties in solutions to governing equations due to the complex and changing geometry between the particles in which the fluid flows. To simplify the geometry, approximating equations were obtained by averaging quantities over a control volume that is large in comparison with the particles and interstices of the porous medium.

By applying the conservation of mass to the control volume, the continuity equation results.

$$\frac{\partial \phi \rho}{\partial t} + \frac{\partial \rho u}{\partial x} + \frac{\partial \rho v}{\partial y} + \frac{\partial \rho w}{\partial z} = 0$$

For the one-dimensional model the continuity equation takes the following form:

$$\frac{\partial}{\partial t} [\phi S_l \rho_l + \phi S_g \rho_g + (1 - \phi) \rho_s] + \nabla \cdot (\rho_l u_l + \rho_g u_g) + \dot{m}_e = 0$$

where ϕ is the porosity, S_l is the liquid phase saturation, S_g is the gas phase saturation, ρ_l is the liquid phase density, ρ_g is the gas phase density, ρ_s is the saturation density, u_l is the liquid phase velocity, u_g is the gas phase velocity and \dot{m}_e is the mass flow rate.

According to Whitaker (1977) and Boehm et al. (1995a, 1995b), the above equation is used in conjunction with the following assumptions:

1. Viscous dissipation and work due to compression is negligible.
2. The medium through which flow occurs is homogeneous.
3. The streamwise component of mass diffusion is negligible compared to convection.
4. Thermophysical properties except nitrogen gas and water vapor are considered to be constant.
5. The solid matrix of the porous media is incompressible and no chemical reactions occur.
6. The system is free of bound moisture in the solid phase.
7. Water vapor and gas components can be treated as ideal gases.

For a one phase one-dimensional flow, the mass flow rate is defined as:

$$\dot{m}_e = \rho \frac{\pi D^2}{4} u_D$$

where D is the diameter of the particle and the filter velocity u_D may be obtained from:

$$\frac{dP}{dx} = \frac{\mu}{K} u_D$$

The above equation represents the change in pressure (P) with respect to x, μ the dynamic viscosity and K the permeability. The Reynolds number of the incoming gas is obtained through the following equation:

$$Re = \frac{\rho u D}{\mu}$$

After taking into consideration the more complex two-phase flow, the equations and analyses develop in the following. The gas velocity through the medium is:

$$u_g = -\frac{k_{rg}K}{\mu_g}(\nabla P_g - \rho_g g)$$

where k_{rg} is the relative permeability of the gas, μ_g is the dynamic viscosity of the gas, P_g and ρ_g are the pressure and density of the gas respectively, and g is the gravitational constant. The velocity of the liquid is represented by the same equation with the exception of properties values indicated by a subscript l where applicable. However, since the bed is assumed to be residually saturated, u_l is assumed to be nearly zero. Bejan (1992) after taking averages over an elemental volume of the porous medium, acquires for the solid phase:

$$(1-\phi)(\rho c)_s \frac{\partial T_s}{\partial t} = (1-\phi) \nabla \cdot (k_s \nabla T_s) + (1-\phi) q_s$$

and for the liquid phase:

$$\phi(\rho c_p)_l \frac{\partial T_l}{\partial t} + (\rho c_p)_l \vec{u} \cdot \nabla T_l = \phi \nabla \cdot (k_l \nabla T_l) + \phi q_l$$

where ϕ is the porosity, T is the temperature, t is the time and \vec{q} is the heat flux per unit volume. Setting $T_s = T_l = T$ and combining the previous two equations, the energy equation becomes:

$$(\rho c)_m \frac{\partial T}{\partial t} + (\rho c)_l \vec{u} \cdot \nabla T = \nabla \cdot (k_m \nabla T) + \dot{q}_m$$

Taking into consideration pressure changes, then the term $\beta T (\partial P / \partial t + \vec{u} \cdot \nabla P)$ is added to the left side of the above equation where:

$$\beta = -\frac{1}{\rho} \left(\frac{\partial \rho}{\partial T} \right)_P$$

β is the volumetric thermal expansion coefficient and is a function of the change in density with respect to temperature at a constant pressure.

Boehm et al. derive the volume-average thermal energy equation for both phases and acquire the total thermal energy equations as:

$$\begin{aligned} & \frac{\partial}{\partial t} [\phi S_l \rho_l h_l + \phi S_g \rho_g h_g + (1 - \phi) \rho_s h_s] + \nabla \cdot (\rho_l u_l h_l + \rho_g u_g h_g) \\ & - \nabla \cdot (k \nabla T) - \left[\frac{\partial P}{\partial t} + (u_l + u_g) \cdot \nabla P \right] + \dot{m}_e h_{vap} \end{aligned}$$

The volume constraint equations are:

$$\begin{aligned} \phi &= \varepsilon_l + \varepsilon_g \\ \varepsilon_l &= \phi S_l \\ \varepsilon_g &= \phi S_g \\ \varepsilon_s &= 1 - \phi \\ S_l + S_g &= 1 \end{aligned}$$

For multicomponent and multiphase flows the total mass is equal to the sum of all the individual masses combined ($m = \sum m_i$). Thus concentration is defined as:

$$C_i = \frac{m_i}{V}$$

and the aggregate density of the mixture is the sum of all the concentrations:

$$\rho = \sum C_i$$

As stated earlier, the water vapor and gas can be treated as ideal gases, therefore the gas law yields the equations:

$$PV = mR_m T$$

or

$$PV = nRT$$

where the gas constant of the mixture (R_m) and the universal gas constant (R) are:

$$R = \frac{R_m}{M}$$

The term n represents the number of moles in the mixture and m is the mass. The partial pressure P_i can be observed in the following two equations:

$$P_i V = m_i R_m T$$

or

$$P_i V = n_i R T$$

Summing these equations over i , Dalton's law results:

$$P = \sum P_i$$

Summing these equations over i , Dalton's law results:

$$P = \sum P_i$$

In this experiment, there are two i components, the nitrogen gas and the water vapor.

From Kaviany's (1991) empirical correlations, the following relationships are used for the relative permeabilities for the gas and the liquid:

$$k_{rl} = S^3$$

$$k_{rg} = 1.2984 - 1.9832S + .7432S^2$$

Capillary pressure is defined as:

$$P_c = P_g - P_l$$

Temperature relation can be derived from the combination of Kelvin's relation and the Clapeyron equation resulting in the equilibrium between liquid and gas phases:

$$T = \frac{T_0(1 + P_c / \rho h_{vap})}{1 - T_0(R_g / h_{vap}) \ln(P_g / P_0)}$$

where T_0 and P_0 are reference temperature and pressure respectively and P_{sg} is the saturated vapor pressure. Relative humidity values can be obtained from:

$$P_g = P_{sg}RH$$

where P_g is the partial pressure of the gas and RH is the relative humidity. For mass transfer, the Sherwood number is defined as:

$$Sh = \frac{h_m \cdot d_p}{D_{12}}$$

where h_m is the mass transfer coefficient, d_p is the diameter of the particle and D_{12} is the binary diffusivity. The total surface area per unit volume of a porous bed is:

$$A = \frac{6}{d_p}$$

The equation for the Schmidt number is:

$$Sc = \frac{\nu}{D_{12}}$$

where ν is the kinematic viscosity.

A mass transfer coefficient may be obtained through use of the equation:

$$n_a = \bar{h}_m A (\rho_{a,s} - \rho_{a,\infty})$$

where n_a is the evaporation rate, A is the total area of the porous bed, $\rho_{a,s}$ is the density of the water on the porous surface, and $\rho_{a,\infty}$ is the density of the bulk flow of gas. If the free stream water vapor is assumed to be an ideal gas

$$\phi_\infty = \frac{\rho_{a,\infty}}{\rho_{a,sat}(T_\infty)}$$

the relative humidity (ϕ_∞) of the bulk gas is represented in terms of the density of the gas ($\rho_{a,\infty}$) and the saturation density ($\rho_{a,sat}$) at the ambient temperature (T_∞). When $\rho_{a,s}$ is equal to $\rho_{a,sat}(T_s)$ (the density of the liquid at the surface temperature), the following equation results:

$$n_a = \bar{h}_m A [\rho_{a,sat}(T_s) - \phi_\infty \rho_{a,sat}(T_\infty)]$$

APPENDIX II

HUMIDITY SENSOR CALIBRATIONS- STEEL

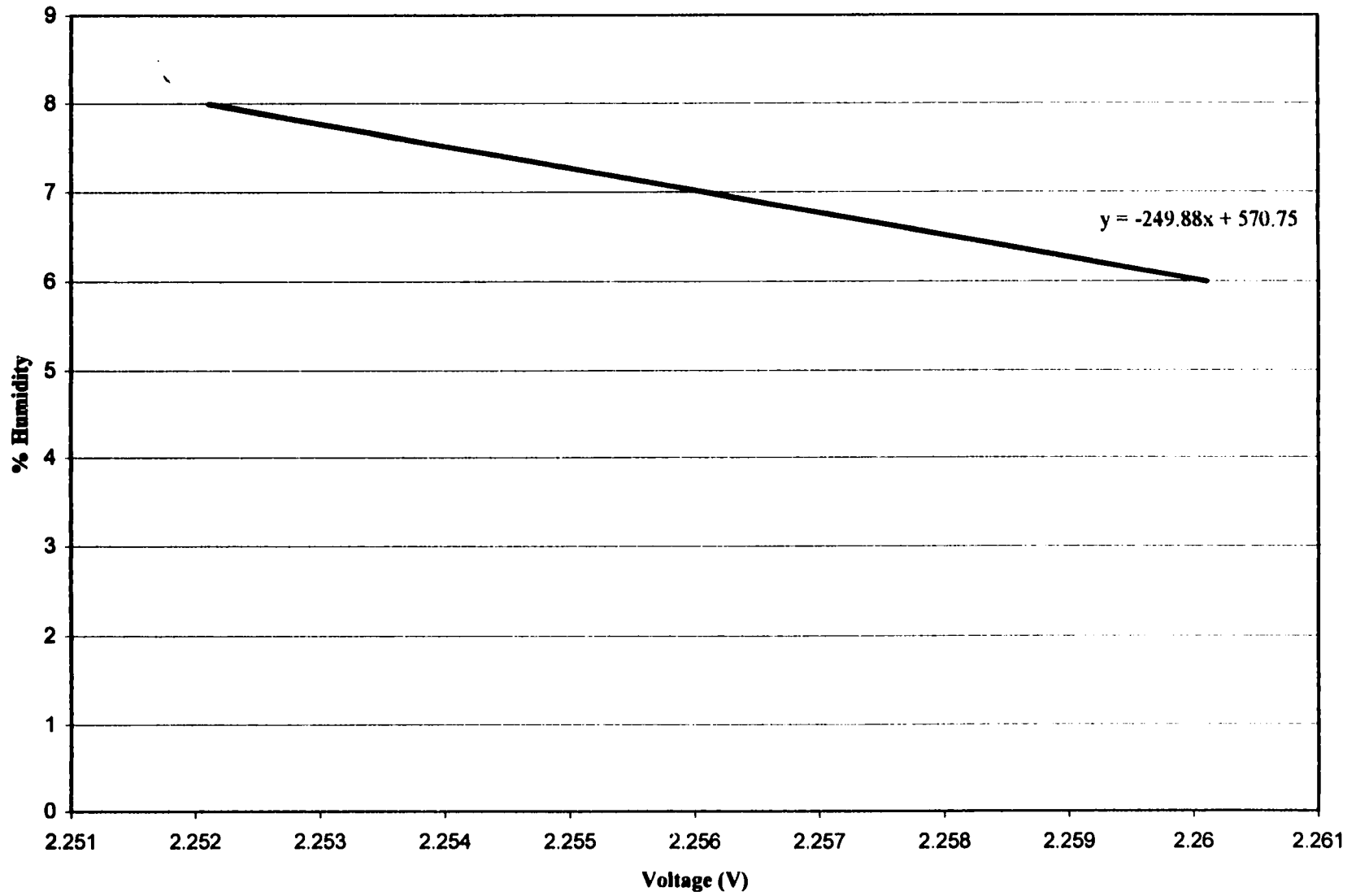


Figure 17. Inlet Humidity of Nitrogen Gas vs. Voltage Calibration- Steel Test # 1

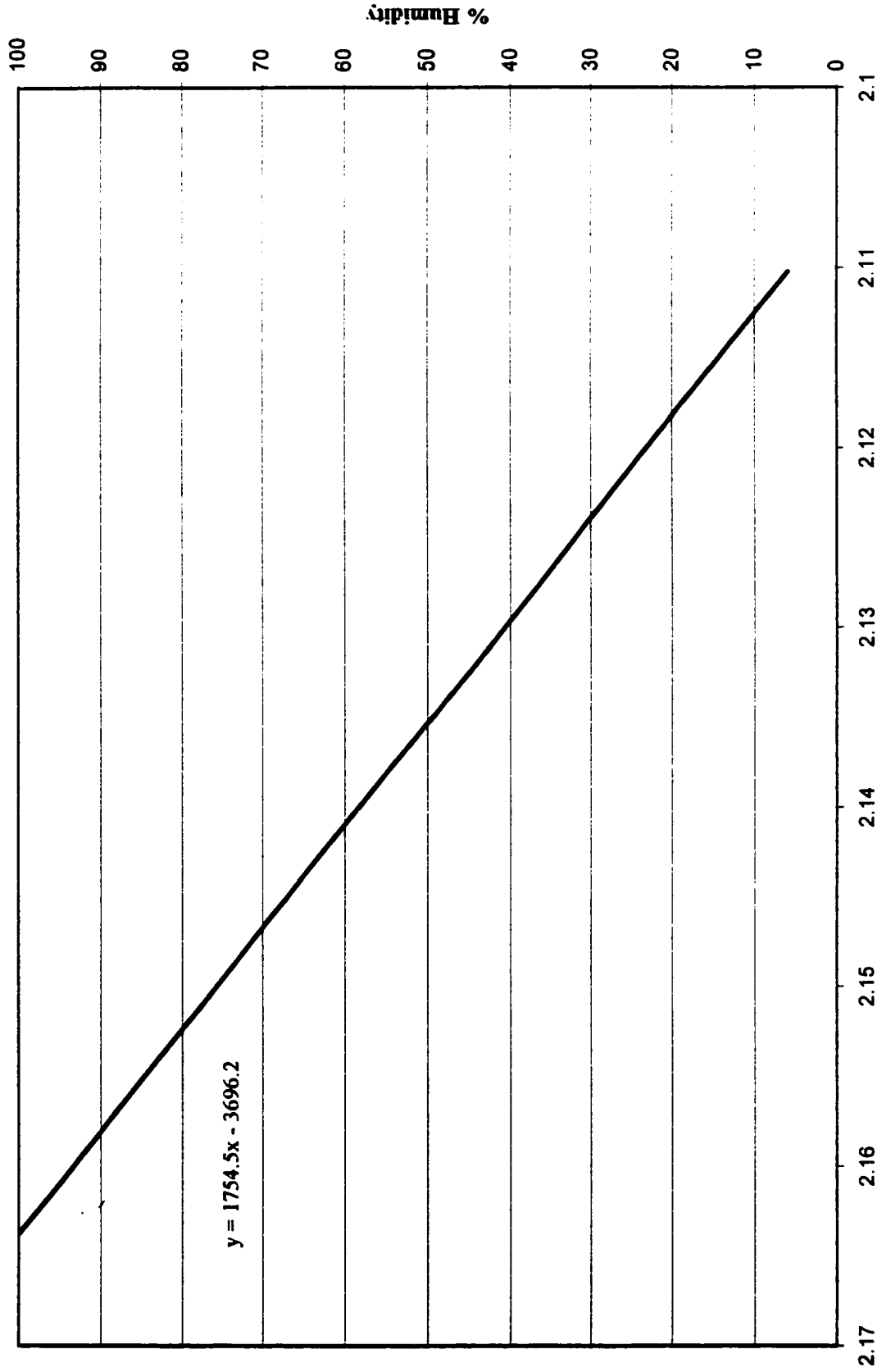


Figure 18. Outlet Humidity vs. Voltage Calibration- Steel Test # 1

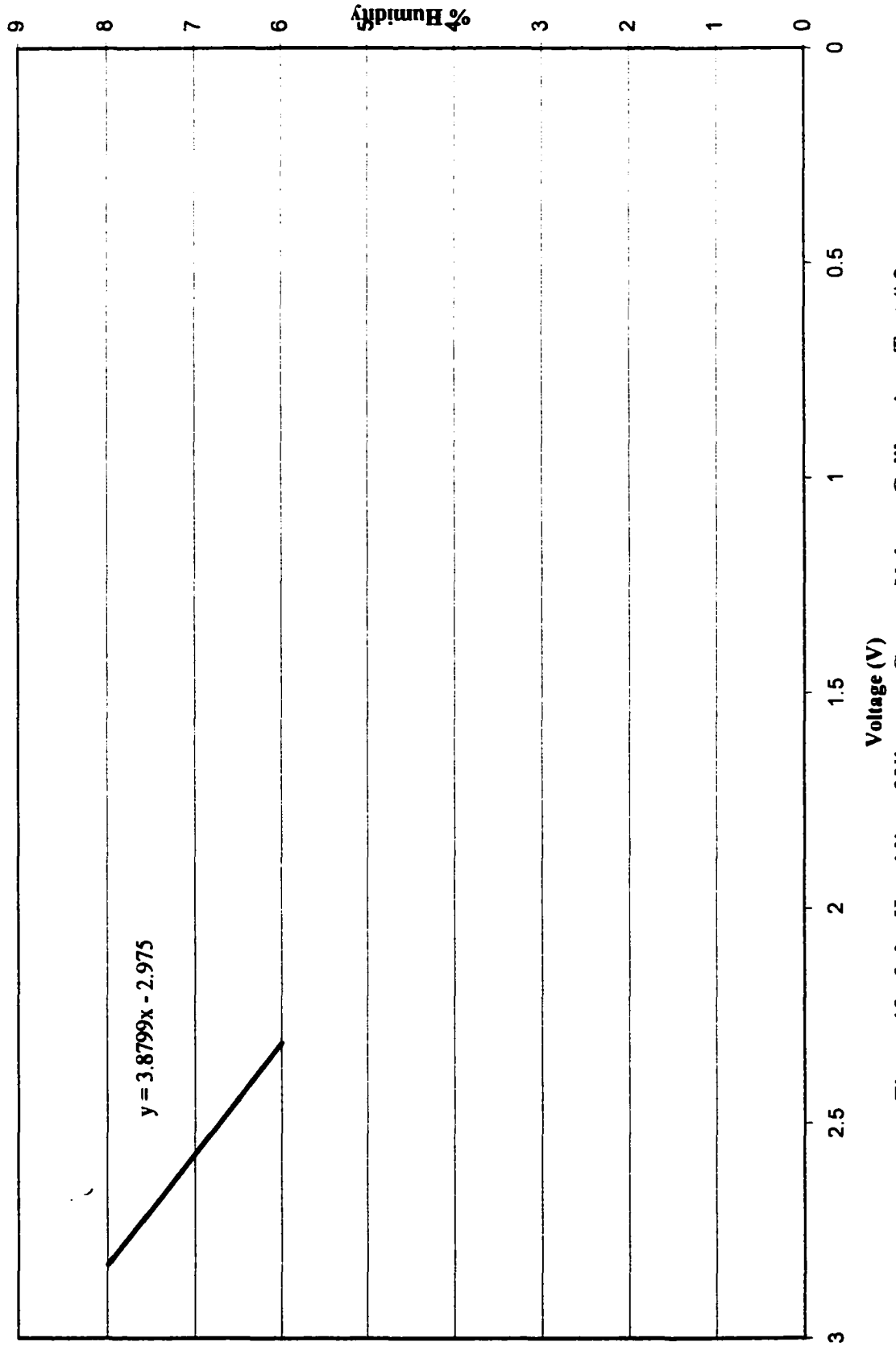


Figure 19. Inlet Humidity of Nitrogen Gas vs. Voltage Calibration- Test # 2

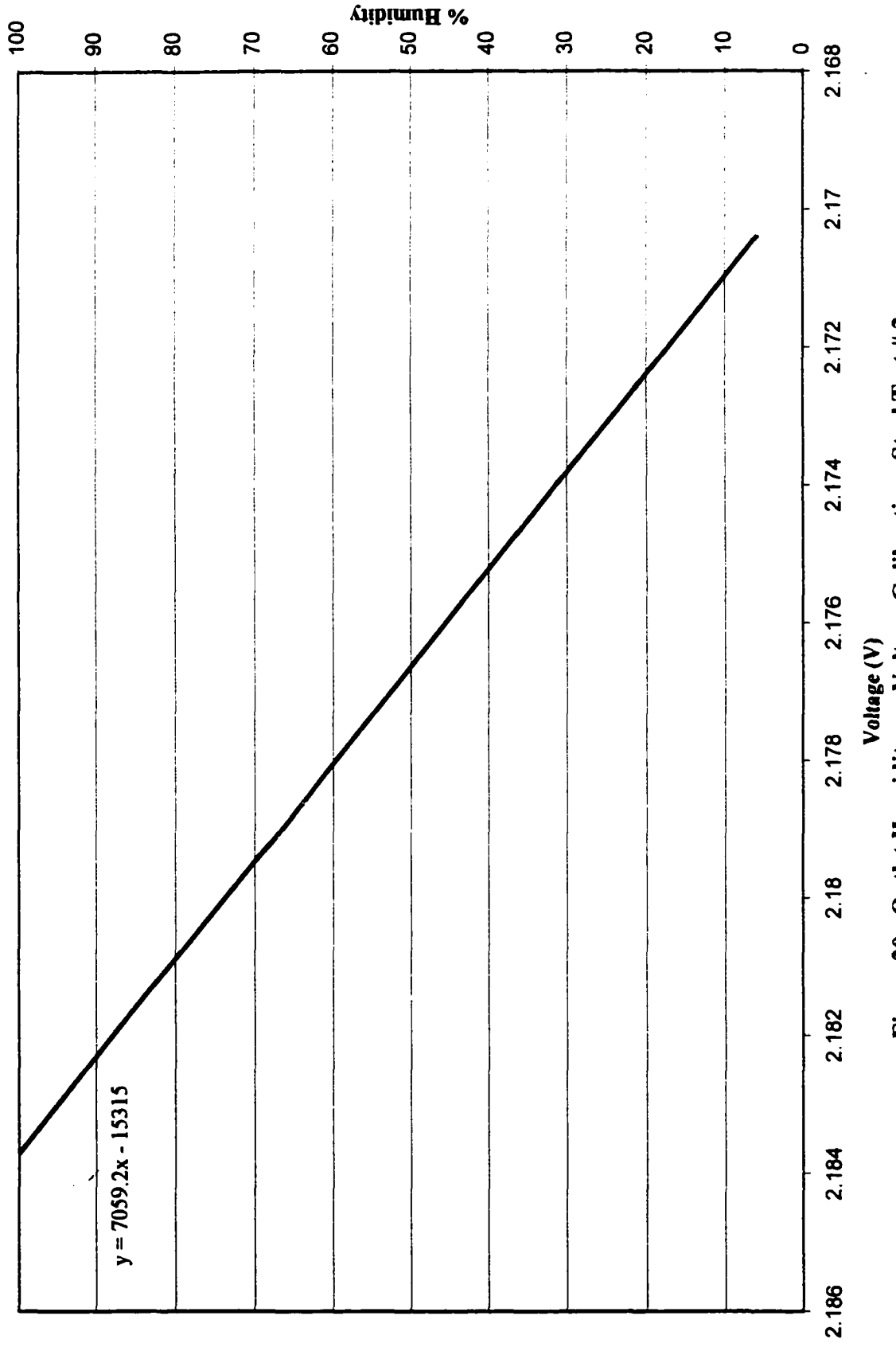


Figure 20. Outlet Humidity vs. Voltage Calibration- Steel Test # 2

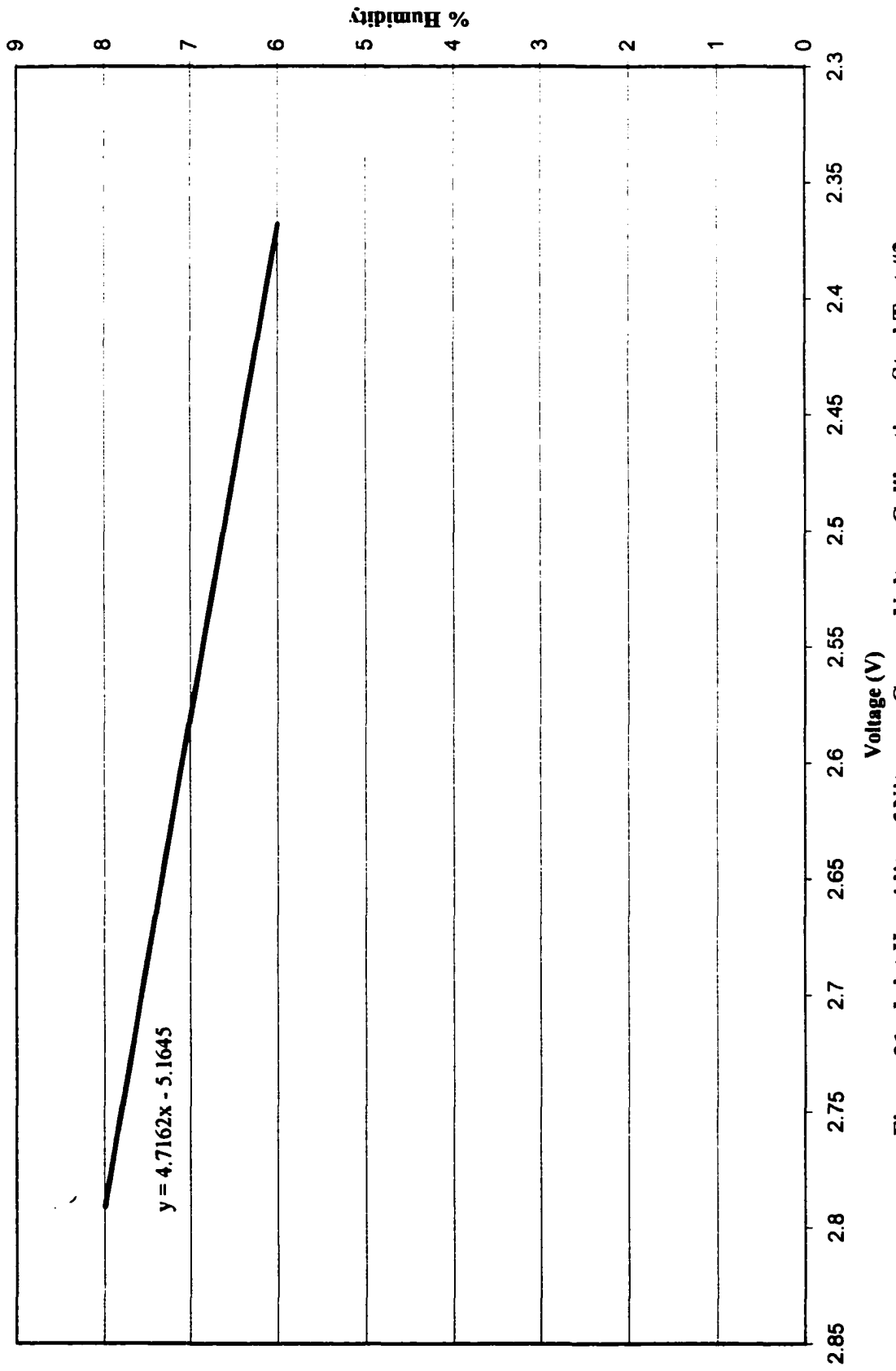


Figure 21. Inlet Humidity of Nitrogen Gas vs. Voltage Calibration- Steel Test #3

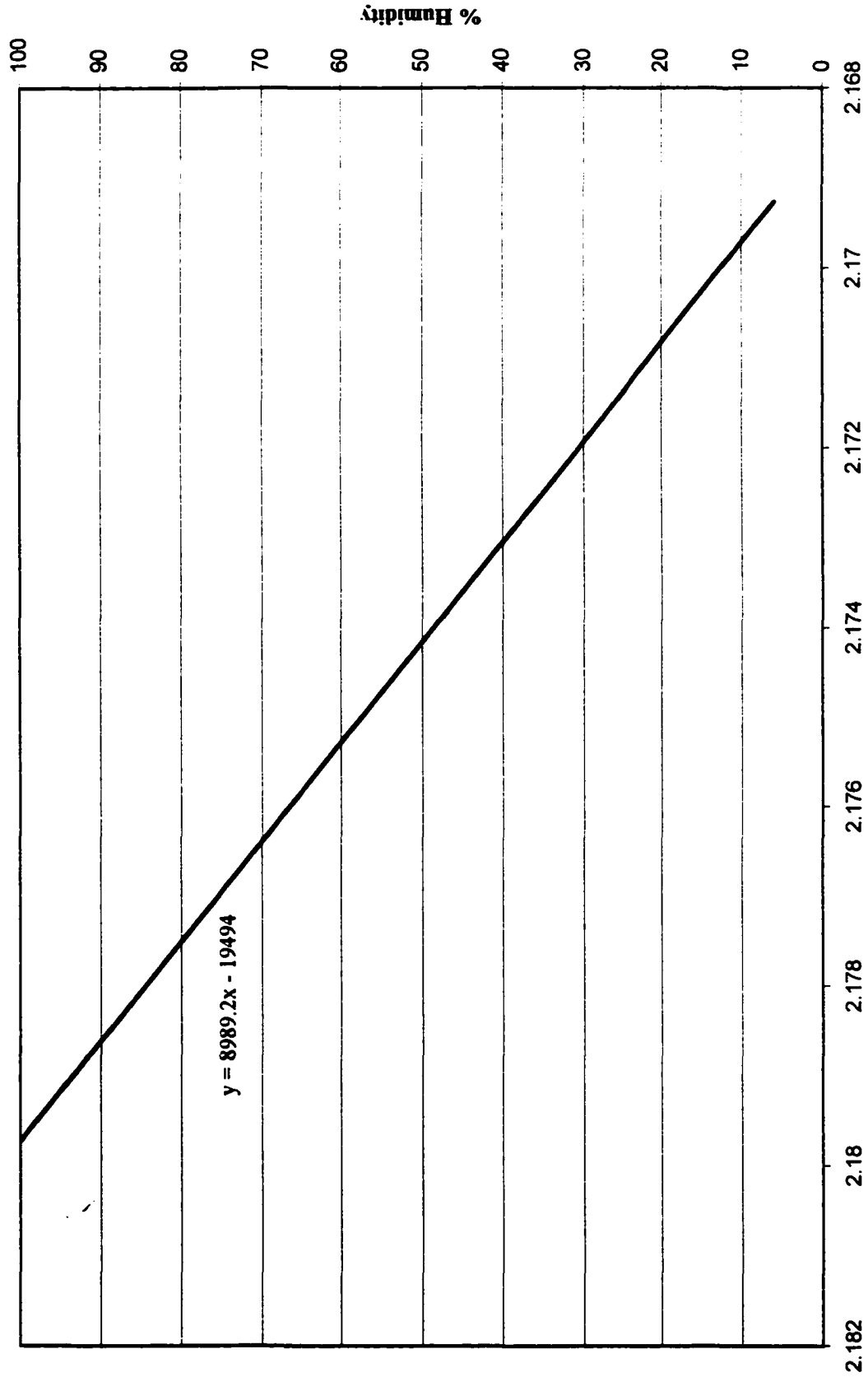


Figure 22. Outlet Humidity vs. Voltage Calibration- Steel Test #3

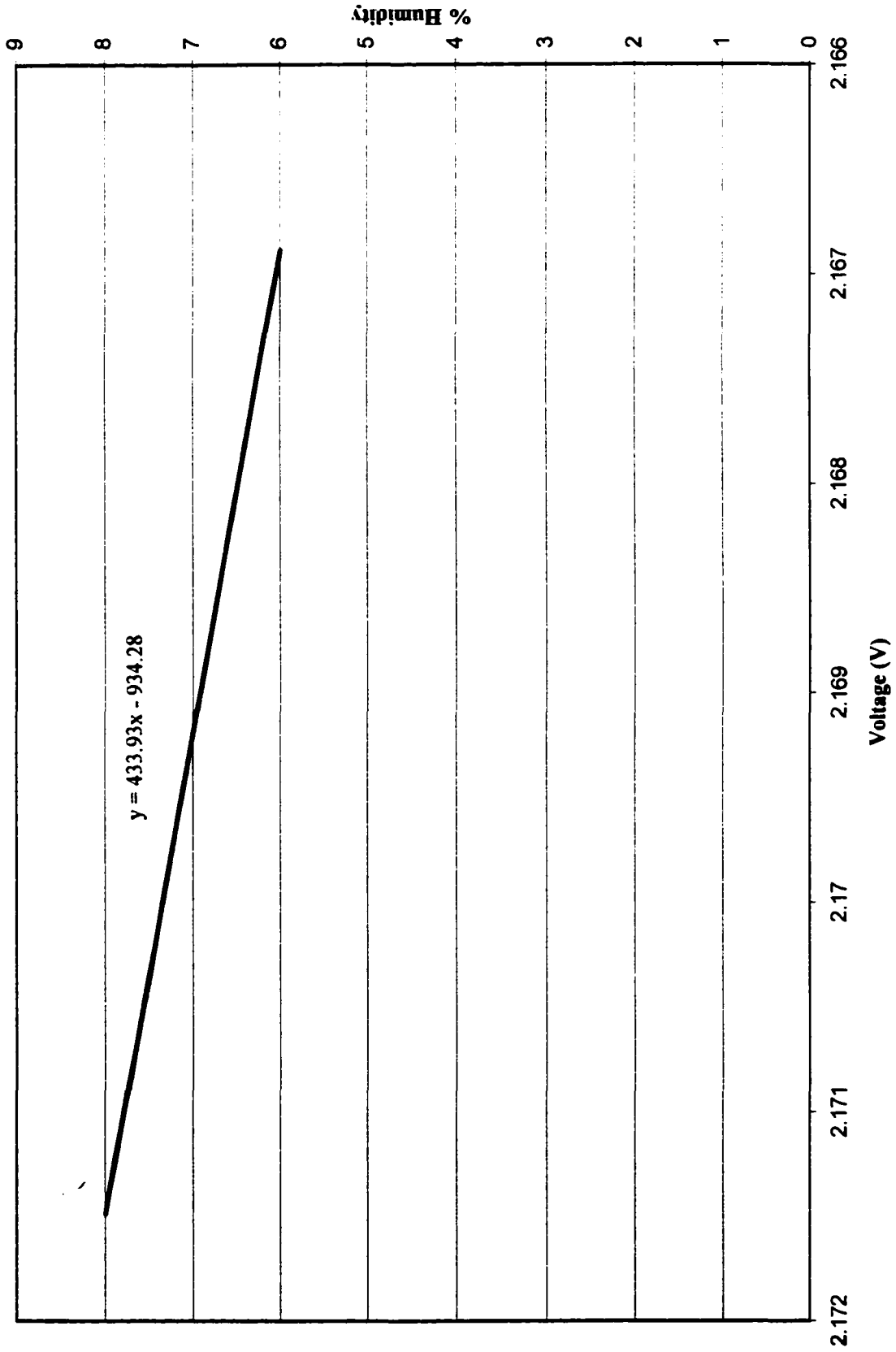


Figure 23. Inlet Humidity of Nitrogen Gas vs. Voltage Calibration- Steel Test # 4

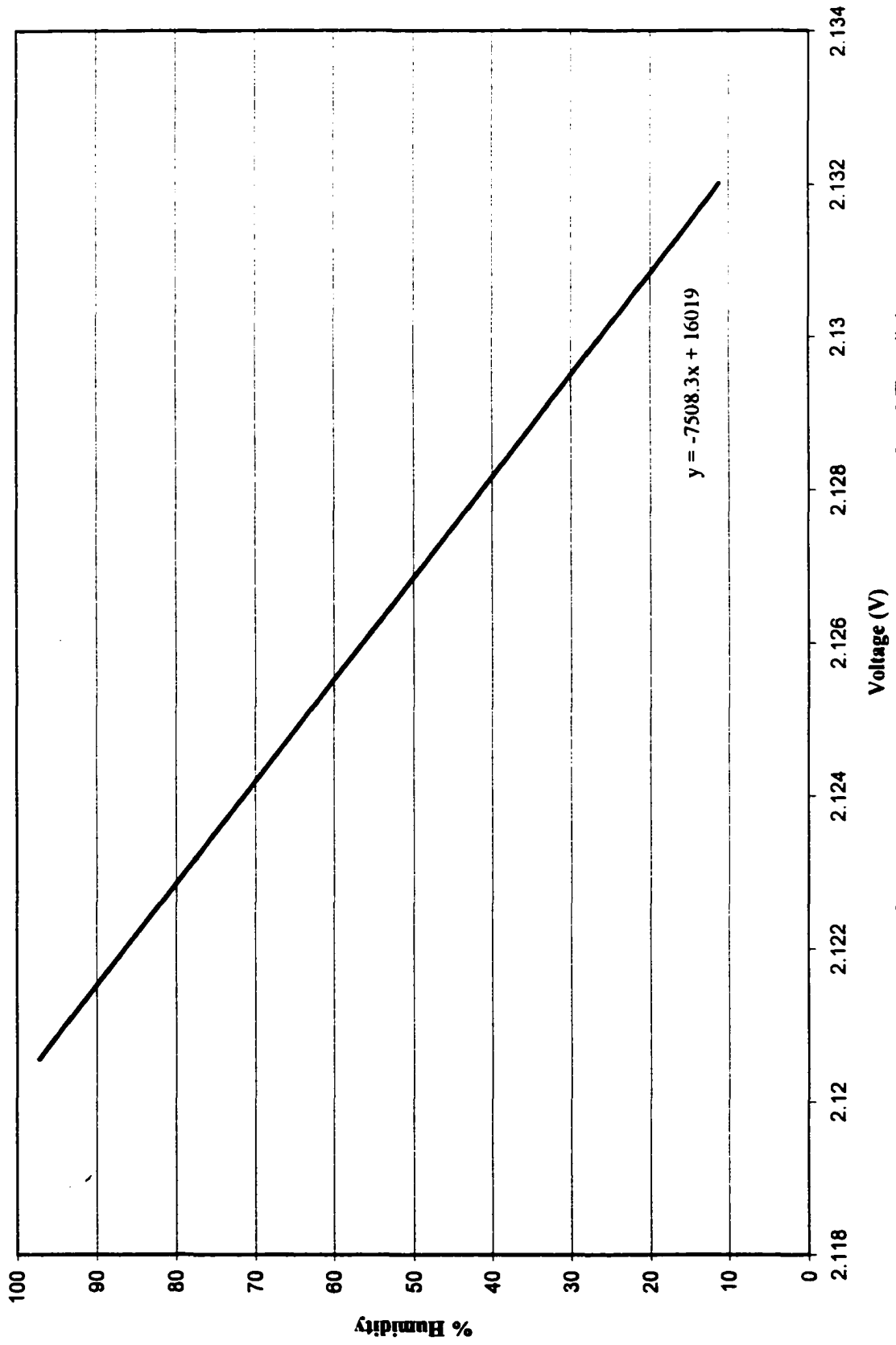


Figure 24. Outlet Humidity vs. Voltage Calibration- Steel Test # 4

APPENDIX III

HUMIDITY SENSOR CALIBRATIONS- CERAMIC

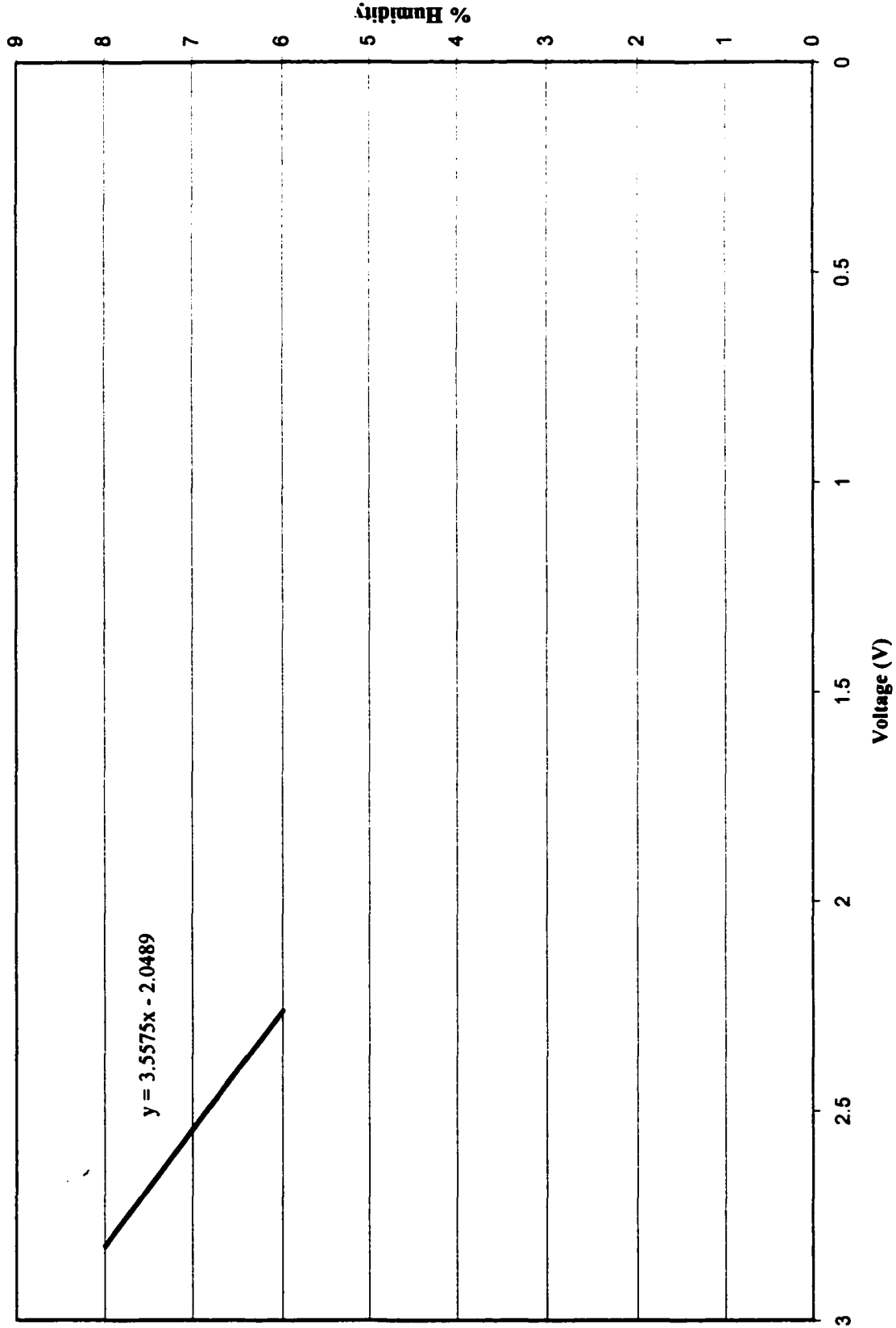


Figure 25. Inlet Humidity of Nitrogen Gas vs. Voltage Calibration - Ceramic Test # 1

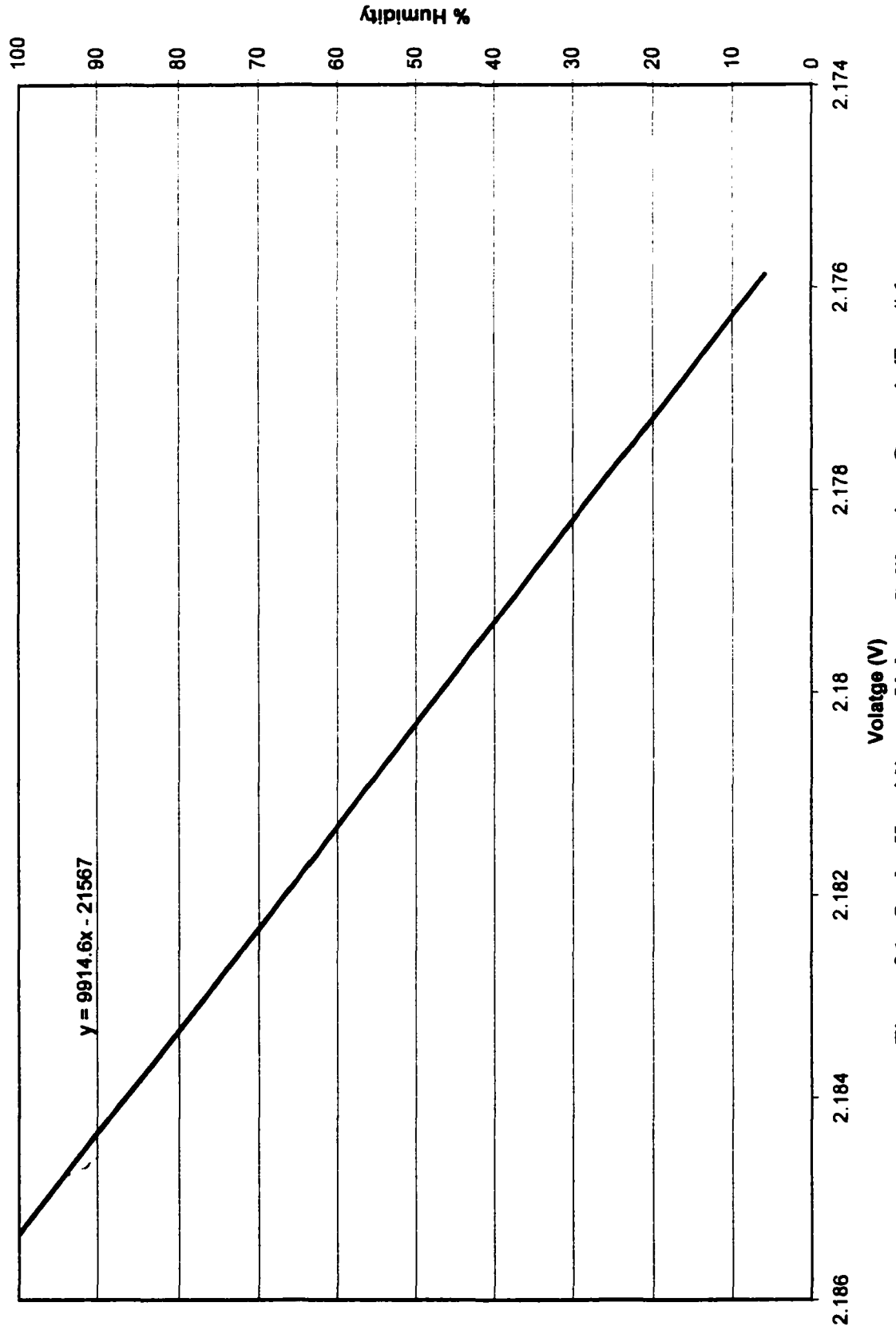


Figure 26. Outlet Humidity vs. Voltage Calibration- Ceramic Test # 1

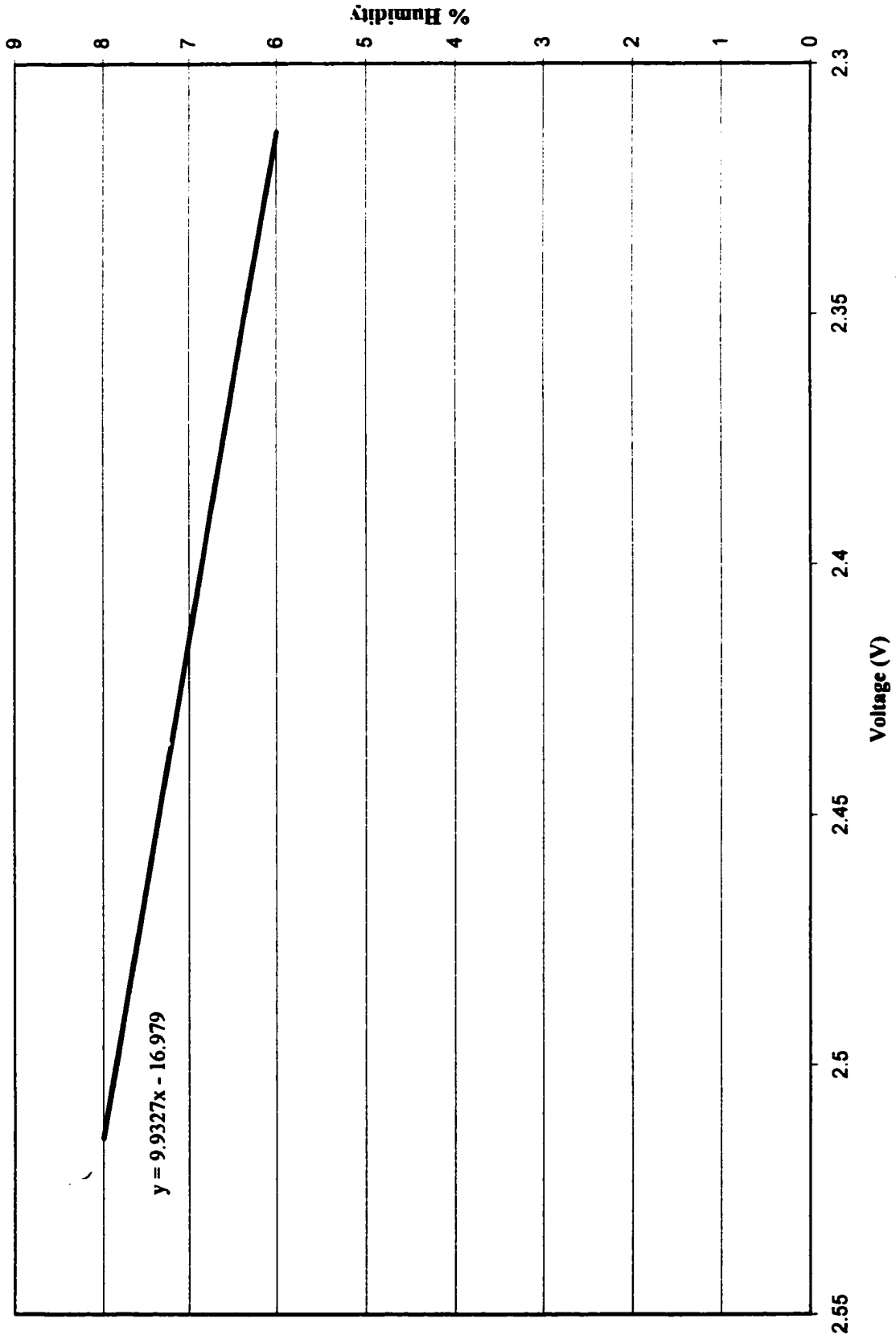


Figure 27. Inlet Humidity of Nitrogen Gas vs. Voltage- Ceramic Test # 2

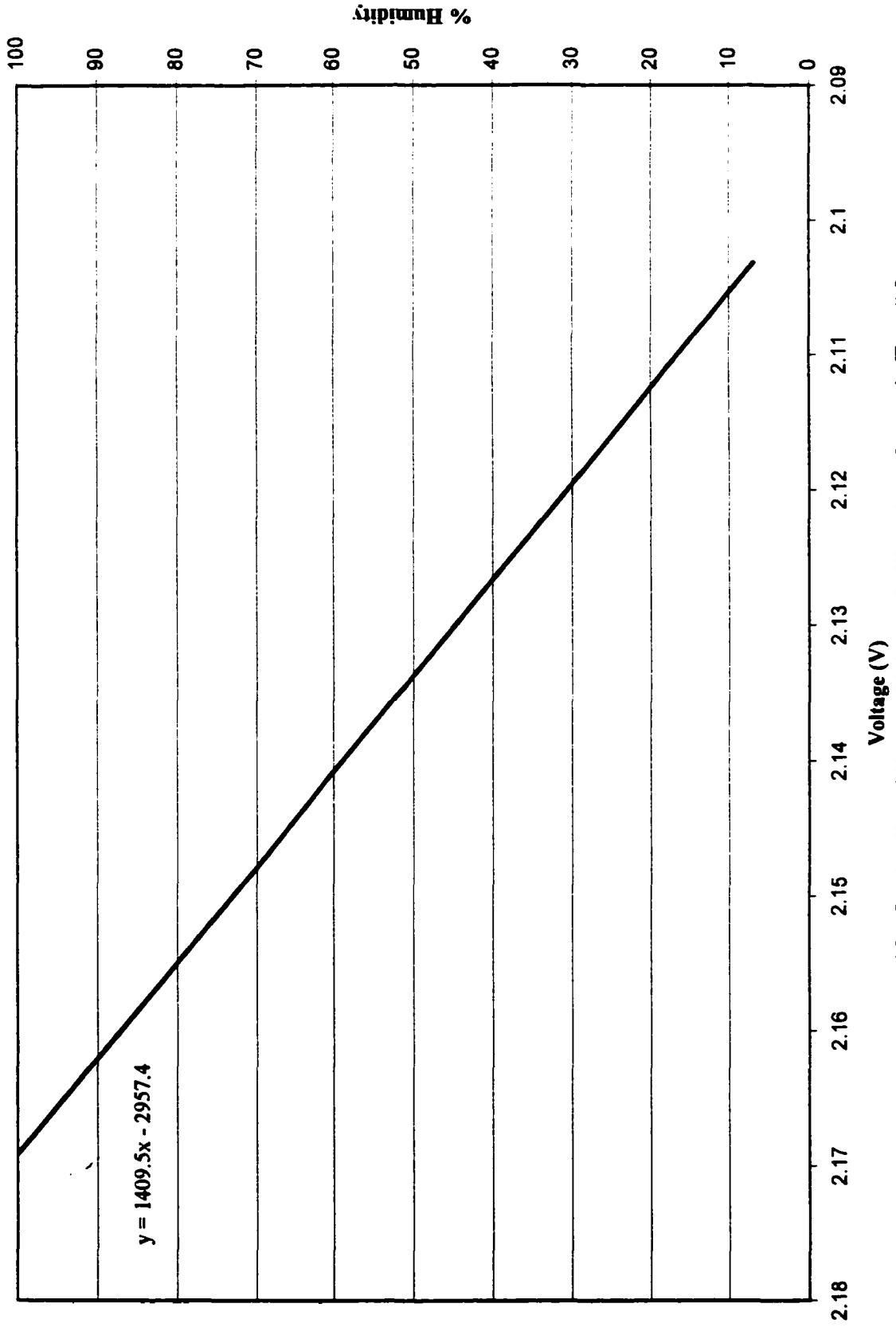


Figure 28. Outlet Humidity vs. Voltage Calibration- Ceramic Test # 2

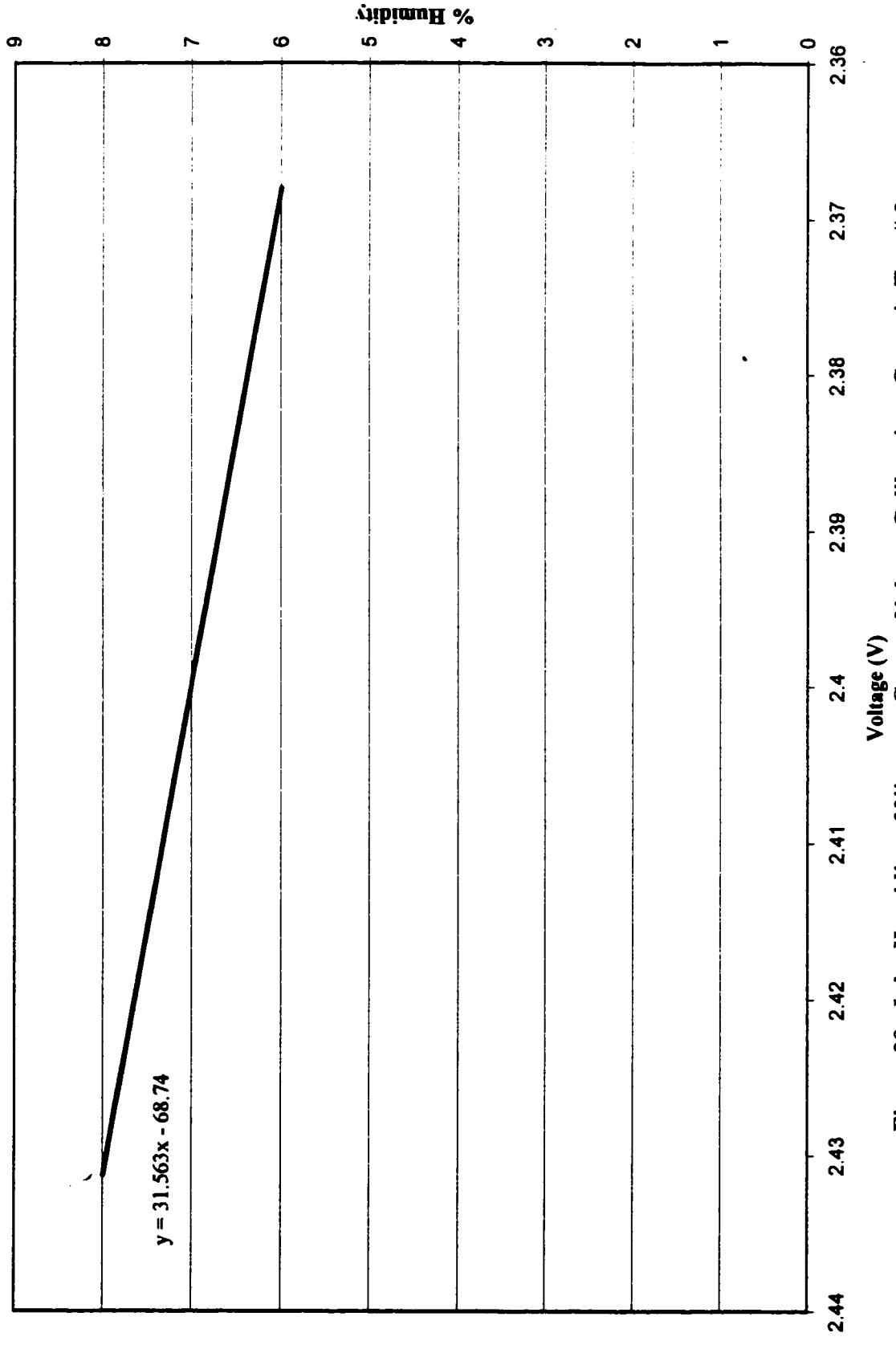


Figure 29. Inlet Humidity of Nitrogen Gas vs. Voltage Calibration- Ceramic Test # 3

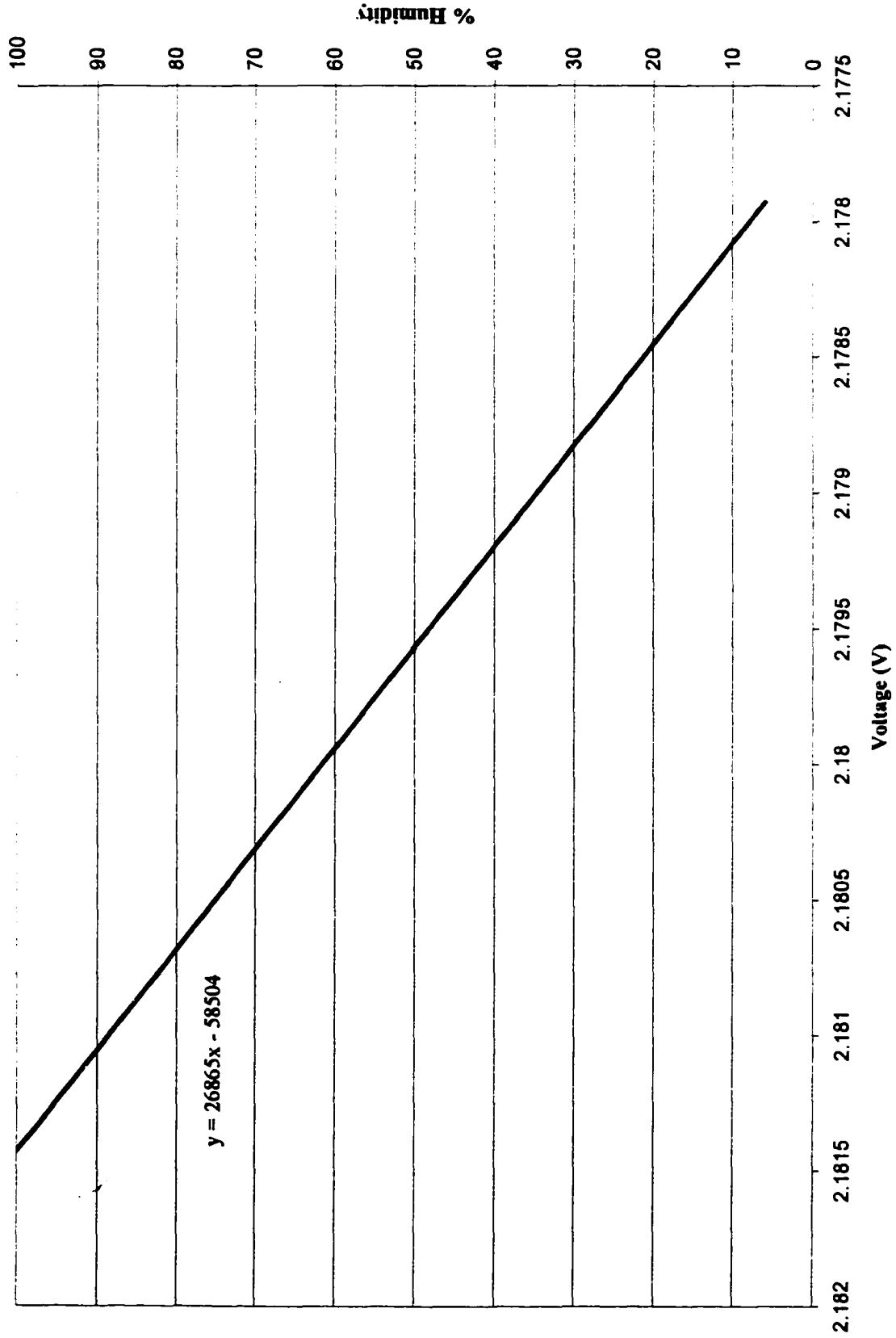


Figure 30. Outlet Humidity vs. Voltage Calibration- Ceramic Test # 3

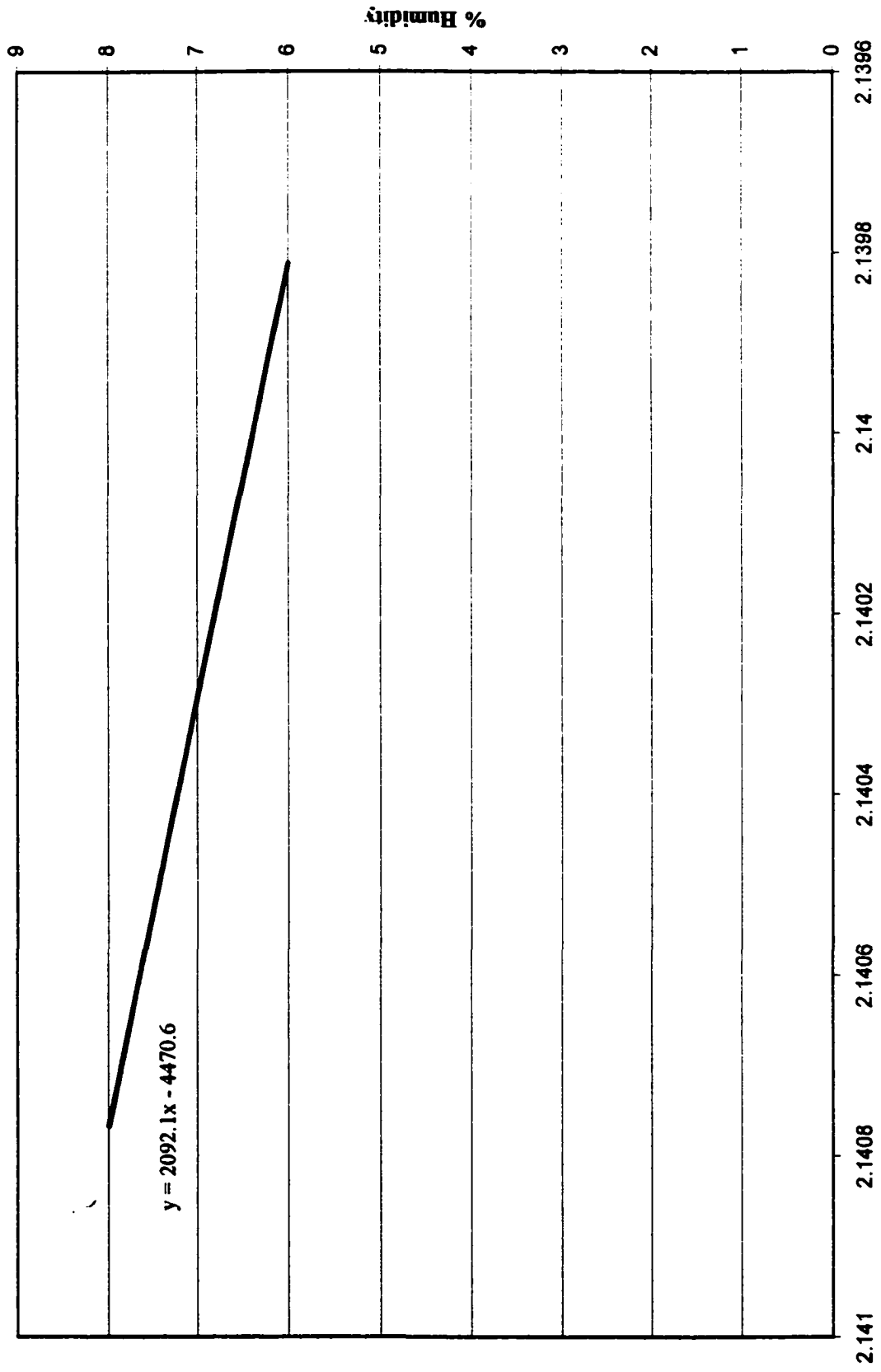


Figure 31. Inlet Humidity of Nitrogen Gas vs. Voltage Calibration- Ceramic Test # 4

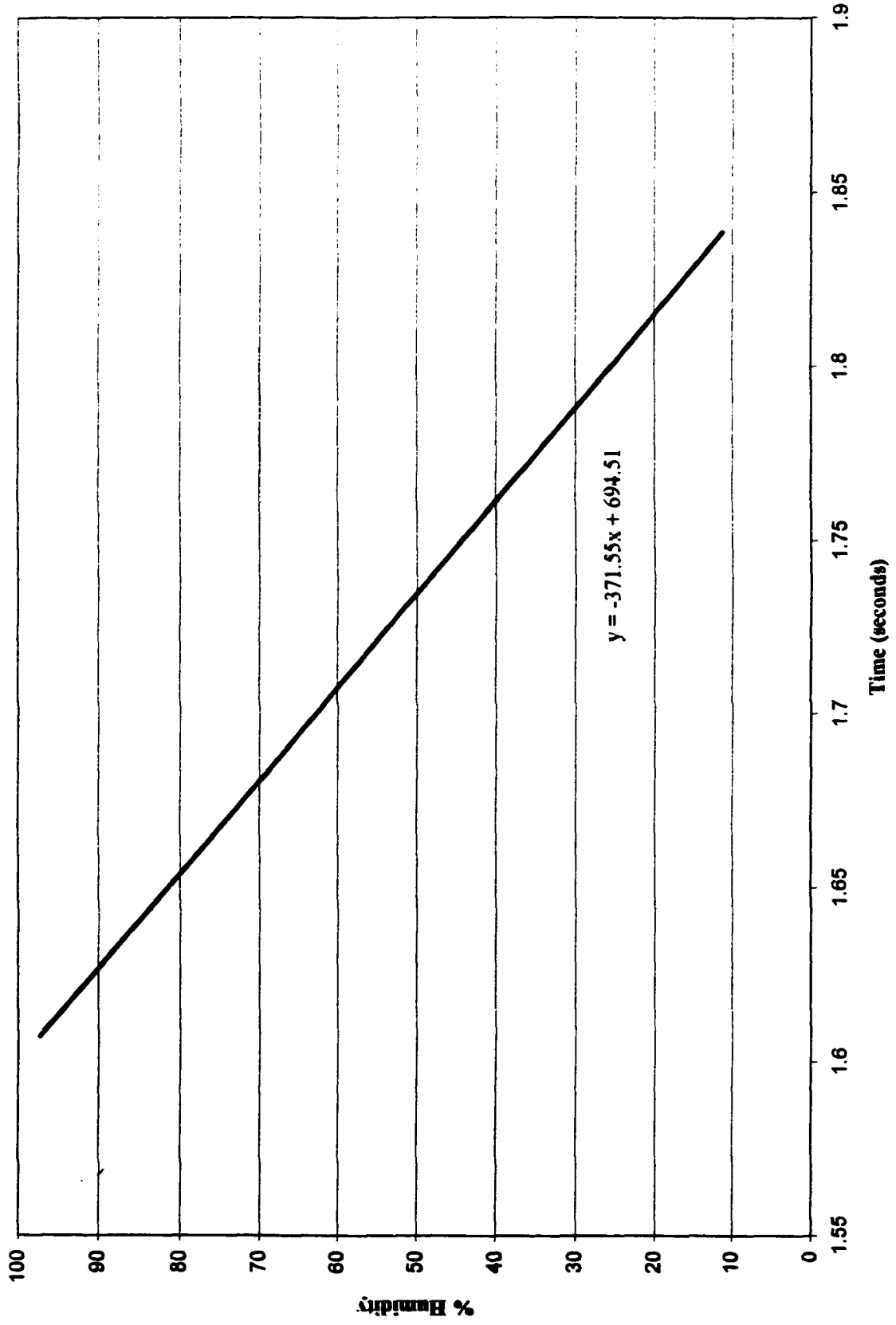


Figure 32. Outlet Humidity vs. Voltage Calibration- Ceramic Test # 4

APPENDIX IV

MASS OF WATER LOST CALIBRATIONS- STEEL

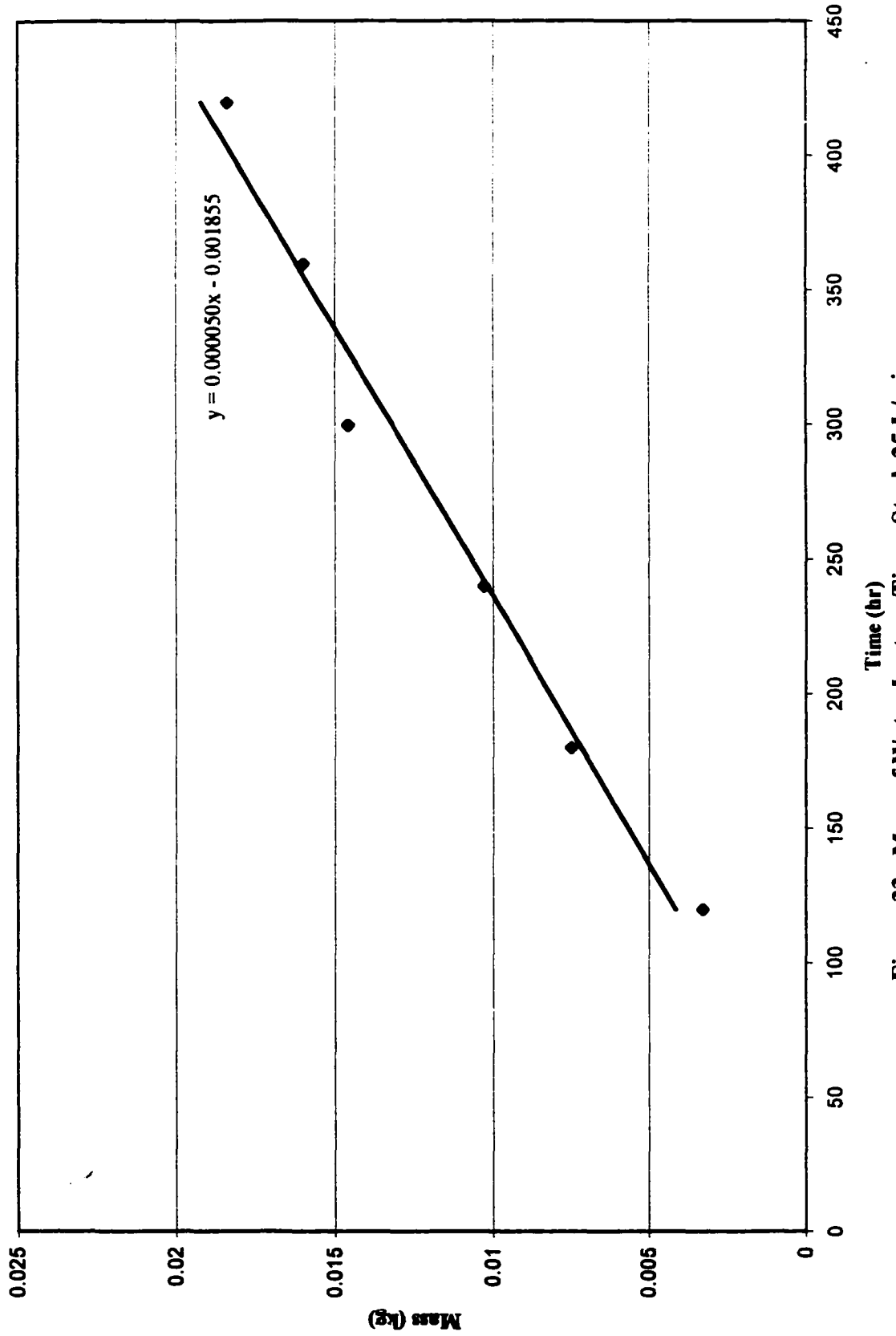


Figure 33. Mass of Water Lost vs. Time-Steel .25 L/min

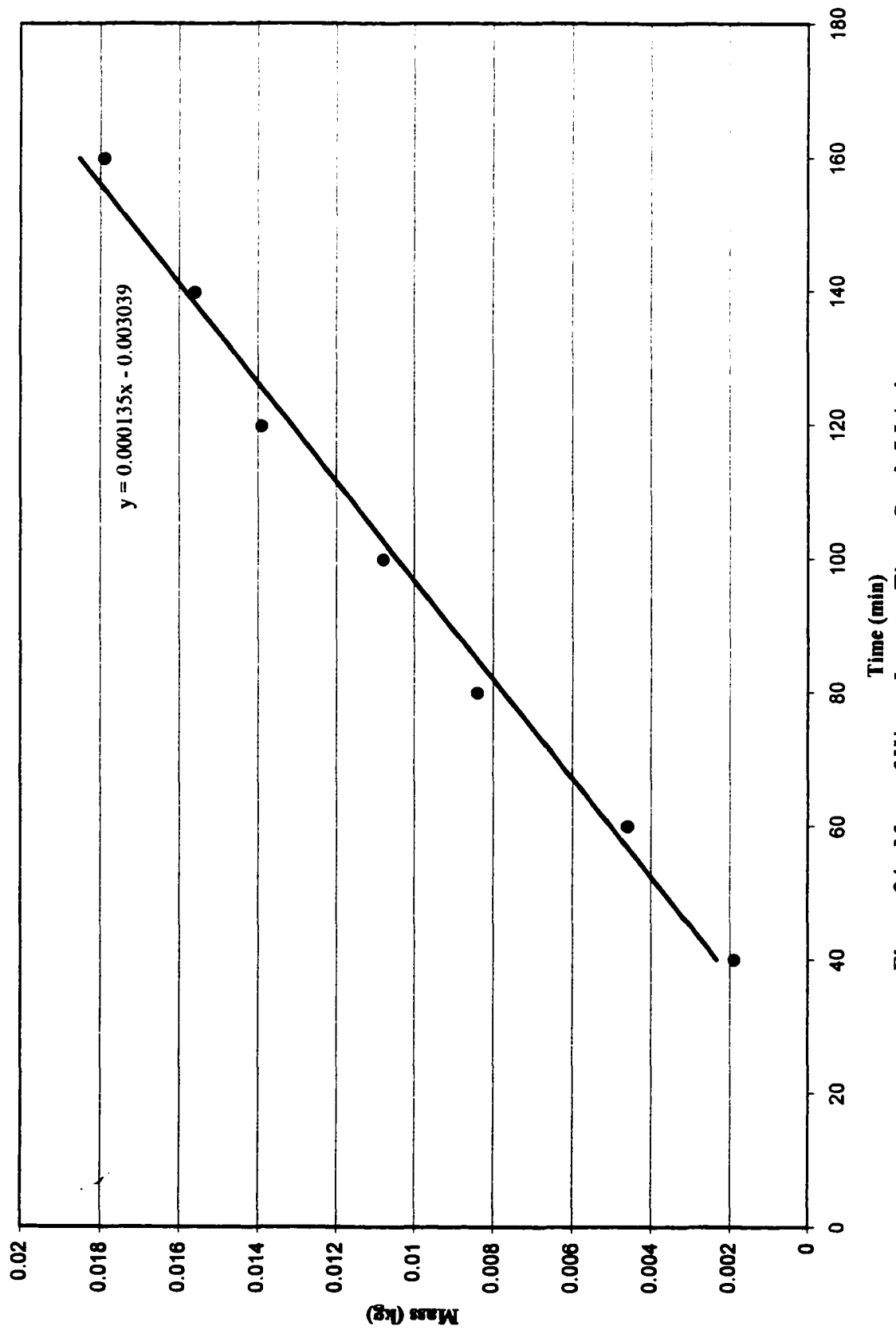


Figure 34. Mass of Water Lost vs. Time- Steel .5 L/min

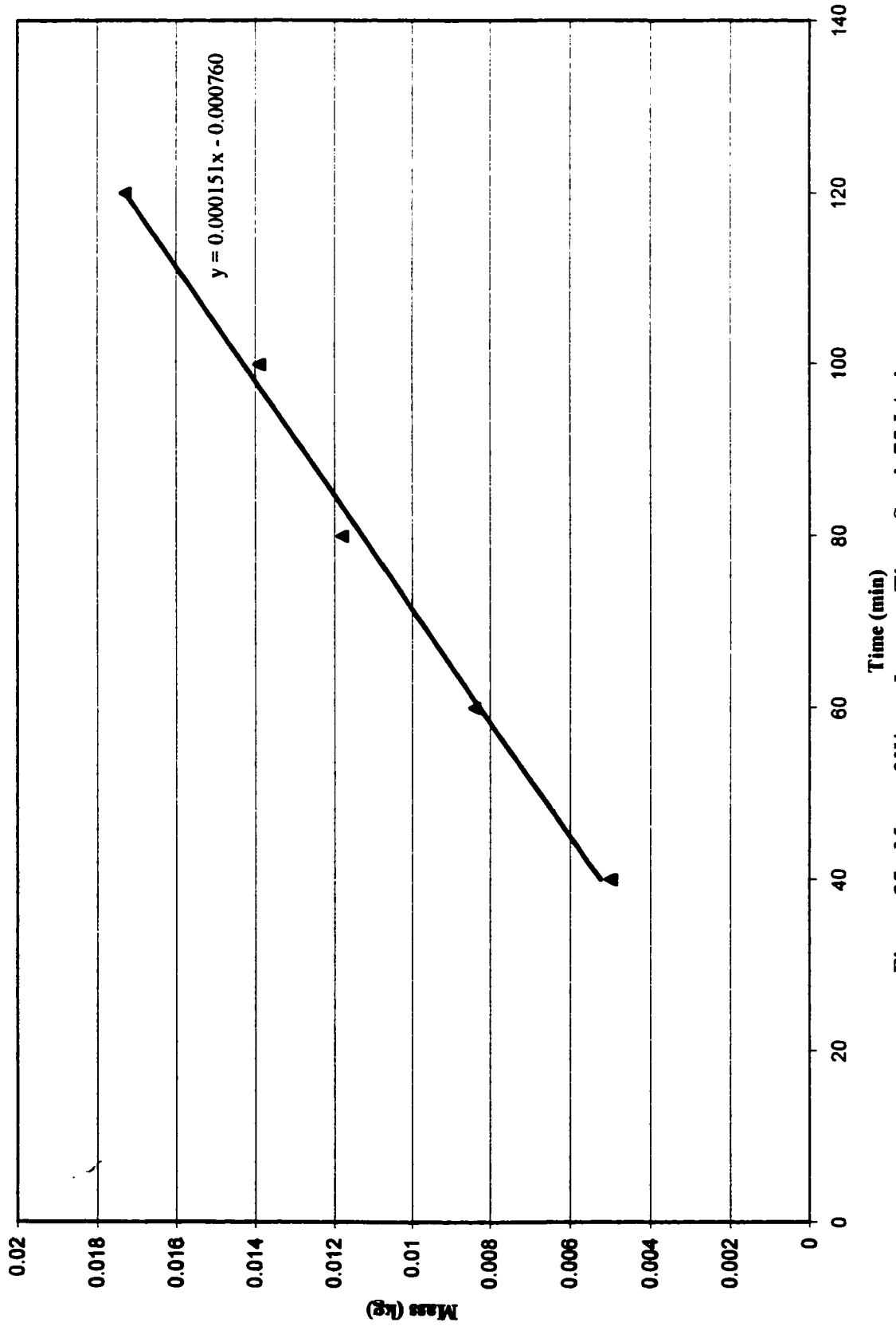


Figure 35. Mass of Water Lost vs. Time-Steel .75 L./min

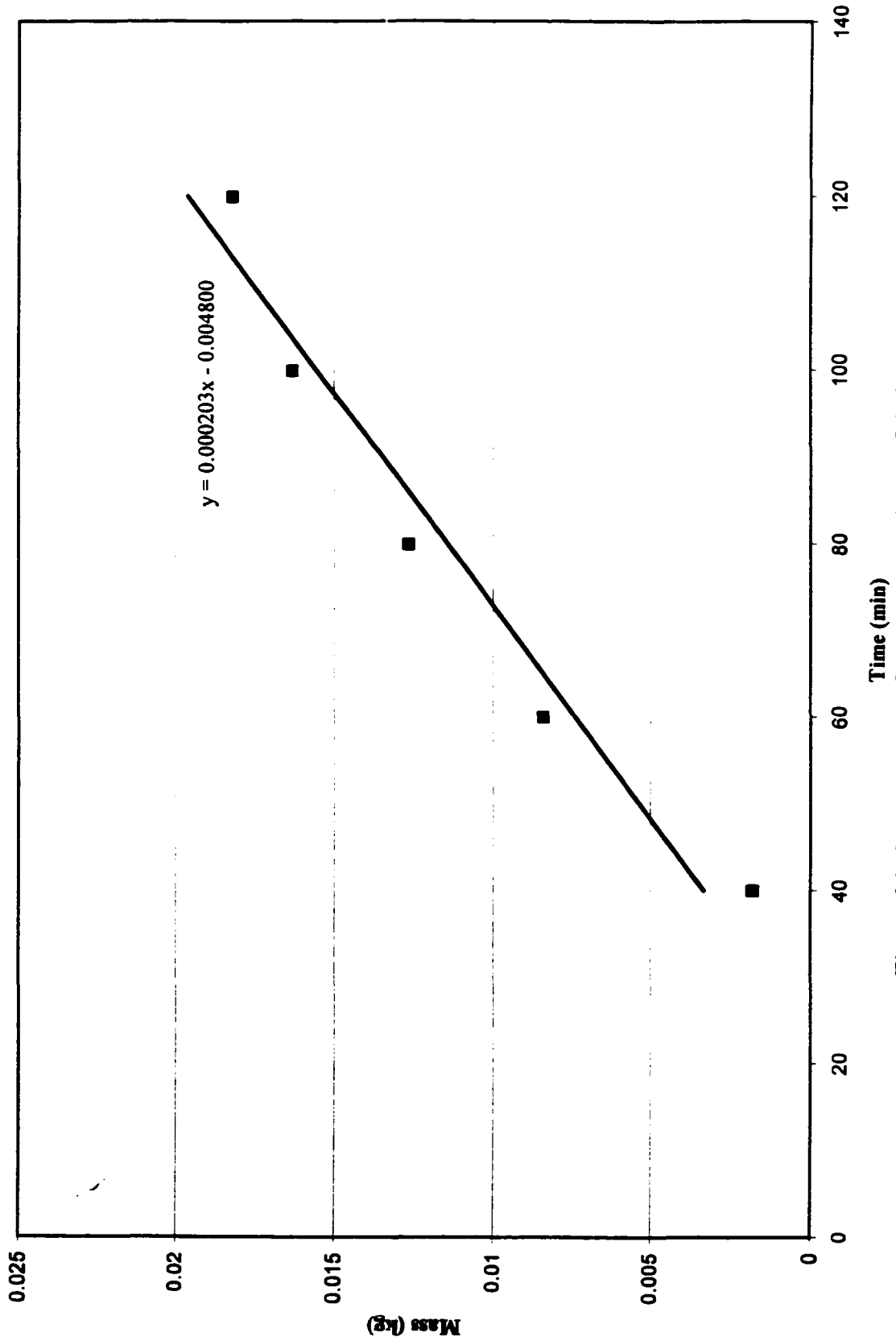


Figure 36. Mass of Water Lost vs. Time- Steel 1 L/min

APPENDIX V

MASS OF WATER LOST CALIBRATIONS- CERAMIC

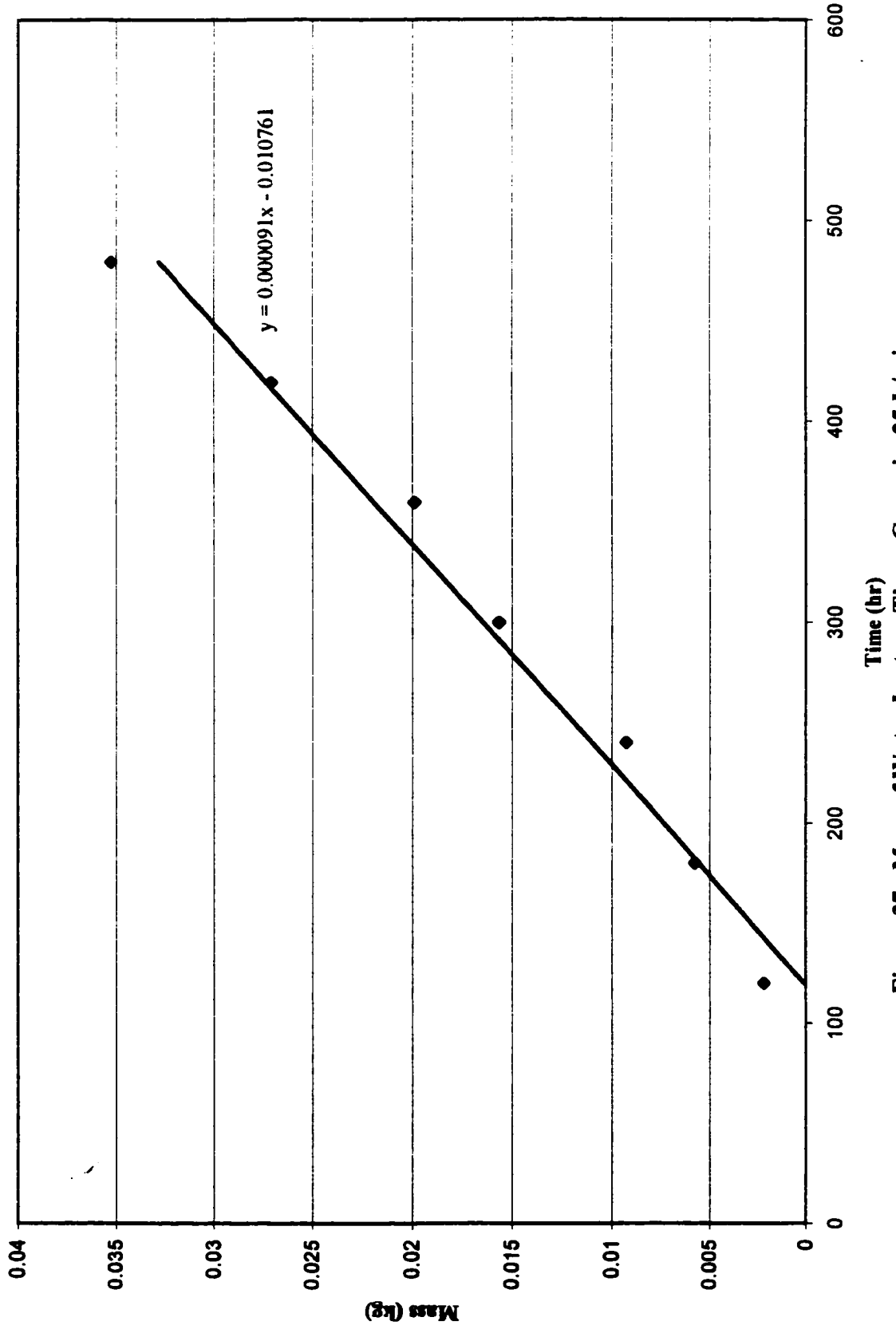


Figure 37. Mass of Water Lost vs. Time- Ceramic .25 L/min

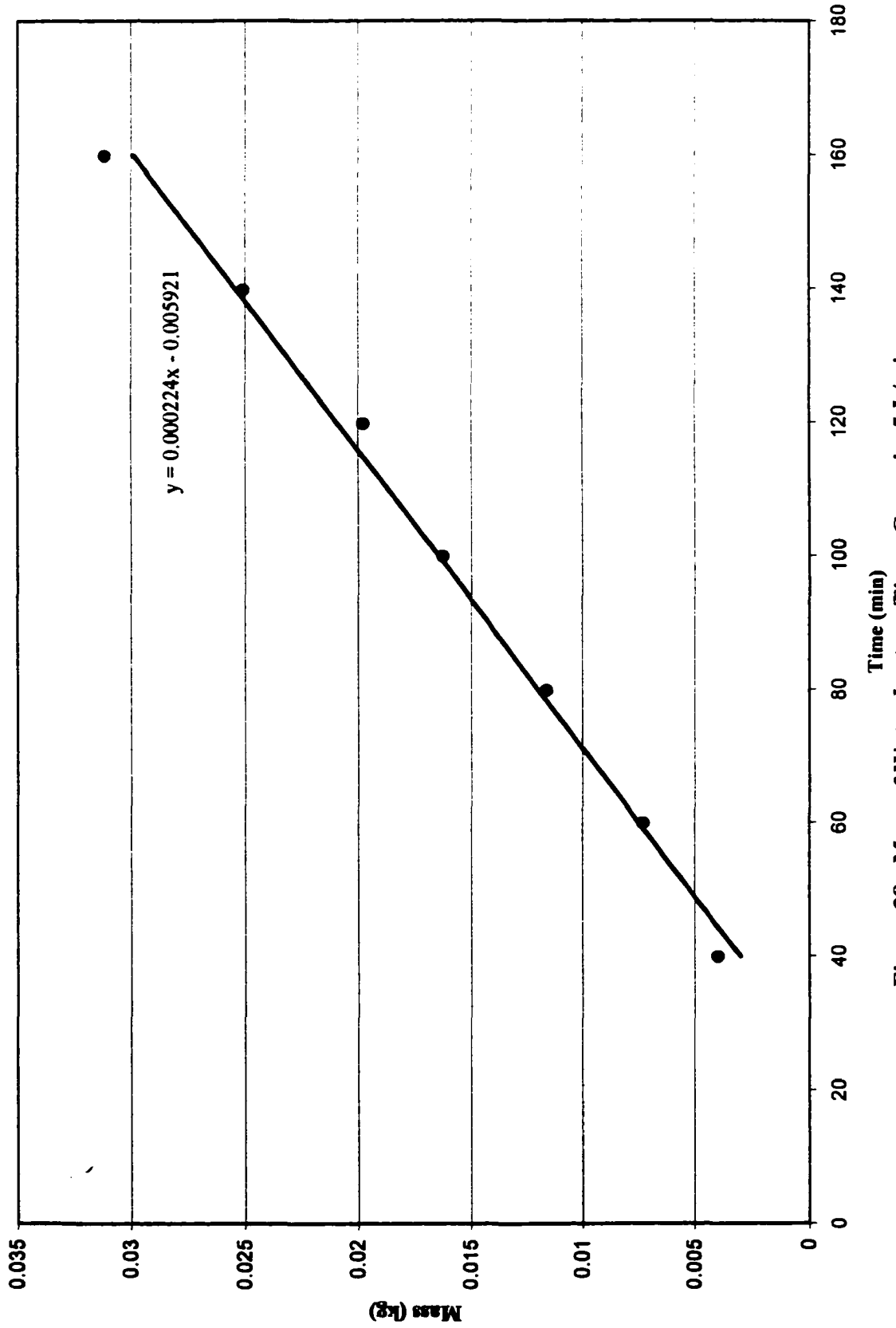


Figure 38. Mass of Water Lost vs. Time- Ceramic .5 L./min

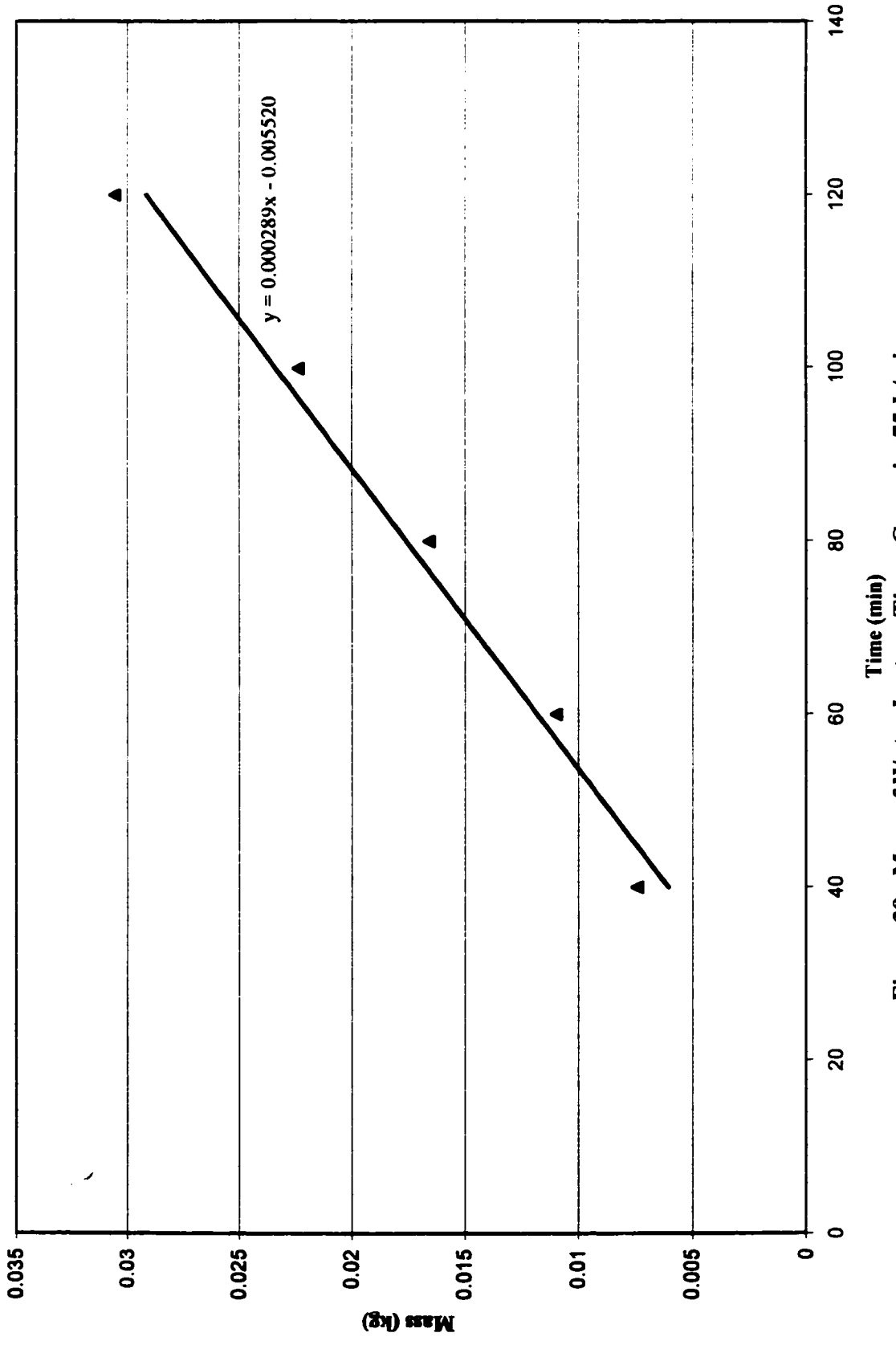


Figure 39. Mass of Water Lost vs. Time- Ceramic .75 L/min

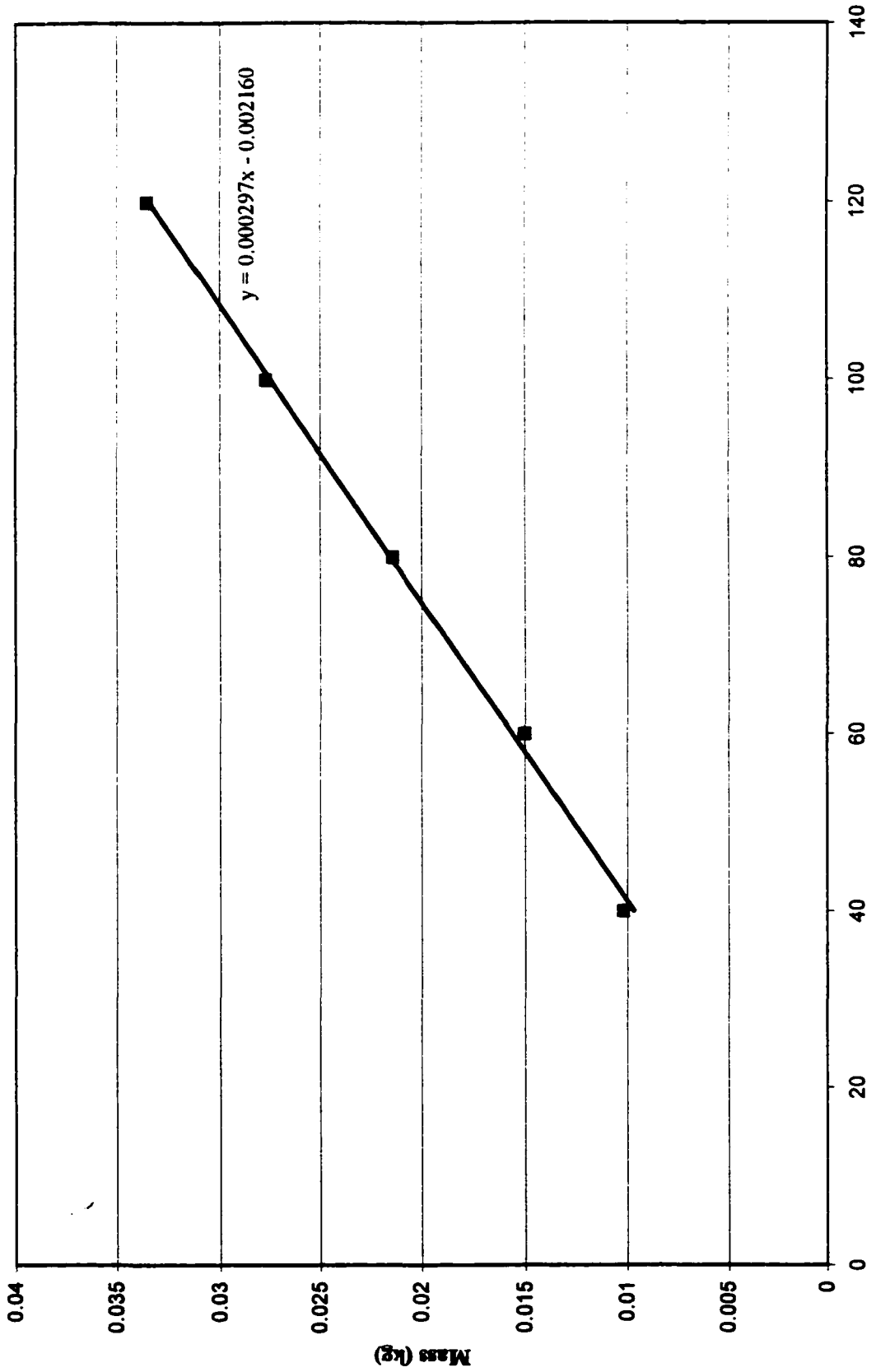


Figure 40. Mass of Water Lost vs. Time- Ceramic 1 L/min

APPENDIX VI

REYNOLDS NUMBER CALCULATIONS

Reynolds Number Calculations

Calculations for .25 L/min Nitrogen Flow Rates

$$\phi = .395$$

Porosity (Kaviany 1995)

$$\rho = 1.1421 \cdot \frac{\text{kg}}{\text{m}^3}$$

Density of Nitrogen gas at 24 degrees C

$$\mu = 17.84 \cdot 10^{-6} \cdot \frac{\text{kg}}{\text{m} \cdot \text{sec}}$$

Dynamic viscosity of Nitrogen gas at 24 degrees C

$$D_{\text{bed}} = .0381 \cdot \text{m}$$

Diameter of tube for incoming Nitrogen gas

$$A = \pi \cdot \left(\frac{D_{\text{bed}}}{2} \right)^2$$

$$A = 1.14 \cdot 10^{-3} \cdot \text{m}^2$$

Area of tube for incoming Nitrogen gas

$$Q = .25 \cdot \frac{\text{liter}}{\text{min}}$$

$$Q = 4.167 \cdot 10^{-6} \cdot \text{m}^3 \cdot \text{sec}^{-1}$$

Flow rate of incoming Nitrogen gas

$$U = \frac{Q}{A \cdot \phi}$$

$$U = 9.252 \cdot 10^{-3} \cdot \text{m} \cdot \text{sec}^{-1}$$

Velocity of incoming Nitrogen gas

$$D_{\text{sphere}} = 4.5 \cdot \text{mm}$$

$$\text{Re}_D = \frac{\rho \cdot U \cdot D_{\text{sphere}}}{\mu}$$

$$\text{Re}_D = 0.267$$

Reynolds number

Calculations for .5 L/min Nitrogen flow Rates

$$Q = .5 \frac{\text{liter}}{\text{min}}$$

Flow rate of incoming Nitrogen gas

$$U = \frac{Q}{A \cdot \phi}$$

$$U = 0.019 \cdot \text{m} \cdot \text{sec}^{-1}$$

Velocity of incoming Nitrogen gas

$$\text{Re}_D = \frac{\rho \cdot U \cdot D_{\text{sphere}}}{\mu}$$

$$\text{Re}_D = 0.533$$

Reynolds Number**Calculations for .75 L/min Nitrogen flow Rates**

$$Q = .75 \frac{\text{liter}}{\text{min}}$$

Flow rate of incoming Nitrogen gas

$$U = \frac{Q}{A \cdot \phi}$$

$$U = 0.028 \cdot \text{m} \cdot \text{sec}^{-1}$$

Velocity of incoming Nitrogen gas

$$\text{Re}_D = \frac{\rho \cdot U \cdot D_{\text{sphere}}}{\mu}$$

$$\text{Re}_D = 0.8$$

Reynolds Number**Calculations for 1 L/min Nitrogen flow Rates**

$$Q = 1 \frac{\text{liter}}{\text{min}}$$

Flow rate of incoming Nitrogen gas

$$U = \frac{Q}{A \cdot \phi}$$

$$U = 0.037 \cdot \text{m} \cdot \text{sec}^{-1}$$

Velocity of incoming Nitrogen gas

$$\text{Re}_D = \frac{\rho \cdot U \cdot D_{\text{sphere}}}{\mu}$$

$$\text{Re}_D = 1.066$$

Reynolds Number

APPENDIX VII

CALCULATIONS- STEEL

Steel Calculations

Test #1 Steel- .25 L/min

$$d_p = 4.5 \cdot \text{mm} \quad \text{Diameter of individual particle in bed}$$

$$S_{\text{bed}} = \frac{6}{d_p}$$

$$S_{\text{bed}} = 1.333 \cdot 10^3 \cdot \text{m}^{-3} \cdot \text{m}^2 \quad \text{Surface area of bed per unit volume}$$

$$D_{\text{test}} = .0381 \cdot \text{m} \quad \text{Diameter of test section}$$

$$L_{\text{test}} = .4064 \cdot \text{m} \quad \text{Length of test section}$$

$$V_{\text{test}} = \pi \cdot \frac{D_{\text{test}}^2}{4} \cdot L_{\text{test}}$$

$$V_{\text{test}} = 4.633 \cdot 10^{-4} \cdot \text{m}^3 \quad \text{Volume of test section}$$

$$A_{\text{test}} = S_{\text{bed}} \cdot V_{\text{test}}$$

$$A_{\text{test}} = 0.618 \cdot \text{m}^2 \quad \text{Total area of test bed}$$

$$n_a = 8.36 \cdot 10^{-7} \cdot \text{kg} \cdot \text{sec}^{-1} \quad \text{Evaporation rate from Mass of Water Lost Calibration}$$

$$v_g = 45.54 \cdot \frac{\text{m}^3}{\text{kg}} \quad \text{Specific volume at 24 degrees C}$$

$$\rho_{\text{satTemp}} = \frac{1}{v_g}$$

$$\rho_{\text{satTemp}} = 0.022 \cdot \text{kg} \cdot \text{m}^{-3} \quad \text{Density at saturation temperature}$$

$$\phi_{\text{N}_2} = .065 \quad \text{Humidity of incoming Nitrogen gas}$$

$$h_m = \frac{n_a}{A_{\text{test}} \rho_{\text{sat}} \text{Temp} \cdot (1 - \phi) N_2}$$

$$h_m = 6.591 \cdot 10^{-5} \cdot \text{m} \cdot \text{sec}^{-1}$$

Mass transfer coefficient

$$D_{12} = .26 \cdot 10^{-8} \cdot \frac{\text{m}^2}{\text{sec}}$$

Binary diffusion coefficient

$$\text{Sh} = \frac{h_m \cdot d_p}{D_{12}}$$

$$\text{Sh} = 114.076$$

Sherwood number

Test #2 Steel- .5 L/min

$$d_p = 4.5 \cdot \text{mm}$$

Diameter of individual particle in bed

$$S_{\text{bed}} = \frac{6}{d_p}$$

$$S_{\text{bed}} = 1.333 \cdot 10^3 \cdot \text{m}^{-3} \cdot \text{m}^2$$

Surface area of bed per unit volume

$$D_{\text{test}} = .0381 \cdot \text{m}$$

Diameter of test section

$$L_{\text{test}} = .4064 \cdot \text{m}$$

Length of test section

$$V_{\text{test}} = \pi \cdot \frac{D_{\text{test}}^2}{4} \cdot L_{\text{test}}$$

$$V_{\text{test}} = 4.633 \cdot 10^{-4} \cdot \text{m}^3$$

Volume of test section

$$A_{\text{test}} = S_{\text{bed}} \cdot V_{\text{test}}$$

$$A_{\text{test}} = 0.618 \cdot \text{m}^2$$

Total area of test bed

$$n_a = 2.25 \cdot 10^{-6} \cdot \text{kg} \cdot \text{sec}^{-1}$$

Evaporation rate from Mass of Water Lost Calibration

$$v_g = 45.54 \cdot \frac{\text{m}^3}{\text{kg}}$$

Specific volume at 24 degrees C

$$\rho_{\text{satTemp}} = \frac{1}{v_g}$$

$$\rho_{\text{satTemp}} = 0.022 \cdot \text{kg} \cdot \text{m}^{-3}$$

Density at saturation Temperature

$$\phi_{\text{N}_2} = .06$$

Humidity of incoming Nitrogen gas

$$h_m = \frac{n_a}{A_{\text{test}} \rho_{\text{satTemp}} (1 - \phi) N_2}$$

$$h_m = 1.764 \cdot 10^{-4} \cdot \text{m} \cdot \text{sec}^{-1} \quad \text{Mass transfer coefficient}$$

$$D_{12} = .26 \cdot 10^{-8} \frac{\text{m}^2}{\text{sec}} \quad \text{Binary diffusion coefficient}$$

$$Sh = \frac{h_m \cdot d_p}{D_{12}}$$

$$Sh = 305.39 \quad \text{Sherwood number}$$

Test #3 Steel- .75 L/min

$$d_p = 4.5 \cdot \text{mm}$$

Diameter of individual particle in bed

$$S_{\text{bed}} = \frac{6}{d_p}$$

$$S_{\text{bed}} = 1.333 \cdot 10^3 \cdot \text{m}^{-3} \cdot \text{m}^2$$

Surface area of bed per unit volume

$$D_{\text{test}} = .0381 \cdot \text{m}$$

Diameter of test section

$$L_{\text{test}} = .4064 \cdot \text{m}$$

Length of test section

$$V_{\text{test}} = \pi \cdot \left(\frac{D_{\text{test}}}{2} \right)^2 \cdot L_{\text{test}}$$

$$V_{\text{test}} = 4.633 \cdot 10^{-4} \cdot \text{m}^3$$

Volume of test section

$$A_{\text{test}} = S_{\text{bed}} \cdot V_{\text{test}}$$

$$A_{\text{test}} = 0.618 \cdot \text{m}^2$$

Total area of test bed

$$n_a = 2.517 \cdot 10^{-6} \cdot \text{kg} \cdot \text{sec}^{-1}$$

Evaporation rate from Mass of Water Lost Calibration

$$v_g = 45.54 \cdot \frac{\text{m}^3}{\text{kg}}$$

Specific volume at 24 degrees C

$$\rho_{\text{satTemp}} = \frac{1}{v_g}$$

$$\rho_{\text{satTemp}} = 0.022 \cdot \text{kg} \cdot \text{m}^{-3}$$

Density at saturation temperature

$$\phi_{\text{N}_2} = .06$$

Humidity of incoming Nitrogen gas

$$h_m = \frac{n_a}{A_{\text{test}} \rho_{\text{satTemp}} (1 - \phi_{N_2})}$$

$$h_m = 1.974 \cdot 10^{-4} \cdot \text{m} \cdot \text{sec}^{-1} \quad \text{Mass transfer coefficient}$$

$$D_{12} = .26 \cdot 10^{-8} \frac{\text{m}^2}{\text{sec}} \quad \text{Binary diffusion coefficient}$$

$$\text{Sh} = \frac{h_m \cdot d_p}{D_{12}}$$

$$\text{Sh} = 341.629 \quad \text{Sherwood number}$$

Test #4 Steel- 1 L/min

$$d_p = 4.5 \cdot \text{mm}$$

Diameter of individual particle in bed

$$S_{\text{bed}} = \frac{6}{d_p}$$

$$S_{\text{bed}} = 1.333 \cdot 10^3 \cdot \text{m}^{-3} \cdot \text{m}^2$$

Surface area of bed per unit volume

$$D_{\text{test}} = .0381 \cdot \text{m}$$

Diameter of test section

$$L_{\text{test}} = .4064 \cdot \text{m}$$

Length of test section

$$V_{\text{test}} = \pi \cdot \frac{D_{\text{test}}^2}{4} \cdot L_{\text{test}}$$

$$V_{\text{test}} = 4.633 \cdot 10^{-4} \cdot \text{m}^3$$

Volume of test section

$$A_{\text{test}} = S_{\text{bed}} \cdot V_{\text{test}}$$

$$A_{\text{test}} = 0.618 \cdot \text{m}^2$$

Total area of test bed

$$n_a = 3.383 \cdot 10^{-6} \cdot \text{kg} \cdot \text{sec}^{-1}$$

Evaporation rate from Mass of water Lost Calibration

$$v_g = 45.54 \cdot \frac{\text{m}^3}{\text{kg}}$$

Specific volume at 24 degrees C

$$\rho_{\text{satTemp}} = \frac{1}{v_g}$$

$$\rho_{\text{satTemp}} = 0.022 \cdot \text{kg} \cdot \text{m}^{-3}$$

Density at saturation temperature

$$\phi_{\text{N}_2} = .073$$

Humidity of incoming Nitrogen gas

$$h_m = \frac{n_a}{A_{\text{test}} \rho_{\text{sat}} \text{Temp} \cdot (1 - \phi) N_2}$$

$$h_m = 2.69 \cdot 10^{-4} \cdot \text{m} \cdot \text{sec}^{-1} \quad \text{Mass transfer coefficient}$$

$$D_{12} = 26 \cdot 10^{-8} \cdot \frac{\text{m}^2}{\text{sec}} \quad \text{Binary diffusion coefficient}$$

$$\text{Sh} = \frac{h_m \cdot d_p}{D_{12}}$$

$$\text{Sh} = 465.61 \quad \text{Sherwood number}$$

APPENDIX VIII

CALCULATIONS- CERAMIC

Ceramic Calculations

Test #1 Ceramic- .25 L/min

$$d_p = 4.5 \cdot \text{mm} \quad \text{Diameter of individual particle in bed}$$

$$S_{\text{bed}} = \frac{6}{d_p}$$

$$S_{\text{bed}} = 1.333 \cdot 10^3 \cdot \text{m}^{-3} \cdot \text{m}^2 \quad \text{Surface area of bed per unit volume}$$

$$D_{\text{test}} = .0381 \cdot \text{m} \quad \text{Diameter of test section}$$

$$L_{\text{test}} = .4064 \cdot \text{m} \quad \text{Length of test section}$$

$$V_{\text{test}} = \pi \cdot \left(\frac{D_{\text{test}}}{2} \right)^2 \cdot L_{\text{test}}$$

$$V_{\text{test}} = 4.633 \cdot 10^{-4} \cdot \text{m}^3 \quad \text{Volume of test section}$$

$$A_{\text{test}} = S_{\text{bed}} \cdot V_{\text{test}}$$

$$A_{\text{test}} = 0.618 \cdot \text{m}^2 \quad \text{Total area of test bed}$$

$$n_a = 1.513 \cdot 10^{-6} \cdot \text{kg} \cdot \text{sec}^{-1} \quad \text{Evaporation rate}$$

$$v_g = 45.54 \cdot \frac{\text{m}^3}{\text{kg}} \quad \text{Specific volume at 24 degrees C}$$

$$\rho_{\text{satTemp}} = \frac{1}{v_g}$$

$$\rho_{\text{satTemp}} = 0.022 \cdot \text{kg} \cdot \text{m}^{-3} \quad \text{Density at saturation temperature}$$

$$\phi_{\text{N}_2} = .06 \quad \text{Humidity of incoming Nitrogen gas}$$

$$h_m = \frac{n_a}{A_{\text{test}} \rho_{\text{sat}} \text{Temp}^{1-\phi} N_2}$$

$$h_m = 1.187 \cdot 10^{-4} \cdot \text{m} \cdot \text{sec}^{-1} \quad \text{Mass transfer coefficient}$$

$$D_{12} = .26 \cdot 10^{-8} \frac{\text{m}^2}{\text{sec}} \quad \text{Binary diffusion coefficient}$$

$$\text{Sh} = \frac{h_m \cdot d_p}{D_{12}}$$

$$\text{Sh} = 205.358 \quad \text{Sherwood number}$$

Test #2 Ceramic- .5 L/min

$$d_p = 4.5 \cdot \text{mm}$$

Diameter of individual particle in bed

$$S_{\text{bed}} = \frac{6}{d_p}$$

$$S_{\text{bed}} = 1.333 \cdot 10^3 \cdot \text{m}^{-3} \cdot \text{m}^2$$

Surface area of bed per unit volume

$$D_{\text{test}} = .0381 \cdot \text{m}$$

Diameter of test section

$$L_{\text{test}} = .4064 \cdot \text{m}$$

Length of test section

$$V_{\text{test}} = \pi \cdot \left(\frac{D_{\text{test}}}{2} \right)^2 \cdot L_{\text{test}}$$

$$V_{\text{test}} = 4.633 \cdot 10^{-4} \cdot \text{m}^3$$

Volume of test section

$$A_{\text{test}} = S_{\text{bed}} \cdot V_{\text{test}}$$

$$A_{\text{test}} = 0.618 \cdot \text{m}^2$$

Total area of test bed

$$n_a = 3.733 \cdot 10^{-6} \cdot \text{kg} \cdot \text{sec}^{-1}$$

Evaporation rate

$$v_g = 45.54 \cdot \frac{\text{m}^3}{\text{kg}}$$

Specific volume at 24 degrees C

$$\rho_{\text{satTemp}} = \frac{1}{v_g}$$

$$\rho_{\text{satTemp}} = 0.022 \cdot \text{kg} \cdot \text{m}^{-3}$$

Density at saturation temperature

$$\phi_{\text{N}_2} = .06$$

Humidity of incoming Nitrogen gas

$$h_m = \frac{n_a}{A_{\text{test}} \cdot p_{\text{sat}} \cdot \text{Temp} \cdot (1 - \phi) N_2}$$

$$h_m = 2.927 \cdot 10^{-4} \cdot \text{m} \cdot \text{sec}^{-1} \quad \text{Mass transfer coefficient}$$

$$D_{12} = .26 \cdot 10^{-8} \cdot \frac{\text{m}^2}{\text{sec}} \quad \text{Binary diffusion coefficient}$$

$$Sh = \frac{h_m \cdot d_p}{D_{12}}$$

$$Sh = 506.676 \quad \text{Sherwood number}$$

Test #3 Ceramic- .75 L/min

$$d_p = 4.5 \cdot \text{mm} \quad \text{Diameter of individual particle in bed}$$

$$S_{\text{bed}} = \frac{6}{d_p}$$

$$S_{\text{bed}} = 1.333 \cdot 10^3 \cdot \text{m}^{-3} \cdot \text{m}^2 \quad \text{Surface area of bed per unit volume}$$

$$D_{\text{test}} = .0381 \cdot \text{m} \quad \text{Diameter of test section}$$

$$L_{\text{test}} = .4064 \cdot \text{m} \quad \text{Length of test section}$$

$$V_{\text{test}} = \pi \cdot \left(\frac{D_{\text{test}}}{2} \right)^2 \cdot L_{\text{test}}$$

$$V_{\text{test}} = 4.633 \cdot 10^{-4} \cdot \text{m}^3 \quad \text{Volume of test section}$$

$$A_{\text{test}} = S_{\text{bed}} \cdot V_{\text{test}}$$

$$A_{\text{test}} = 0.618 \cdot \text{m}^2 \quad \text{Total area of test bed}$$

$$n_a = 4.817 \cdot 10^{-6} \cdot \text{kg} \cdot \text{sec}^{-1} \quad \text{Evaporation rate}$$

$$v_g = 45.54 \cdot \frac{\text{m}^3}{\text{kg}} \quad \text{Specific volume at 24 degrees C}$$

$$\rho_{\text{satTemp}} = \frac{1}{v_g}$$

$$\rho_{\text{satTemp}} = 0.022 \cdot \text{kg} \cdot \text{m}^{-3} \quad \text{Density at saturation temperature}$$

$$\phi_{\text{N}_2} = .06 \quad \text{Humidity of incoming Nitrogen gas}$$

$$h_m = \frac{n_a}{A_{\text{test}} \rho_{\text{sat}} \text{Temp} \cdot 1 - \phi_{\text{N2}}}$$

$$h_m = 3.778 \cdot 10^{-4} \cdot \text{m} \cdot \text{sec}^{-1} \quad \text{Mass transfer coefficient}$$

$$D_{12} = .26 \cdot 10^{-8} \cdot \frac{\text{m}^2}{\text{sec}} \quad \text{Binary diffusion coefficient}$$

$$\text{Sh} = \frac{h_m \cdot d_p}{D_{12}}$$

$$\text{Sh} = 653.806 \quad \text{Sherwood number}$$

Test #4 Ceramic- 1 L/min

$$d_p = 4.5 \cdot \text{mm} \quad \text{Diameter of individual particle in bed}$$

$$S_{\text{bed}} = \frac{6}{d_p}$$

$$S_{\text{bed}} = 1.333 \cdot 10^3 \cdot \text{m}^{-3} \cdot \text{m}^2 \quad \text{Surface area of bed per unit volume}$$

$$D_{\text{test}} = .0381 \cdot \text{m} \quad \text{Diameter of test section}$$

$$L_{\text{test}} = .4064 \cdot \text{m} \quad \text{Length of test section}$$

$$V_{\text{test}} = \pi \cdot \left(\frac{D_{\text{test}}}{2} \right)^2 \cdot L_{\text{test}}$$

$$V_{\text{test}} = 4.633 \cdot 10^{-4} \cdot \text{m}^3 \quad \text{Volume of test section}$$

$$A_{\text{test}} = S_{\text{bed}} \cdot V_{\text{test}}$$

$$A_{\text{test}} = 0.618 \cdot \text{m}^2 \quad \text{Total area of test bed}$$

$$n_a = 4.95 \cdot 10^{-6} \cdot \text{kg} \cdot \text{sec}^{-1} \quad \text{Evaporation rate}$$

$$v_g = 45.54 \cdot \frac{\text{m}^3}{\text{kg}} \quad \text{Specific volume at 24 degrees C}$$

$$\rho_{\text{satTemp}} = \frac{1}{v_g}$$

$$\rho_{\text{satTemp}} = 0.022 \cdot \text{kg} \cdot \text{m}^{-3} \quad \text{Density at saturation temperature}$$

$$\phi_{\text{N}_2} = .078 \quad \text{Humidity of incoming Nitrogen gas}$$

/

$$h_m = \frac{n_a}{A_{\text{test}} \rho_{\text{sat}} \text{Temp} \cdot 1 - \phi_{N2}}$$

$$h_m = 3.958 \cdot 10^{-4} \cdot \text{m} \cdot \text{sec}^{-1} \quad \text{Mass transfer coefficient}$$

$$D_{12} = .26 \cdot 10^{-8} \cdot \frac{\text{m}^2}{\text{sec}} \quad \text{Binary diffusion coefficient}$$

$$\text{Sh} = \frac{h_m \cdot d_p}{D_{12}}$$

$$\text{Sh} = 684.974 \quad \text{Sherwood number}$$

BIBLIOGRAPHY

Adler, P.M., 1992, *Porous Media-Geometry and Transports*, Butterworth-Heinemann, Boston.

ASTM Designation: E 104-85- Standard Practice for Maintaining Constant Relative Humidity by Means of Aqueous Solutions, 1991.

Bastian, G., 1997, "Heat and Moisture Transfer in Capillary-Porous Bodies- Some Experimental Methods of Investigation", *Drying Technology*, Vol. 15, No. 9, pp. 2145-2164.

Bejan, A., and Nield, D.A., 1992, *Convection in Porous Media*, Springer-Verlag, New York.

Bermeister, L.C., 1993, "*Convective Heat Transfer-2nd Edition*", Wiley, New York.

Bertomieu, J., Bueve, S. and LeLong, T., 1997, "From Simulation to the Design of an Industrial Drier for Natural Rubber in Granule Form", *Drying Technology*, Vol. 15, No. 10, pp. 2541-2555.

Boehm, R.F., Chen, Y.-T., and Lingineni, S., 1995a, "On the Extension of Multi-Phase Models to Sub-Residual Saturation", Proceedings of the 30th National Heat Transfer Conference, HTD-Vol. 309, Vol. 7, ASME, pp. 41-48.

Boehm, R.F., Chen, Y.-T., and Lingineni, S., 1995b, "Transport Processes in Unsaturated Soils at Sub-Residual Saturations", Proceedings of the 6th Annual International High level Radioactive Waste Material Conference, Las Vegas, Nevada, pp. 297-298

Bories, S.A., 1991 "Fundamentals of Drying of Capillary Porous Bodies", *Convective Heat Transfer and Mass Transfer in Porous Media*, Luwer Academic Publishers.

Çorapcioglu, Y.M., 1991, *Advances in Porous Media*, Vol. 1 & 2, Elsevier, Amsterdam.

Eckert, E.R.G., and Drake, R.M., 1972, "*Analysis of Heat and Mass Transfer*", McGraw-Hill, New York.

Francis, N.D. and Wepfer, W.J., 1996, "Jet Impingement Drying of a Moist Porous Solid", *International Journal of Heat and Mass Transfer*, Vol. 39, No.9, pp. 1911-1923.

Fogiel, M., 1994, "*Handbook of Mathematical, Scientific, and Engineering Formulas, Tables, Functions, Graphs, Transforms*", Research and Education Association, Piscataway.

Gong, Z.X. and Mujumdar, A.S., 1995, "The Influence of an Impermeable Surface on Pore Steam Pressure During Drying of Refractory Concrete Slabs", *International Journal of Heat and Mass Transfer*, Vol.38, No.7, pp. 1297-1303.

Izzeldin, A.A., 1994, "*Experimental Study of Heat Transfer and Fluid Flow in Unsaturated Porous Media*".

Incropera, F.P. and De Witt, D.P., 1990 "*Fundamentals of Heat and Mass Transfer*", Wiley, New York.

Kaviany, M., 1995, *Principles of Heat Transfer in Porous Media- 2nd Edition*, Springer, New York.

Keey, R.B., 1992. *Drying of Loose and Particulate Materials*, Hemisphere Publishing Corporation.

Keey, R.B., Shusheng, P. and Langrish, T.A.G., 1995, "Modelling the Temperature Profiles Within Boards During High-Temperature Drying of Pinus radiata Timber: The Influence of Airflow Reversals", *International Journal of Heat and Mass Transfer*, Vol. 38, No.2, pp. 189-205.

La Comber, P., Ward, S., and Lynch, J., 1997, "The Effect of Particle Size on the Drying of Milled Peat", *Drying Technology*, Vol. 15, No. 3 & 4, pp. 1083-1093.

Plumb, O.A., Lee, W.C. and Gong, L., 1992, "An Experimental Study of Heat and Mass Transfer During Drying of Packed Beds", *Journal of Heat and Mass Transfer*, Vol. 114, pp. 727-734.

Sun, D.W. and Woods, J.L., 1997, "Simulation of The Heat and Moisture Transfer Process During Drying in Deep Grain Beds", *Drying Technology*, Vol. 15, pp. 2479-2508.

Vafai, K. and Sozen, M., 1990, "A Comparative Analysis of Multiphase Transport Models in Porous Media", *Annual Review of Heat Transfer*, Vol. 3, Hemisphere Publishing Corporation.

Walker, G.M., Magee, C.R., and Ahmad, M.N., 1997, "Effect of Humidity on NPK Fertilizer Drying", *Drying Technology*, Vol.15, pp. 2565-2575.

Whitaker, S., 1977, "Simultaneous Heat, Mass, and Momentum Transfer in Porous Media: A Theory of Drying", *Advances in Heat Transfer*, Vol. 13, Academic Press, Inc.

VITA

Graduate College
University of Nevada, Las Vegas

Jason C. Viggato

Local Address:

Las Vegas, NV

Home Address:

Las Vegas, NV

Degree:

Bachelor of Technology, Mechanical Engineering, 1996

State University of New York College at Buffalo

Thesis Title: A Study of the Influence of Physical Parameters on the Drying of Porous Media

Thesis Examination Committee:

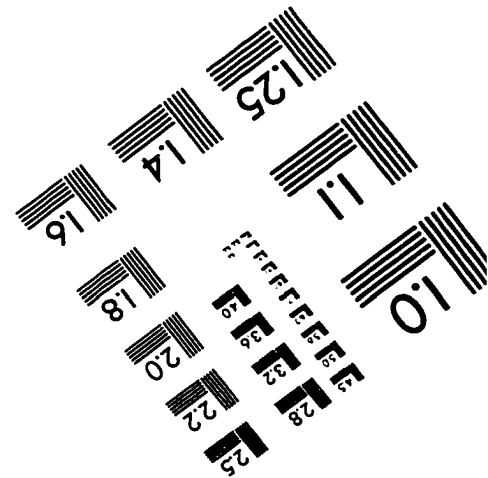
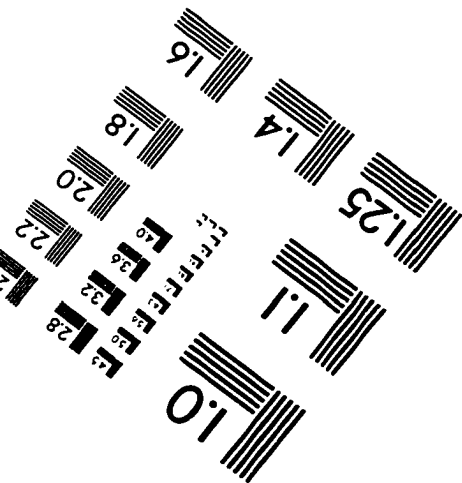
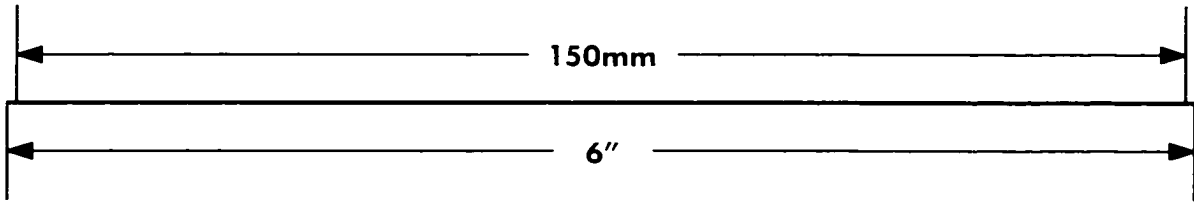
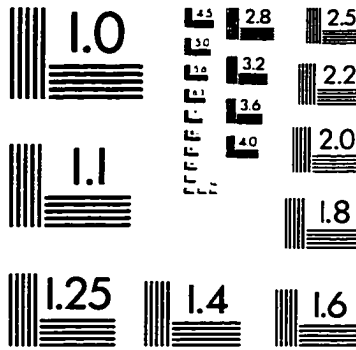
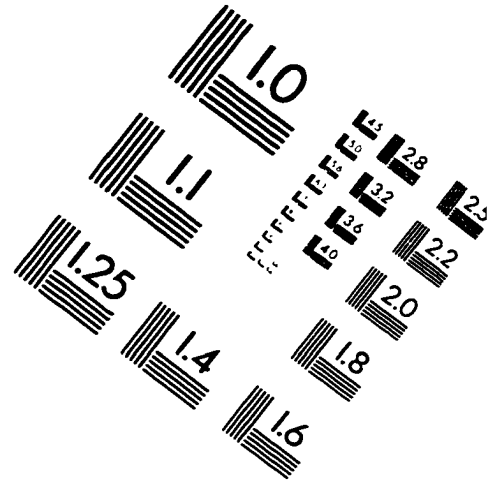
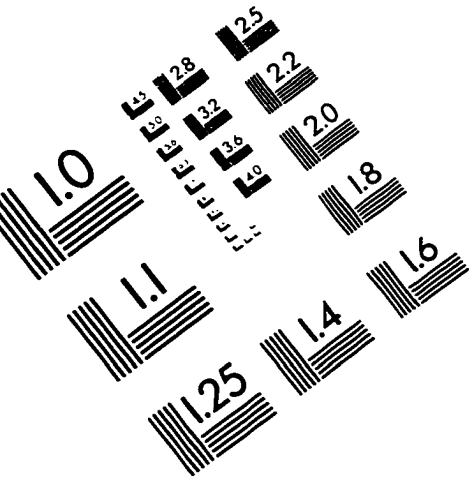
Chairperson, Dr. Robert Boehm, Ph.D.

Committee Member, Dr. Yi-Tung Chen, Ph.D.

Committee Member, Dr. William Culbreth, Ph.D.

Graduate Faculty Representative, Dr. George Miel, Ph.D.

IMAGE EVALUATION TEST TARGET (QA-3)



APPLIED IMAGE, Inc
 1653 East Main Street
 Rochester, NY 14609 USA
 Phone: 716/482-0300
 Fax: 716/288-5989

© 1993, Applied Image, Inc., All Rights Reserved